Assessing the impact of vaccination and behavior change on outbreaks of emerging respiratory diseases

by

Mohammed Hameed Alharbi

Presented to the Faculty of the Graduate School of
The University of Texas at Arlington
in Partial fulfillment of the Requirements
for the Degree of

Doctor of Philosophy

The University of Texas at Arlington
May 2021

ACKNOWLEDGEMENTS

I want to thank the Almighty Allah (God) for all his blessings in my life. I want to thank my parents, Eidah and Hameed Alharbi, for their immeasurable love and support to my upbringing and education and for all their sacrifices to ensure my success.

Special thanks go to my lovely wife, Walaa Alkharmani, for her enormous sacrifices and support throughout my doctoral program. I also want to thank all my brothers, sisters, relatives, and friends for their prayers, support, and encouragement throughout my studies.

My sincere gratitude goes to my supervisor, Dr. Christopher Kribs, for his immense support and guidance in this journey. Without his instruction and guidance, this dissertation would not have been possible. I am grateful to the other committee members Dr. Hristo Kojouharov, Dr. James Grover, Dr. Gaik Ambartsoumian, and Dr. Souvik Roy, for their valuable feedback.

I want to thank the Mathematics Department at UT Arlington for the help they have provided me over the past years.

Special appreciation goes to the Saudi Arabia Cultural Mission (SACM) and the University of Jeddah for their generous financial support for my doctoral program.

April 12, 2021

Assessing the impact of vaccination and behavior change on outbreaks of emerging respiratory diseases

Mohammed Hameed Alharbi

The University of Texas at Arlington

Supervising Professor: Dr. Christopher Kribs

Abstract

The purpose of this dissertation is to use mathematical models to evaluate the impact of characteristics of respiratory diseases like influenza and COVID-19 either alone or co-circulating and how might influenza vaccine affect this interplay. First, we assess the effects of matching and mismatching between vaccine strains and circulating strains during the Hajj. Then we evaluate the impact of the proportion of asymptomatic COVID-19 infections on the magnitude of an epidemic under three different behavior change scenarios. Finally, we model the co-circulation of influenza and COVID-19 to investigate whether the influenza vaccine increases the combined disease burden of influenza and COVID-19 in a dual epidemic.

The influenza virus causes severe respiratory illnesses and deaths worldwide every year. It spreads quickly in an overcrowded area like the annual Hajj pilgrimage in Saudi Arabia.

Vaccination is the primary strategy for protection against influenza. Due to the occurrence of antigenic shift and drift of the influenza virus, a mismatch between vaccine strains and circulating strains of influenza may occur. We study the impact of mismatch between vaccine strains and circulating strains during Hajj, which brings together individuals from all over the globe. We develop deterministic mathematical models of influenza with different populations and strains from the Northern and Southern hemispheres. Results show that the existence and duration of an influenza outbreak during Hajj depend on vaccine efficacy. In this concern, we discuss four scenarios: vaccine strains for both groups match/mismatch circulating strains, and vaccine strains match their target strains and mismatch the other strains. Further, a scenario where a novel pandemic strain arises. Results show that as long as the influenza vaccines match their target strains, there will be no outbreak of strain H1N1, and only a small outbreak of strain H3N2. Mismatching for non-target strains causes about 10,000 new H3N2 cases, and mismatching for both strains causes about 2,000 more new H1N1 cases and 6,000 additional H3N2 cases during Hajj. Complete mismatch in a pandemic scenario may infect over 342,000 additional pilgrims (13.75%) and cause more cases in their home countries.

SARS-CoV-2 has caused severe respiratory illnesses and deaths since late 2019 and spreads globally. While asymptomatic cases play a crucial role in transmitting COVID-19, they do not contribute to the observed prevalence, which drives behavior change during the pandemic. We develop a new mathematical model to identify the effect of the proportion of asymptomatic infections on the magnitude of an epidemic under behavior change scenarios. In this interest, we discuss three different behavior change cases separately: constant behavior change, instantaneous behavior change response to the disease's perceived prevalence, and piecewise constant behavior change response to government policies. Our results imply that the proportion of asymptomatic infections which maximizes the spread of the epidemic depends on the nature of the dominant force driving behavior changes.

Demand for influenza vaccine rose as countries prepared for the second COVID-19 wave over the winter months of 2020-2021. High coverage of the influenza vaccine can significantly reduce morbidity and mortality of the burden of influenza. Natural influenza infection creates short-term non-specific immunity against respiratory viruses (virus interference). We model two viral diseases, both of the SEIR type, to investigate whether the influenza vaccine increases the combined disease burden of influenza and COVID-19 in a dual epidemic. We show that the combined disease burden's behavior depends on virus interference factors and the proportion of the population vaccinated against influenza. Our results indicate that influenza vaccination only lowers the overall disease burden when net virus interference is relatively low.

Contents

Chapter 1

Introduction

Infectious diseases are well known in today's era. Influenza, COVID-19, malaria, and cholera are just a few recent outbreaks that are commonly seen in today's news. Infectious diseases can be transmitted in a variety of ways: airborne (COVID-19, influenza), food or waterborne (cholera, botulism), vector-borne (malaria, dengue), to mention a few. Modeling is a beneficial tool to provide the fundamental dynamics of a disease as it spreads through populations. Mathematical models have been used for over a hundred years to track and understand the mechanism of disease spread, predict the future of epidemics, and identify strategies to protect human health. Many initial studies in mathematical epidemiology are due to public health officials. In 1760, a famous mathematician, Daniel Bernouilli, published a defense of vaccination against smallpox that was the first known result in mathematical epidemiology. Modern mathematical models were developed from the contributions of people such as Sir R.A. Ross, W.H. Hamer, A.G. McKendrick, and W.O. Kermack. One of the especially illuminating contributions is the work of Sir R.A. Ross on malaria. He was awarded the Nobel Prize in Medicine in 1902 for his work on the transmission of malaria. He used differential equations to describe the change in time in susceptible and infected human and mosquito populations and identified a threshold mosquito density under which malaria could be eradicated. Years afterward, George

Macdonald continued the work of Sir R.A. Ross. He introduced the basic reproductive number (BRN), the average number of secondary cases caused by one primary infected individual in a wholly uninfected population, of malaria [1, 2].

Our study uses compartmental models (SEIR, SEIR with vaccination) and nonlinear ordinary differential equations (ODEs) to describe the population's change in size and predict diseases' spread. Fundamental analysis techniques such as equilibria analysis and calculations of the BRN, qualitative analysis, and quantitative analysis are used to analyze each model in this dissertation.

Respiratory disease is the umbrella term for diseases of the lung, bronchi, tubes, trachea, and larynx. These diseases range from mild to moderate to life-threatening (bacterial pneumonia, common cold, influenza, MERS, or COVID-19, for example). Viral respiratory diseases can be spread through airborne respiratory droplets (cough or sneeze), skin-to-skin contact (handshakes or hug), saliva (kissing or shared drinks), or by touching a tainted surface (blanket or doorknob). Influenza (or the flu) is a viral infection that attacks the human respiratory system. The flu epidemics are responsible for 3 to 5 million severe cases and 290,000 to 650,000 respiratory deaths worldwide every year [3]. For more than 50 years, the influenza vaccine is the primary strategy for the protection against influenza [4, 5]. Due to antigenic variations of influenza viruses, individuals are susceptible to the new subtypes (strains) [6, 7, 8]. The influenza vaccine is updated every year by the WHO based on the most common strains circulating from the previous season. The influenza vaccine's efficacy essentially varies depending on mismatching between influenza vaccine strains and the circulating strains [9]. Coronavirus disease 2019 (COVID-19) is a respiratory disease that belongs to a large family of viruses called coronaviruses. COVID-19 was first identified in Wuhan, China, in December 2019. Since then, COVID-19 has spread rapidly worldwide and has been declared a pandemic by the World Health Organization (WHO) on March 11th, 2020. While COVID-19 shares some symptoms

with influenza, it is essential to note that some individuals become infected and do not develop any symptoms (asymptomatic infected) or feel ill [10, 11, 12, 13].

There are fundamental ways to prevent individuals from getting respiratory diseases, whether vaccines or reducing contacts; however, sometimes, these prevention measures have consequences that would not initially be intended. For instance, a mismatch that occurs in the influenza vaccine is an unintended consequence of intervention measures. We want to have some way to measure and evaluate those unintended consequences. Hence, this thesis investigates the impacts of unique characteristics of respiratory viral diseases like influenza and COVID-19, either alone or co-circulating, and how might influenza vaccine affect this interplay. This goal is broken into three parts. First, in Chapter 2, we evaluate the impact of mismatch between vaccine strains and circulating strains in Hajj (Muslim pilgrimage). Mainly, we focus on a scenario where pilgrims from the northern and southern hemispheres carry genetically different strains of infection. In Chapter 3, we seek to identify the effect of the proportion of asymptomatic COVID-19 infections on the magnitude of an epidemic under three different behavior change scenarios. Finally, in Chapter 4, we model the co-circulation of influenza and COVID-19 to evaluate whether the influenza vaccine increases the combined disease burden of influenza and COVID-19 in a dual epidemic.

Chapter 2

A mathematical modeling study: assessing impact of mismatch between influenza vaccine strains and circulating strains in Hajj

2.1 Introduction

Influenza viruses circulating worldwide cause respiratory tract infection known as seasonal influenza. In general, there are four types of influenza viruses, type A, B, C, and D. Usually, influenza infections are caused by influenza A and B viruses. Seasonal influenza presently infects one of each six people every year, with 3 to 5 million severe illness, and 290,000 to 650,000 respiratory deaths worldwide. Influenza viruses can be spread by airborne respiratory droplets (cough or sneeze), skin-to-skin contact (handshakes or hug), saliva (kissing or shared drinks), or by touching a tainted surface (blanket or doorknob). Seasonal influenza spreads readily in overcrowded areas like mass gatherings [3].

For more than a half-century, vaccination has been the primary strategy for protecting and controlling influenza [4, 5], and influenza vaccines continue to decrease the impact of infection [9]. However, individuals are repeatedly infected by seasonal influenza due to two types of antigenic variation: antigenic drift and antigenic shift. These variations make people susceptible to new subtypes that are genetically different enough from the old ones, regardless of prior infection by other influenza subtypes. In other words, if the

new strains of influenza are genetically different enough from the old strains, people will be susceptible to them. If the genetic distance between the new strain and old strain is not very big, then people will have partial immunity [6, 7, 8]. Hence, the influenza vaccine is updated yearly based on the most common strains circulating from the previous season, in order to match with new circulating strains that are predicted to cause infections [14]. WHO monitors influenza worldwide and recommends vaccine compositions twice each year for the Northern and Southern hemisphere influenza seasons.

Mismatching or poor matching is defined to be the case if the strains that are included in the vaccine are antigenically different from the circulating strains. The mismatch between the vaccine strains and circulating strains may take place when a drifted virus emerges after vaccine strains have been selected or a novel pandemic strain has spread [3]. Vaccine effectiveness (VE) primarily varies depending on matching or mismatching between influenza vaccine strains and the circulating strains [9]. A systematic review shows that the VE was 77% (95% confidence interval (CI) 67% to 86%) for the live attenuated influenza vaccine (LAIV) and 65% (95% CI 57% to 72%) for the trivalent inactivated vaccine (TIV) when the vaccine strains and circulating strains are matched. Furthermore, when the vaccine strains and circulating strains are mismatched, VE was 60% (95% CI 44% to 71%) for LAIV and 56% (95% CI 43% to 66%) for (TIV) [15]. These findings prove that there is cross-protection even when vaccine strains do not match circulating strains. Kelly et al. demonstrated that the seasonal vaccine has no protection against a pandemic influenza strain in any age group [16]. Vaccine failure or low efficacy refers to poor matching between vaccine strains and circulating strains [17, 18]. Matching and mismatching, in actuality, is not binary, i.e., vaccination is not a perfect match or a perfect mismatch with the circulating strains.

Co-infection, i.e. infection by more than one strain of influenza, also known as concurrent infection, has been detected in seasonal influenza in different parts of the world (e.g.,

[7, 19, 20, 21, 22, 23, 24, 25, 26, 27, 28, 29, 30, 31, 32, 33, 34, 35, 36, 37]). Individuals can be either infected by both strains at the same time [38] or infected by one strain and then infected by the other before recovery from the first strain. The phenomenon of co-infection is different from re-infection, where an individual who has been infected by one strain and then recovered is then infected by another strain, usually called a secondary infection.

Every year about three million Muslims perform Hajj to Makkah, Saudi Arabia. The Hajj is an annual Muslim pilgrimage and a mandatory religious obligation for all Muslims who are physically and financially capable of the commitment, the travel, and support of their family during their absence. This obligation is only mandatory once in a lifetime. The Hajj occurs during the last month (12th) of the Islamic calendar, and the Hajj ritual is held within six specific days during the month. Some pilgrims come only for the Hajj ritual, while others prefer to stay sometime before or after performing Hajj. At these times, pilgrims are in such close contact that transmission of respiratory tract infection is extremely high because of immense overcrowding.

The Hajj is epidemiologically significant because it brings together large numbers of people from all over the world who may be carrying different strains of influenza that other people may not be vaccinated against. Vaccination against influenza is recommended for all pilgrims by the Saudi Ministry of Health [39]. A proportion of those people may come to the Hajj while they are vaccinated against their home influenza circulating strains, which are often different than strains circulating during Hajj. A detailed analysis at the Hajj covering the period between 2003 and 2015 demonstrated that mismatching between strains that included in the vaccine and the circulating strains is frequent [40]. Different vaccines are made available for the Northern and Southern hemispheres due to significant differences between strains circulating in the Northern and Southern hemispheres. In this regard, Hajj is similar to events like the Olympics and World Cup, but it is unique

in its extremely high population density, which generates homogeneous mixing in an extraordinarily large population.

Many mathematical studies have been done to better understand the dynamics of influenza transmission in one host population (since influenza is an air-borne disease) and multi-strains of influenza with varying levels of cross-immunity [41, 42, 43, 44, 45, 46, 47, 48, 49, 50, 51, 52, 53, 54, 55, 56]. Some influenza mathematical models have studied the dynamics of infection with two different populations and one strain of influenza [57, 58]. Evaluating the role of cross-immunity and determining the condition(s) for co-existence have been concentrated, overall, on these studies. Nune et al. demonstrated that host isolation and cross-immunity may stimulate sustained periodic oscillations [52]. Bremermann and Thieme manifest the occurrence of competitive exclusion, where one strain with the largest reproduction number persists and excludes the other strains [59]. The reproduction number of the 1918–1919 influenza pandemic and other seasonal strains of influenza have been estimated to be in the range between 1.5 and 5.4 [55]. To the best of our knowledge, there is no mathematical model that incorporates both: two different populations, with the possibility that a proportion of each population is vaccinated, and two different strains of influenza. Any vector-borne disease (VBD) models, however, naturally involve two different populations (host and vector) that interact among each other. Some VBD models have considered two populations and two strains [60, 61, 62], or two diseases [63, 64].

The focus of our study is to assess the impact of matching and mismatching between vaccine strains and circulating strains during the Hajj, in a scenario where pilgrims from the Northern and Southern hemispheres carry genetically different strains of infection. A new deterministic model will be built to attain this goal.

2.2 Model Development

Because of the complexity of the model, we build up to it by adapting a basic SEIR model with vaccination to first two strains, and then two populations.

2.2.1 Simple SEIR Model with Vaccination (One Population, One or Two Strains)

We begin with a simple SEIR model with vaccination, see Fig. 2.1, to explain the underlying assumptions and why we have different versions of it in the full model. In brief, the population is classified into susceptible, vaccinated, exposed, infected, and recovered classes (S, V, E, I, R). Susceptible and vaccinated individuals can be infected through their contact with infected individuals in class I, with a reduced rate for vaccinated individuals due to the vaccine's protection. Infected individuals are moving to exposed class, E, and remaining noninfectious for an incubation period. Individuals in class E are moving to the infected class, I, and becoming infectious after the incubation period. Lastly, individuals in class I are moving to recovered class, R, after recovery. For the simple model, Fig. 2.1, there is only one class for each stage of the course of the infection. The simple model can be applied to an influenza disease model that considers one population and one strain.

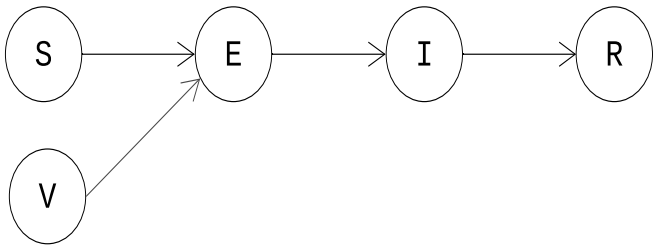

Figure 2.1: Simple SEIR with vaccination.

In order to include two different strains of influenza, multiple copies of the simple model are required. Since the model describes a single mixing population with only one type of vaccine, there remain only one S_i class and one V_i class. However, those vaccinated individuals infected by one strain retain partial protection against the other strain, requiring a separate chain of exposed (F_{ij}), infective (K_{ij}), and recovered (W_{ij}) compartments for each strain. Thus vaccination history remains important until not the first exposure (as in the one-strain model), but the second. Initial infection of the S_i or V_i population with strain 1 or 2 therefore leads to four SEIR chains, as in Fig. 2.2. Although we are only considering one mixing population at this stage, we introduce the notation that will be used in the final model: each compartment's first subscript i designates the population (1 or 2) to which it belongs, while a second subscript j indicates the strain (1 or 2) with which it has been infected.

To add the co-exposed classes and complete the model, each of the six pairs (E_{1j}, F_{1j}), (I_{1j}, K_{1j}), (R_{1j}, W_{1j}), $j = 1, 2$, in Fig. 2.2 will serve in the full model as the starting points (corresponding to (S, V)) of an SEIR cycle. Since co-infection is incorporated, there are classes exposed, E_{13}, infected, I_{13}, and recovered, R_{13}, from both strains. Plus, there are classes exposed by one strain and infected, L_{1j}, or recovered, G_{1j} by the other strain and classes for infected by a strain and recovered from the other strain, J_{1j} and $j = 1, 2$, see Fig. 2.3 when i=1 only.

2.2.2 Full Model (Two Populations, Two Strains)

We divide the population who attend Hajj into two groups: pilgrims from the Northern hemisphere, $i = 1$, and pilgrims from the Southern hemisphere, $i = 2$, based on their influenza vaccine strains. Each group is categorized into 23 compartments according to vaccination and infection status for both strains, with total population for each group denoted by N_i and the total population denoted by N. We define n_i as the proportion

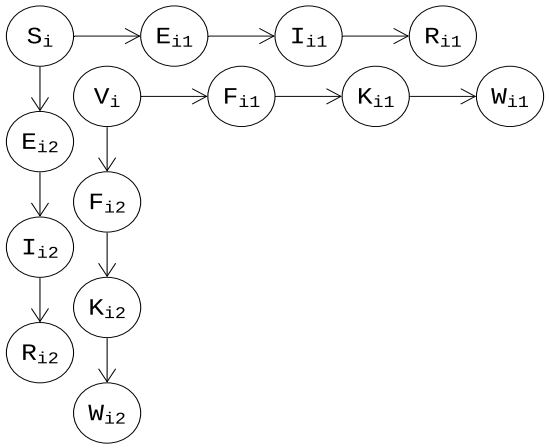

Figure 2.2: Single-infection SEIR chains for one population (i) and two strains (1,2), starting from susceptible or vaccinated

of the total population occupied by each group. Again, a compartment's first subscript indicates population or hemisphere of origin, i = 1 or 2, and any second subscript denotes the strain of most recent infection, j = 1 or 2 (3 for co-infection). A complete list of the state variables used in this model is shown in Table 2.1. A flow chart for the complete model would include two copies of Fig. 2.3–one for each population of origin–coupled only by the infection rates, which sum over all compartments infected with a given strain in both populations.

Since we examine transmission during the short timeline of Hajj, we do not include birth and death rates. The infection rate of susceptible individuals through their contacts with infectives in the model is standard incidence since the contact rate in Hajj is saturated, due to the large numbers of pilgrims. Furthermore, during the entire model, we assume nearly all of the pilgrims' contact time is with other pilgrims. Thus, we are restricting our attention only to infections among pilgrims. We use multiple infection rates, β_{mnj}, for each combination of infecting group, receiving group, and strain types. The infection rates, β_{mnj}, are defined as the rate of infectious contacts from individuals in a group m to individuals in a group n multiplied by the probability of transmission

of a strain j per contact. Susceptibles from both groups are at risk of getting infected by either strain. Each group has a proportion of individuals who have received the vaccine for their region $\phi_i \in (0,1)$. Vaccinated individuals can be infected at a reduced rate based on the matching/mismatching measures, q_{ij}. We assume that an individual can be co-infected from both strains; to get that, he/she must first be infected by one strain and then infected by the other. An individual will get permanent immunity from one strain after recovery, but he/she will still be susceptible to the other strain. For an individual to be permanently immunized from both strains, he/she must be infected by both strains, either co-infected or one after another, and then recover from both of them. For each strain, we assume there is a different recovery rate γ_j. We incorporate the idea of vaccine matching as a parameter, q_{ij}, that can tune between 0 and 1. If $q_{ij} = 1$, that means there is a complete mismatch, between vaccine strain i and circulating strain j, and no protection at all. If $q_{ij} = 0$, it is a perfect match between vaccine strain i and circulating strain j. In reality, it is going to be somewhere in between. A list of all parameters used in the model is shown in Table 2.1.

We will consider three versions of this model. The first case, where individuals do not arrive or leave (no recruitment or departure rates), is considered for the specific six days of the Hajj ritual. Case two, where individuals arrive and depart at constant rates, is a more complex approximation to Hajj pilgrims' population dynamics. Case three, where individuals arrive before the six days of Hajj rituals and leave after these six days, mirrors the actual timeline at Hajj. In case three, there are three time periods. The first period, the arrival phase, is when pilgrims arrive gradually, the 38 days before the Hajj worship. The second period, the worship stage, is the actual intense six days of the Hajj ritual. The third period, the departure stage, is when pilgrims leave, 27 days after the Hajj ritual. Thus, we consider an approximate time frame of 90 days for the model.

	Notation	Definition
State variables	S_i	Susceptible in group i who have never been infected or received vaccine from either strains
	V_i	Individuals in group i who have received vaccine i
	E_{ij}	Individuals in group i who have been exposed to strain j
	E_{i3}	Individuals in group i who have been exposed to both strains
	F_{ij}	Individuals in group i who have received vaccine i and exposed to strain j
	I_{ij}	Individuals in group i who have been infected by strain j
	I_{i3}	Individuals in group i who have been co-infected by both strains
	K_{ij}	Individuals in group i who have received vaccine i and infected by strain j
	L_{ij}	Individuals in group i who have been infected by strain j and expose to the other strain, $\neq j$
	R_{ij}	Individuals in group i who have recovered from strain j
	R_{i3}	Individuals in group i who have recovered from both strains
	G_{ij}	Individuals in group i who have been exposed to strain j and immunized by the other strain due to recovery
	J_{ij}	Individuals in group i who have been infected by strain j and immunized by the other strain due to recovery
	W_{ij}	Individuals in group i who have been immunized from strain j due to recovery and received vaccine i
	N_i	Total population of group i
Parameters	Λ_i	Recruitment rate for group i ($\frac{\text{individual}}{\text{time}}$)
	μ	Departure rate (time^{-1})
	β_{mnj}	Individuals from group m to individuals from group n infection rate by strain j (time^{-1})
	η_j	1/Incubation period for strain j (time^{-1})
	γ_j	Influenza strain j recovery rate (time^{-1})
	q_{ij}	Mismatching reduced rate for group i strain j (Dimensionless)
	ϕ_i	The proportion of individuals who have received vaccine for group i (Dimensionless)
	p_i	Prevalence of influenza among individuals from group i who have arrived (Dimensionless)

Table 2.1: State variable and parameter definitions and their units.

2.2.3 Model Equations

A flowchart of the three cases of this model is illustrated in Fig. 2.3. The solid arrows only represent the case one model. The solid and dotted arrows represent cases two and three. The system of equations for case one model is given by system (2.1), when $\Lambda_i = \mu = 0$ and

for cases two and three by system (2.1), when Λ_i and $\mu \neq 0$.

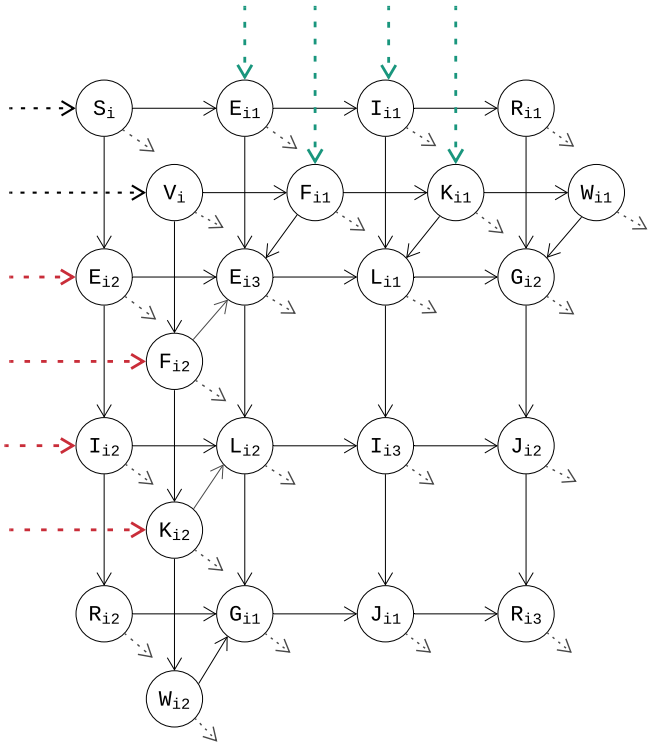

Figure 2.3: Compartmental diagram of the model for group i, $i = 1, 2$. The diagram without dotted arrows represents case one model, and the dotted arrows indicate incoming infected pilgrims in cases two and three. Group 1 imports infections of strain one only (green arrows) while group 2 imports strain two only (red arrows).

$$
\begin{aligned}
\frac{dS_i}{dt} &= (1-p_i)(1-\phi_i)\Lambda_i - d_{i1}S_i - d_{i2}S_i - \mu S_i \\
\frac{dE_{i1}}{dt} &= \frac{p_i}{2}(1-\phi_i)\Lambda_i + d_{i1}S_i - d_{i2}E_{i1} - \eta_1 E_{i1} - \mu E_{i1} \\
\frac{dE_{i2}}{dt} &= \frac{p_i}{2}(1-\phi_i)\Lambda_i + d_{i2}S_i - d_{i1}E_{i2} - \eta_2 E_{i2} - \mu E_{i2} \\
\frac{dV_i}{dt} &= (1-p_i)\phi_i\Lambda_i - q_{i1}d_{i1}V_i - q_{i2}d_{i2}V_i - \mu V_i \\
\frac{dF_{i1}}{dt} &= \frac{p_i}{2}\phi_i\Lambda_i + q_{i1}d_{i1}V_i - q_{i2}d_{i2}F_{i1} - \eta_1 F_{i1} - \mu F_{i1} \\
\frac{dF_{i2}}{dt} &= \frac{p_i}{2}\phi_i\Lambda_i + q_{i2}d_{i2}V_i - q_{i1}d_{i1}F_{i2} - \eta_2 F_{i2} - \mu F_{i2} \\
\frac{dE_{i3}}{dt} &= d_{i1}E_{i2} + d_{i2}E_{i1} + q_{i1}d_{i1}F_{i2} + q_{i2}d_{i2}F_{i1} - (\eta_1+\eta_2)E_{i3} - \mu E_{i3} \\
\frac{dI_{i1}}{dt} &= \frac{p_i}{2}(1-\phi_i)\Lambda_i + \eta_1 E_{i1} - d_{i2}I_{i1} - \gamma_1 I_{i1} - \mu I_{i1} \\
\frac{dI_{i2}}{dt} &= \frac{p_i}{2}(1-\phi_i)\Lambda_i + \eta_1 E_{i2} - d_{i1}I_{i2} - \gamma_2 I_{i2} - \mu I_{i2} \\
\frac{dK_{i1}}{dt} &= \frac{p_i}{2}\phi_i\Lambda_i + \eta_1 F_{i1} - q_{i2}d_{i2}K_{i1} - \gamma_1 K_{i1} - \mu K_{i1} \\
\frac{dK_{i2}}{dt} &= \frac{p_i}{2}\phi_i\Lambda_i + \eta_2 F_{i2} - q_{i1}d_{i1}K_{i2} - \gamma_2 K_{i2} - \mu K_{i2} \\
\frac{dL_{i1}}{dt} &= \eta_1 E_{i3} + d_{i2}I_{i1} + q_{i2}d_{i2}K_{i1} - \gamma_1 L_{i1} - \eta_2 L_{i1} - \mu L_{i1} \\
\frac{dL_{i2}}{dt} &= \eta_2 E_{i3} + d_{i1}I_{i2} + q_{i1}d_{i1}K_{i2} - \gamma_2 L_{i2} - \eta_1 L_{i2} - \mu L_{i2} \\
\frac{dI_{i3}}{dt} &= \eta_1 L_{i2} + \eta_2 L_{i1} - (\gamma_1+\gamma_2)I_{i3} - \mu I_{i3} \\
\frac{dJ_{i1}}{dt} &= \eta_1 G_{i1} + \gamma_2 I_{i3} - (\gamma_1+\mu)J_{i1}, \qquad
\frac{dJ_{i2}}{dt} = \eta_2 G_{i2} + \gamma_1 I_{i3} - \gamma_2 J_{i2} - \mu J_{i2} \\
\frac{dR_{i1}}{dt} &= \gamma_1 I_{i1} - d_{i2}R_{i1} - \mu R_{i1}, \qquad
\frac{dR_{i2}}{dt} = \gamma_2 I_{i2} - d_{i1}R_{i2} - \mu R_{i2} \\
\frac{dW_{i1}}{dt} &= \gamma_1 K_{i1} - q_{i2}d_{i2}W_{i1} - \mu W_{i1}, \qquad
\frac{dW_{i2}}{dt} = \gamma_2 K_{i2} - q_{i1}d_{i1}W_{i2} - \mu W_{i2} \\
\frac{dG_{i1}}{dt} &= d_{i1}R_{i2} + q_{i1}d_{i1}W_{i2} + \gamma_2 L_{i2} - \eta_1 G_{i1} - \mu G_{i1} \\
\frac{dG_{i2}}{dt} &= d_{i2}R_{i1} + q_{i2}d_{i2}W_{i1} + \gamma_1 L_{i1} - \eta_2 G_{i2} - \mu G_{i2} \\
\frac{dR_{i3}}{dt} &= \gamma_1 J_{i1} + \gamma_2 J_{i2} - \mu R_{i3},
\end{aligned}
\tag{2.1}
$$

where "d_{i1}" and "d_{i2}", the infection rates, are given by

$$d_{i1} = \sum_{m=1}^{2} \beta_{mi1} \frac{I_{m1} + K_{m1} + J_{m1} + L_{m1} + I_{m3}}{N},$$
$$d_{i2} = \sum_{m=1}^{2} \beta_{mi2} \frac{I_{m2} + K_{m2} + J_{m2} + L_{m2} + I_{m3}}{N}.$$

Case 1: Model with No Recruitment and Departure Rate

The system of nonlinear differential equations corresponding to the case one model is depicted in Fig. 2.3 for group i, $i = 1, 2$, without dotted arrows, and given by (2.1) for all $i = 1, 2$, with recruitment and departure rates are zeros. When $i = 1$, $\Lambda_1 = \mu = 0$, (2.1) describe the compartments for the group one population, which represents pilgrims who are coming from the Northern hemisphere. Group two population consisting of pilgrims coming from the Southern hemisphere is described when $i = 2$, $\Lambda_2 = \mu = 0$ in (2.1). Further, the initial conditions for all $i = 1, 2$ in case one model are described as

$$\frac{V_i(0)}{S_i(0) + V_i(0)} = \phi_i.$$

There are at most few individuals in the other classes. This would make $V_i(0)$ approximately $\phi_i N_i$ and $S_i(0)$ approximately $(1 - \phi_i)N_i$.

Case 2: Model with Constant Recruitment and Departure Rates

The system of nonlinear differential equations corresponding to the cases two and three is portrayed in Fig. 2.3 and given by (2.1), where recruitment rates (Λ_i, $i = 1, 2$) and departure rate (μ) for the case two are going to be constant rates. We assume that strain one is only coming from Northern pilgrims (green arrows in Fig. 2.3 and terms in (2.1)), and strain two from Southern pilgrims (red arrows in Fig. 2.3 and terms only in (2.1)). Furthermore, there is a proportion of arriving infected pilgrims, namely

prevalences of strain one and strain two are described as (p_1) and (p_2), respectively. Moreover, the distributions of infected states of the arriving pilgrims are evenly separated between infected ($p_i/2$) and exposed ($p_i/2$) compartments for both groups. Since infections are considered only to be among pilgrims, initial conditions for cases two and three are zero.

Case 3: Model with Non-Constant Recruitment and Departure Rates

Since the system of nonlinear differential equations corresponding to case three model is going to be similar to case two equations, with non-constant recruitment (Λ_i, $i = 1, 2$) and departure (μ) rates, descriptions for the case three model will not be given. The case three model mirrors the actual timeline of the Hajj season, which has three phases. Phase one (arrival phase) occurs between day one and 38 of Hajj season, when individuals are arriving, and no one is leaving. Phase two (the Hajj worship phase) mainly happens between days 38 and 43 for the specific six days of the Hajj ritual, where everyone must be there to complete their rites. In other words, this phase represents the case one model, with no recruitment nor departure rates. Phase three (departure phase) mainly occurs between days 43 and the end of the season. All pilgrims must leave Saudi Arabia after the Hajj ritual no later than the 10th of Muharram of each year, which is 27 days after the Hajj ritual [65]. In this phase, pilgrims have ended their worship and ready to go back to their home country. Consequently, we will not have the departure rate (μ) for phase one, and no recruitment rates (Λ_i,$i = 1, 2$) for phase three, while we will have neither recruitment rates nor departure rate for phase two. Thereupon, Λ_i equals $\frac{N_i}{38}$, $i = 1, 2$ when t goes from 0 to 38, zero everywhere else, and μ represents the reciprocal of average time that pilgrims stay after Hajj worship ends, which we assume to be $\frac{1}{27}$ day^{-1} for t between 44 and 90, and zero everywhere else [65].

2.3 Analysis

Although equilibria have little practical meaning in a study of short-term dynamics, we nevertheless perform an equilibrium analysis in order to derive the control reproductive number (CRN), which is a measure of whether the disease would spread or not. We will study the infection's ability to spread using CRN as a threshold quantity. It is called CRN instead of basic reproductive number (BRN) because it includes vaccination as a control measure. The point where the disease does not exist within the population is called disease free equilibrium (DFE).

2.3.1 Control Reproduction Number for Case One Model

DFE occurs for the case one model equations when $I_{ij} = K_{ij} = L_{ij} = J_{ij} = I_{i3} = 0 \ \forall \ i, j = 1, 2$. By setting all the nonlinear differential equations in case one model equations equal to zero, we get $E^*_{ij} = E^*_{i3} = F^*_{ij} = G^*_{ij} = 0$ and infinitely many non-zero DFEs of the form DFE $= (S^*_1, S^*_2, V^*_1, V^*_2, 0, 0, 0, 0, 0, 0, 0, 0, 0, 0, 0, 0, 0, 0, 0, 0, 0, 0, 0, 0, 0, R^*_{11}, R^*_{12}, R^*_{21}, R^*_{22}, R^*_{13}, R^*_{23}, 0, 0, 0, 0, 0, 0, 0, 0, 0, 0, 0, 0, W^*_{11}, W^*_{12}, W^*_{21}, W^*_{22})$, where S^*_i, V^*_i, R^*_{ij}, R^*_{i3}, W^*_{ij} are free real valued variables $\forall \ i, j = 1, 2$ and

$$\sum_{j=1}^{2} [S^*_i + V^*_i + R^*_{ij} + R^*_{i3} + W^*_{ij}] = N_i.$$

(If equilibrium components are required to take on whole-number values, then the number of equilibria is finite but very large). Although the next generation methods normally assume an isolated disease free equilibrium, by [1] it is sufficient to consider the disease free equilibrium where everyone is susceptible. In order to derive the control reproduction number (CRN), denoted by $\mathcal{R}_c$, for the case one model equations, we use the next generation operator approach proposed by[66]. $\mathcal{R}_c$ is the spectral radius, the dominant eigenvalue, of the next generation matrix (NGM) obtained from this method. Evaluating

the NGM at DFE where everyone is susceptible, i.e. $R^*_{ij} + R^*_{i3} = W^*_{ij} = 0$ for all $i, j = 1, 2$, and computing the spectral radius of the NGM, we have $\mathcal{R}_c = \max\{\mathcal{R}_1, \mathcal{R}_2\}$ where:

$$\mathcal{R}_1 = \frac{\beta_{111}\tau_{11} + \beta_{221}\tau_{21} + \sqrt{(\beta_{111}\tau_{11} - \beta_{221}\tau_{21})^2 + 4\beta_{121}\beta_{211}\tau_{11}\tau_{21}}}{2\gamma_1},$$
$$\mathcal{R}_2 = \frac{\beta_{112}\tau_{12} + \beta_{222}\tau_{22} + \sqrt{(\beta_{112}\tau_{12} - \beta_{222}\tau_{22})^2 + 4\beta_{122}\beta_{212}\tau_{12}\tau_{22}}}{2\gamma_2}.$$

τ_{ij} refers to the average susceptibility for strain j in group i. Then by applying the initial conditions for case 1, we get

$$\begin{aligned}
\tau^*_{ij} &= \frac{S^*_i + q_{ij}V^*_i}{N_1 + N_2} \\
&= \frac{(1-\phi_i)N_i + q_{ij}\phi_{ij}N_i}{N_1 + N_2} \\
&= \frac{(1-(1-q_{ij})\phi_i)N_i}{N_1 + N_2} \\
&= \sigma_{ij}n_i,
\end{aligned}$$

where

$$n_i = \frac{N_i}{N_1 + N_2},$$
$$\sigma_{ij} = 1 - (1 - q_{ij})\phi_i.$$

2.3.2 Control Reproduction Number for Case Two Model

In order to compute CRN for case two model, we need to consider the special case when both p_1 and p_2 equal zero. In this matter, DFE occurs for the case two model equations when $I_{ij} = K_{ij} = J_{ij} = L_{ij} = I_{i3} = 0 \ \forall \ i, j = 1, 2$. By setting all the equations equal to zero, we get DFE $= ((1-\phi_1)N^*_1, (1-\phi_2)N^*_2, \phi_1 N^*_1, \phi_2 N^*_2, 0, 0, 0, 0, 0, 0, 0, 0, 0, 0, 0, 0, 0, 0, 0, 0,$

0, 0, 0, 0, 0, 0, 0, 0, 0, 0, 0, 0, 0, 0, 0, 0, 0, 0, 0, 0, 0, 0, 0, 0) and where for all $i = 1, 2$

$$N_i^* = \frac{\Lambda_i}{\mu}.$$

Similarly, $\mathcal{R}_c$ for case 2 is calculated as the spectral radius of the NGM, where $\mathcal{R}_c = \max\{\mathcal{R}_1, \mathcal{R}_2\}$ and

$$\mathcal{R}_1 = \frac{\eta_1}{\mu + \eta_1} \frac{\beta_{111} n_1^* \sigma_{11} + \beta_{221} n_2^* \sigma_{21} + \sqrt{(\beta_{111} n_1^* \sigma_{11} - \beta_{221} n_2^* \sigma_{21})^2 + 4\beta_{121}\beta_{211} n_1^* n_2^* \sigma_{11}\sigma_{21}}}{2(\mu + \gamma_1)},$$
$$\mathcal{R}_2 = \frac{\eta_2}{\mu + \eta_2} \frac{\beta_{112} n_1^* \sigma_{12} + \beta_{222} n_2^* \sigma_{22} + \sqrt{(\beta_{112} n_1^* \sigma_{12} - \beta_{222} n_2^* \sigma_{22})^2 + 4\beta_{122}\beta_{212} n_1^* n_2^* \sigma_{12}\sigma_{22}}}{2(\mu + \gamma_2)},$$

where for all $i, j = 1, 2$, we have:

$$n_i^* = \frac{N_i^*}{N_1 + N_2},$$
$$\sigma_{ij} = 1 - (1 - q_{ij})\phi_i.$$

Lemma 2.3.1. *$\mathcal{R}_c$'s are equal for both cases as long as N_i approaches N_i^* for all $i = 1, 2$ and μ goes to zero.*

Proof. We notice that as N_i approaches N_i^* for all $i = 1, 2$, we get

$$\begin{aligned}\tau_{ij} &= \sigma_{ij} \frac{N_i}{N_1 + N_2} \\ &= \sigma_{ij} \frac{N_i^*}{N_1 + N_2} \\ &= \sigma_{ij} n_i^*.\end{aligned}$$

And as μ goes to zero, we have for all $i = 1, 2$

$$\frac{\eta_j}{\mu + \eta_j} = 1.$$

□

Following the text of [1], we choose specifically the equilibrium where everyone is susceptible. By the initial conditions, we suppose that $S_i = (1 - \phi_i)N_i$ and $V_i = \phi_i N_i$. From 2.3.1, we will have $\tau_{ij} = \sigma_{ij} n_i^*$. Then the CRN for both cases will be $\mathcal{R}_c = \max_j \{\mathcal{R}_j\}$, $j = 1, 2$

$$\mathcal{R}_j = \frac{a_{11j} + a_{22j} + \sqrt{(a_{11j} - a_{22j})^2 + 4a_{12j}a_{21j}}}{2},$$

and where

$$a_{mnj} = \begin{cases} \frac{\beta_{mnj} n_m^* \sigma_{mj}}{\gamma_j} & \text{case 1} \\ \frac{\beta_{mnj} n_m^* \sigma_{mj}}{(\mu + \gamma_j)} & \text{case 2.} \end{cases}$$

a_{11j} refers to the transmission of influenza strain j within group one. Through pilgrims' interaction, susceptible and a proportion of vaccinated pilgrims become infected by strain j, $j = 1, 2$. In a similar way, a_{22j} describes the rate of development of infected individuals by strain j, $j = 1, 2$ in group 2 through contact with other individuals in group 2. Infected individuals from either group are recruited through interaction with other infected individuals from the same group, such as through accommodation in the same place or walking with nearby infected individuals from the same group. Both terms, a_{11j} and a_{22j}, are the primary ways that influenza strain j develops within the system. The

other recruitment is given by the terms a_{12j} and a_{21j}. a_{12j} is the transmission of strain j from an infected pilgrim from group 1 to an individual from group 2, and vice-versa a_{21j}. This occurs everywhere in Hajj due to the overcrowding in every holy site area. For each model, case 1 and case 2, the interpretation of the CRN for a strain j is the ability to spread. Strain j is spreading with efficiency a_{11j} in population one and spreading with efficiency a_{22j} in population two.

In order to interpret the CRN, we use two useful mathematical facts:

$$\sqrt{x+y} \leq \sqrt{x} + \sqrt{y},$$
$$\max\{x, y\} = \frac{x + y + |x - y|}{2}$$

Applying these facts to the CRN we have

$$\max_{1\leq k\leq 2}\{a_{11j}, a_{22j}\} \leq \mathcal{R}_j \leq \max_{1\leq k\leq 2}\{a_{11j}, a_{22j}\} + \sqrt{a_{12j}a_{21j}}].$$

The CRN is the ability of strain j to spread either in population one or in population two. It makes sense that $\mathcal{R}_c$ should be at least as great as its ability to spread in either population alone. In fact, it is greater because it is spreading in both populations. The square root is the geometric mean of the ability of strain j to spread from group one to group two and then back from group two to group one which is a complete cycle. Geometric mean is sort of the average of that ability to spread from group one to group two and then back or from group two to group one and then back. This is a form of $\mathcal{R}_0$ that has actually been seen lots of times before [67].

To obtain the basic reproductive number (BRN) from the CRN, we set $\phi_i = 0$ for all

$i = 1, 2$. By doing this we get BRN, $\mathcal{R}_0 = \max_j \{\mathcal{R}_j\}$, $j = 1, 2$

$$\mathcal{R}_j = \frac{a^*_{11j} + a^*_{22j} + \sqrt{(a^*_{11j} - a^*_{22j})^2 + 4a^*_{12j}a^*_{21j}}}{2},$$

and where

$$a^*_{mnj} = \frac{\beta_{mnj} n^*_m}{\gamma_j}.$$

2.3.3 Control Reproduction Number for Case Three Model

Since the case three model has three phases, it is not very easy to discuss the CRN. Furthermore, the first phase of the case three model has no equilibria; thus, we cannot compute CRN for the first phase. For the second phase, CRN is the same as the case one model. Additionally, all equilibria for phase three are extinction equilibria, which means CRN equals zero.

2.4 Parameter Estimates

To evaluate the impact of vaccine matching and mismatching, we provide some values of each parameter. Before estimating those values, we need to choose specific strains to consider. Since 1977, H1N1 and H3N2 have been co-circulating worldwide [68]. Therefore, we take into account these two strains, respectively, in the model. Most of the model's parameters can be estimated directly from the literature, with the only exception being the infection rates for which a more heuristic approach is required.

By carefully looking at studies of vaccination proportions in the last 20 years, we see a massive variation from basically no one to everyone. To make sense of this variation, despite there being some variation from country to country, however, what seems very

important for us is variation by year. To that end, we notice that influenza 2009 pandemic temporarily and permanently changed the way people view influenza vaccination. So before 2009, the rate of influenza vaccine compliance was shallow, about 10.9% [69, 70, 71, 72, 73, 74, 75]. Then in 2009, the rate of compliance was very high. It was mandatory by Saudi Arabia for pilgrims from some countries to receive the vaccine to obtain the Hajj visa. The average rate of vaccine compliance from studies that we have seen with data in 2009 was about 95.7% [76, 77, 78, 79]. After 2009, the compliance goes down, but it goes down to still a much higher level than before 2009. The average rate of vaccine compliance after 2009 was around 75% [80, 81, 82].

To estimate the total number of Northern and Southern pilgrims, we examine individuals who attend Hajj based on their nationalities and the type of vaccine that has been recommended in their home countries. We obtain the total number of pilgrims from Saudi Arabia's official records [83], and the type of recommended vaccine by WHO [84], and then calculate the total number of pilgrims who came from countries where the vaccine is Northern hemisphere vaccine and countries where the vaccine is Southern hemisphere vaccine. The total estimate for the Northern pilgrims (N_1) was 1771576, and for the Southern pilgrims (N_2) was 717830.

The estimation of the prevalence of influenza strain 1 (H1N1) among arrived pilgrims was 0.2% and 0.1% in Hajj season 2009 and 2013, respectively; strain 2 (H3N2) was 0.2% and 0.6% in Hajj season 2009 and 2013, respectively[85, 86].

To estimate infection rates, we used a two-part process: first, relating different infection rates to each other and then applying a back-estimation approach to estimate the baseline values of each strain. We first observe that, for each strain, we have two distinct infection rates: cross-group β_{mnj} and within-group infection rate β_{mmj}, for all $m, n, j = 1, 2$ and $m \neq n$. The nature of the contact while individuals are mixing, is different from the nature of contact while they are not mixing. For instance, several individuals sitting

around a table, talking, or eating generates potentially infectious contacts, but not as many as when individuals are walking around the holy sites in the middle of intensive crowds. To relate the different infection rates for each strain, we must estimate how many hours per day individuals are mixing with individuals in the other group, sitting with their group, not mixing, and sleeping. We may assume that on average, individuals during Hajj spend 8 hours a day mixing with individuals in both groups, 8 hours a day sitting with their group, not mixing, and 8 hours a day sleeping. The kind of contact while they are mixing with individuals in the other group is so dense that their chance of getting infected is twice as high as when they are not mixing, for the same amount of time. Thereby, within-group infection rate (β_{mmj}) would be expected to be 50% more than the cross-group infection rate (β_{mnj}, $m \neq n$) because an individual would stay with his/her group while mixing with individuals in both groups or sitting with their group, not mixing. Consequently, we assume that cross-group infection rates (β_{mnj}, $m \neq n$) are the baseline rates for each strain, and $\beta_{12j} = \beta_{21j}$, $j = 1, 2$ (for simplification). Thus, the infection rates are reduced from eight different rates to two distinct baseline rates, one for each strain, and the other rates are described as follows: for all $m, j = 1, 2$, we have

$$\beta_{mmj} = 1.5\beta_{12j}.$$

The back-estimation approach is an inverse problem where first, we compute the basic reproductive number ($\mathcal{R}_0$) for a simple SEIR model for each strain. For the simple SEIR model with no demographic change, $\mathcal{R}_j = \beta_{12j}/\gamma_j$. Then, by using the published values of $\mathcal{R}_0$ and γ_j for each strain j, we calculate the baseline values of β_{121} and β_{122}. The median value of $\mathcal{R}_0$ for strain 1 (H1N1) is set to 1.46, and strain 2 (H3N2) is set to 1.8 [87]. Values for γ_j are taken from Table 2.2. The resulting estimates for β_{121} and β_{122}

Table 2.2: Summary of estimated model parameters

Par. (unit)	Value	Reference
N_1 (People)	1771576	[83]
N_2 (People)	717830	[83]
β_{121} (days^{-1})	0.4320	This study
β_{122} (days^{-1})	0.6570	This study
β_{mm1} (days^{-1})	0.6480	This study
β_{mm2} (days^{-1})	0.9855	This study
η_1 (days^{-1})	1/2.62	[88]
η_2 (days^{-1})	1/1.9	[89]
γ_1 (days^{-1})	1/3.38	[88]
γ_2 (days^{-1})	1/2.74	[89]

are 0.4320 and 0.6570 days^{-1}, respectively. From these baseline values, we can estimate the other infection rates. Table 2.2 shows parameter values and the estimated values of infection rates.

2.5 Numerical Simulations

Rites of pilgrimage can be completed between 5-6 days, beginning from the 8th of Dhu'l-Hijjah (12th month of Islamic Calendar), while the Hajj season starts on the first of Dhu'l-Qadah (11th month of Islamic Calendar), where pilgrims begin arriving in Saudi Arabia. In this section, we will consider the three cases: the first case is a simulation of the specific six days, where there are no recruitment nor departure rates. The case two model has pilgrims arriving and departing continuously. In this case, we will consider constant rates for recruitment and departure. The case three model has pilgrims arriving and departing during different periods. In this case, non-constant recruitment and departure rates will be considered.

To address the goal of this study, we separate the model's compartments as susceptible, exposed, infected, and recovered for each strain. In this manner, the compartments that

are susceptible to strain one (H1N1) are $\{S_1, S_2, V_1, V_2, E_{12}, E_{22}, F_{12}, F_{22}, I_{12}, I_{22}, K_{12}, K_{22}, R_{12}, R_{22}, W_{12}, W_{22}\}$, exposed to strain one are $\{E_{11}, E_{21}, E_{13}, E_{23}, F_{11}, F_{21}, L_{12}, L_{22}, G_{11}, G_{21}\}$, infected by strain one are $\{I_{11}, I_{21}, K_{11}, K_{21}, L_{11}, L_{21}, I_{13}, I_{23}, J_{11}, J_{21}\}$ and recovered from strain one are $\{R_{11}, R_{21}, W_{11}, W_{21}, G_{12}, G_{22}, J_{12}, J_{22}, R_{13}, R_{23}\}$. Likewise, the compartments that are susceptible to strain two (H3N2) are $\{S_1, S_2, V_1, V_2, E_{11}, E_{21}, F_{11}, F_{21}, I_{11}, I_{21}, K_{11}, K_{21}, R_{11}, R_{21}, W_{11}, W_{21}\}$, exposed to strain two are $\{E_{12}, E_{22}, E_{13}, E_{23}, F_{12}, F_{22}, L_{11}, L_{21}, G_{12}, G_{22}\}$, infected by strain two are $\{I_{12}, I_{22}, K_{12}, K_{22}, L_{12}, L_{22}, I_{13}, I_{23}, J_{12}, J_{22}\}$ and recovered from strain two are $\{R_{12}, R_{22}, W_{12}, W_{22}, G_{11}, G_{21}, J_{11}, J_{21}, R_{13}, R_{23}\}$.

Since the case one model is only applicable over six-day periods where pilgrims are not coming nor leaving, it could be considered a particular case of the model of the case three. We will not discuss the numerical simulation of case one here, but rather as part of the case three simulation.

Numerical simulation will be provided for the case two and three models with section 4 parameter values, the post-2009 era for the proportion of individuals who have received the vaccine (ϕ_i), and for the estimation of the prevalence of influenza strains one and two (p_1 and p_2).

2.5.1 Case Two Model: Constant Arrival and Departure Rates

Pilgrims start arriving in Saudi Arabia from the 1st day of the Hajj season (38 days before Hajj's ritual started) til the 8th of Dual-Hijjah, which is the day when all pilgrims gathered at Mena (a holy place near Makkah) to begin their pilgrimage journey. After the pilgrimage's rites finish on the 13th day of Dual-Hijjah, pilgrims begin to leave Makkah. Pilgrims may stay in Makkah until the Hajj season ends. In this matter, we divide the total number of northern pilgrims (N_1) and southern pilgrims (N_2) by the total number of arrival days (38 days), which gives us recruitment rates (Λ_1 and Λ_2). For the departure

rate (μ), since a pilgrim who comes on the first day of the Hajj season has to stay until the Hajj rites finish (on the 44th day of the Hajj season), we may assume that 44 days is the average time that pilgrims remain in Saudi Arabia.

We provide numerical simulations of case two model equations with constant recruitment and departure rates. Figures 2.4(a) and 2.4(b) indicate how variations in vaccine protections against strain 1 (q_{11} and q_{21}) and strain 2 (q_{22} and q_{12}) affect strain 1 and strain 2, respectively, outbreaks during the Hajj. The horizontal axis is the mismatch rate for the strain that the vaccine targets (q_{ii}), and $(1-q_{ii})$ represents the efficacy of the strain i. The vertical axis is the mismatch rate for the other strain, and $(1-q_{ij})$ represents the efficacy of the other strain. Figures 2.4(a) and 2.4(b) are created by incrementing the target strain mismatch rate q_{ii} along the horizontal axis, and then for each value of q_{ii} decreasing the non-target mismatch rate q_{ij} along the vertical axis until the threshold behavior is observed for both strains. The first threshold, between regions I and II, is whether the outbreak occurs for both strains. This corresponds to the CRN equaling 1; below this threshold, although some new infections occur, increases come primarily from imported cases, and the numbers of cases for both strains are concave down over time (see Fig. 2.4(c)), unlike in the other regions. The second threshold is between regions II and III, where the peak of the outbreak occurs on day 66 for both strains. The third threshold is between regions III and IV for strain two only, where the peak of the outbreak occurs on day 44. The fourth threshold is between regions IV and V for strain two only, where the peak of the outbreak occurs on day 38. We assume that the efficacy of the target strain is better than the efficacy of the other strain (i.e., $q_{ij} > q_{ii}$ for all i,j=1,2). With this in mind, our attention will be restricted above the diagonal line of Figs. 2.4(a) and 2.4(b). Figures 2.4(c) – 2.4(f) give a time series of data of infections over time for a given strain.

Figures 2.4(a) and 2.4(b) consist of the final results of strain 1 (H1N1) and strain 2

(H3N2), respectively, spread simulations with different amounts of mismatching reduced rates (q_{ij}). They show that there are three regions for strain 1 (H1N1) and five regions for strain 2 (H3N2) for the peak of the absolute number of cases. Under the conditions in region I, there is no outbreak, and both strains will go extinct for any value of mismatching reduced rates (q_{ij}) in this region (see Fig. 2.4(c)). The relatively low infection level in Fig. 2.4(c) is caused by constant importation of infectives from the two hemispheres. This behavior does not represent an outbreak because the growth is not due to transmission, but to direct importation of infection. For parameter values in region II, there is a small outbreak which peaks at the end of the season between day 66 and day 90 of the Hajj season (see Fig. 2.4(d)). For parameter values in region III, there is an outbreak that peaks after Hajj rites and before everyone goes back to their home country between day 44 and day 66 (see Fig. 2.4(e)). For parameter values in region IV, there is an outbreak that peaks during Hajj rites, which is between day 38 and day 44 of the Hajj season, where all pilgrims are arrived and practicing their rituals. For parameter values in region V, there is an outbreak that peaks before Hajj rites started and before all pilgrims have arrived, which is between day 35 and day 38 of the Hajj season (see Fig. 2.4(f)). Hence, unless the vaccine efficacy is enormously high, there will be an outbreak of both influenza strains. Approximately, the peak of an outbreak will occur before pilgrims return to their home country if the vaccine efficacy is between 0% to 40% strain 2 (H3N2), and 0% to 10% for strain 1 (H1N1). Otherwise, if the vaccine efficacy is between 40% to 80%, the peak of an outbreak will occur after pilgrims have gone home.

2.5.2 Case Three Model: Non-Constant Arrival and Departure Rates

Figures 2.5(a) and 2.5(b) were generated similar to (Figs. 2.4(a) and 2.4(b)), and indicate the different result regions for each strain for varying values of q_{ii} and q_{ij} $\forall i, j = 1, 2$ and

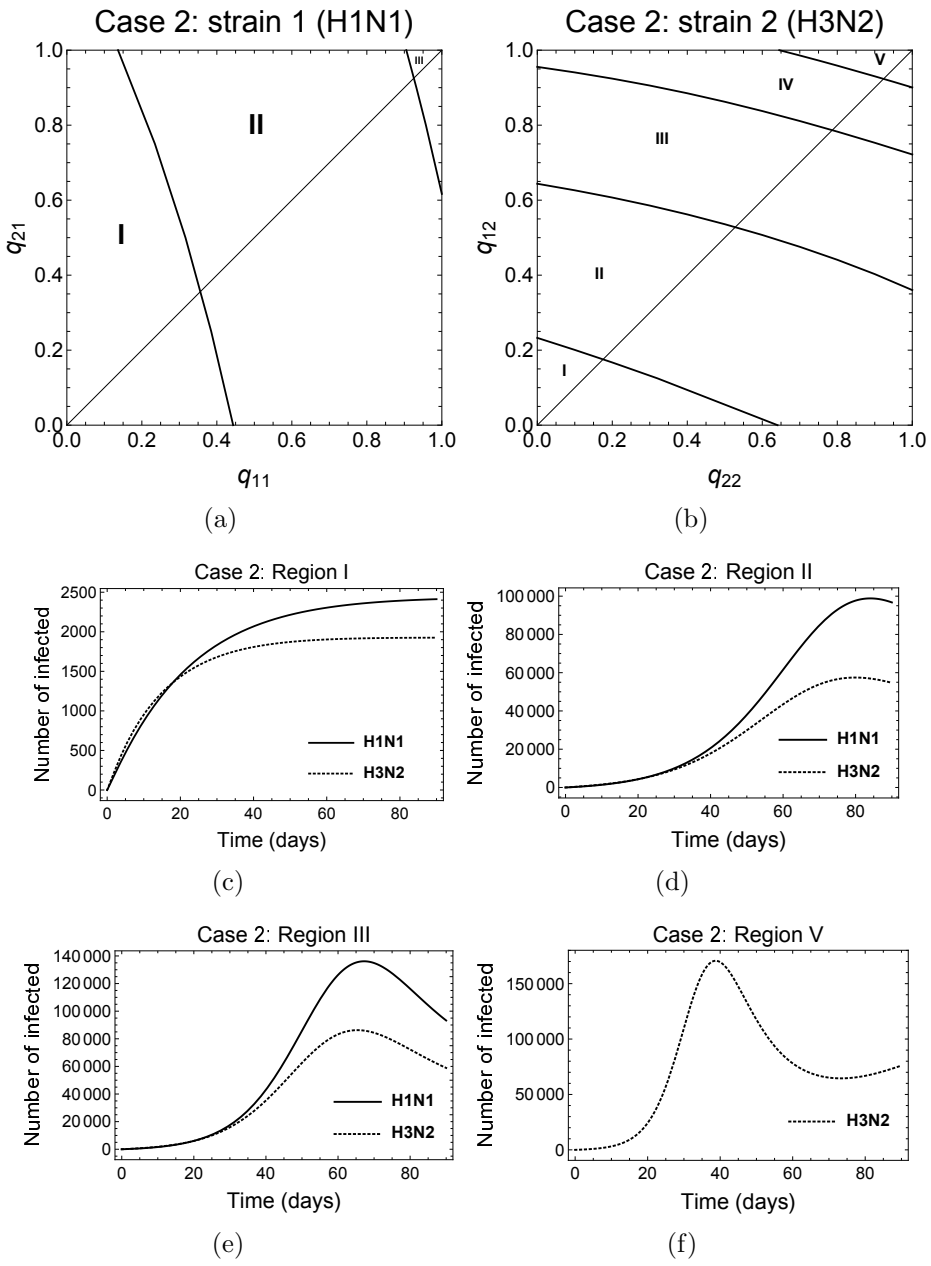

Figure 2.4: Case two: (a) Variations in mismatch rates (q_{11} and q_{21}) against strain 1 (H1N1); (b) Variations in mismatch rates (q_{22} and q_{12}) against strain 2 (H3N2); (c) For q_{ij} $\forall i, j = 1, 2$ in region I, no outbreak will occur for both strains; (d) For q_{ij} $\forall i, j = 1, 2$ in region II, a small outbreak will occur for both strains at the end of the Hajj season; (e) For q_{ij} $\forall i, j = 1, 2$ in region III, an outbreak will occur for both strains before everyone has gone home ; (f) For q_{22} and q_{12} in region V, an outbreak will occur for H3N2 before Hajj ritual started, before day 38 of the Hajj season.

$i \neq j$. Figures 2.5(c)–2.5(j) show the strain 1 (H1N1) and strain 2 (H3N2) simulation with different q_{ij}, $i, j = 1, 2$. The upper and lower figures of 2.5(c)–2.5(f) and 2.5(g)–2.5(j) indicate the prevalence and the absolute number of cases, respectively, for H1N1 and H3N2.

For parameter values in region I, there is no outbreak for both strains and they will become extinct, since this region represents the values of q_{ij}, $i, j = 1, 2$ such that CRN (for phase two) is less than one (see Fig. 2.5(c)). For parameter values in region II, the peak of the absolute number of cases occurs on the last day of the Hajj worship phase, day 43, (see Fig. 2.5(h)), and the peak of prevalence occurs on last days of Hajj season, between days 60 and the end of the season, (see Fig. 2.5(d)). For the parameter values in region III, there is an outbreak whose peaks of the absolute number of cases and prevalence occur after the Hajj worship phase, between day 43 and end of the season (see Figs. 2.5(e) and 2.5(i)). For the parameter values in region IV for H3N2, there is an outbreak whose peaks of the absolute number of cases and prevalence occur at the same time during Hajj ritual time, between days 38 and 43 (see Figs. 2.5(f) and 2.5(j)). For the parameter values in region V for H3N2, there is an outbreak whose peak of the absolute number of cases and prevalence occur during the arrival phase, between days 33 and 37.

For all parameter values (q_{ij}) in all regions, except region I, there will be an outbreak of both strains of influenza. If vaccine efficacy $(1 - q_{ij})$ for q_{ij} is in region II, then the peak of an outbreak of the absolute number of cases occurs in the Hajj worship phase (see Fig. 2.5(h)), and the peak of prevalence occurs in the departure phase (see Fig. 2.5(d)). The peak of an outbreak will occur in the departure phase for both strains on the condition that the vaccine efficacy $(1 - q_{ij})$ for parameter values q_{ij} lies in region III (see Figs. 2.5(e) and 2.5(i)). In the sequel, the peak of an outbreak will occur in the worship phase and the arriving phase for H3N2 if the vaccine efficacy $(1 - q_{ij})$ for parameter values (q_{22} and q_{12}) lies in regions IV and V, respectively (see Figs. 2.5(f) and 2.5(j)).

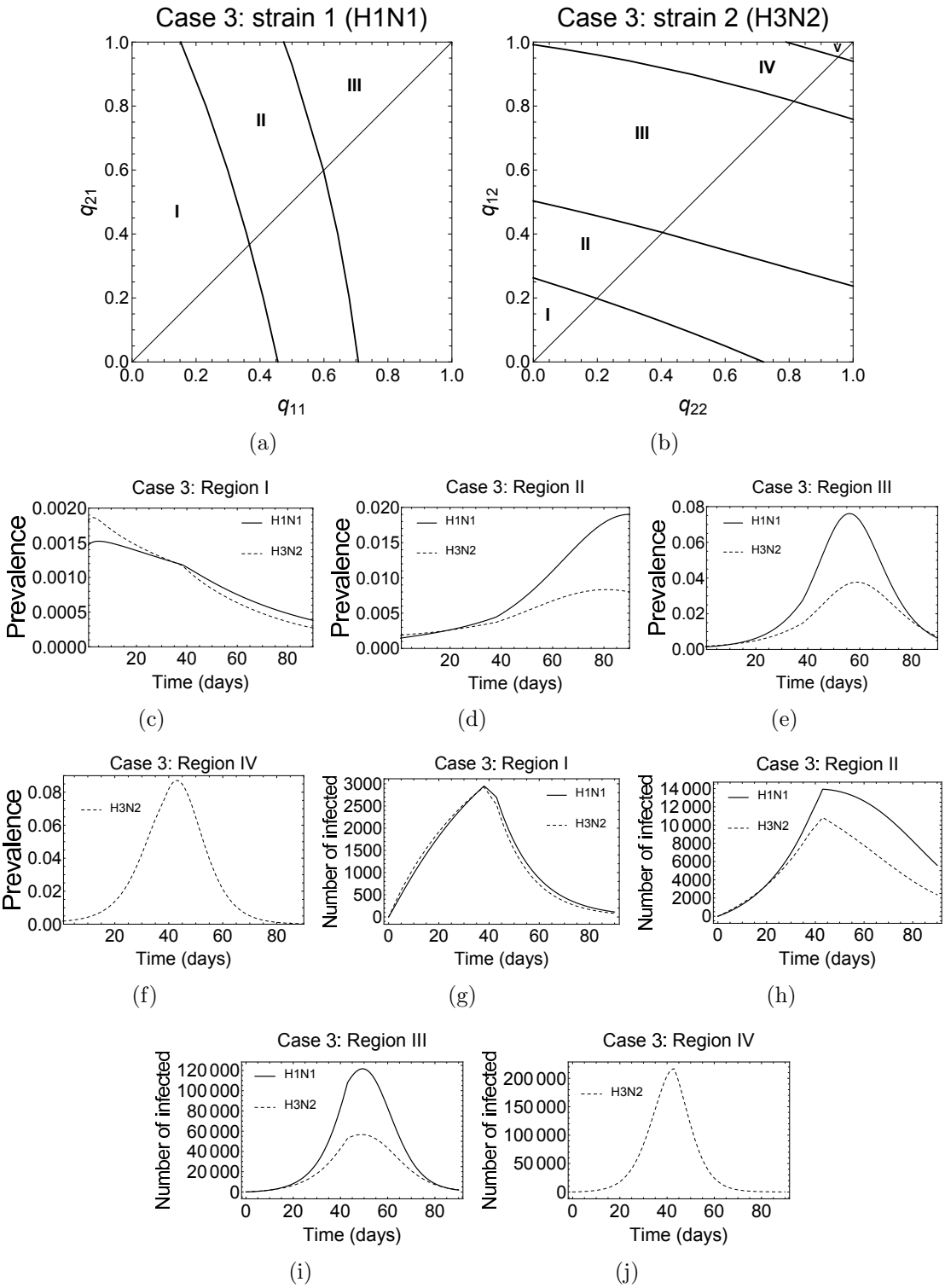

Figure 2.5: Case three: (a) and (b) Variations in mismatch rates (q_{11} and q_{21}) and (q_{22} and q_{12}) against H1N1 and H3N2, respectively; (c)–(f) prevalence, 2.5(g)–2.5(j) the absolute number of cases of H1N1 and H3N2, respectively, for varying values of q_{ii} and q_{ij} $\forall i, j = 1, 2$ and $i \neq j$

2.6 Discussion and Conclusions

Mathematical models are useful in forecasting disease dynamics and estimating significant parameters that can be incorporated to resist the spread of disease. This study analyzed deterministic models for two populations and two strains of influenza to evaluate the impact of mismatch between influenza vaccine strains and circulating strains.

Based on this work, an outbreak occurs for both strains unless the vaccine's effectiveness is tremendously high for both populations (see Figs. 2.4(c) and 2.5(c)). Whether we have an outbreak at the end of Hajj season (see Fig. 2.4(d)), during the Hajj ritual (see Fig. 2.5(h)), or even before that (see Figs. 2.4(f) and 2.5(j)), depends on the vaccine's efficacy. When the case three model is considered, our results show that the peak of the absolute number of cases occurs at the end of the Hajj ritual (the Hajj worship phase) for region II for both strains with low prevalence at the end of the Hajj season. Further, if the mismatch rates for both strains fall in region III, then the peak of absolute numbers of cases and prevalence occurs in the departure phase (see Fig. 2.5(e)). Nonetheless, for extremely low vaccine efficacy (between 0% to 20% for strain H3N2), we have a severe outbreak that occurs during or a couple of days before the Hajj ritual (see Fig. 2.5(j)).

We study the CRN for the case one model, which is equivalent to phase two (the Hajj worship phase) of the case three model. We show that any outbreak will be in the process of dying out during phase two as long as the amount of mismatch reduced rates (q_{ij}) is within region I (see Fig. 2.5(c)), which indicates that CRN is less than one. When CRN is greater than one, we introduce region II, where averaged CRN is between 1 and 1.32 for strain 1 (H1N1) and between 1 and 1.36 for strain 2 (H3N2). In this region, any outbreak will peak during the Hajj worship phase (see Fig. 2.5(h)), with low prevalence peak at the last days of the Hajj season (see Fig. 2.5(d)). Additionally, in region III, the averaged CRN is between 1.32 and 1.90 for H1N1 and between 1.36 and 2.11 for H3N2. In this region, an outbreak will occur in the departure phase, with a peak of prevalence at the

same phase (see Fig. 2.5(i)). Ultimately, regions IV (see Figs. 2.5(f) and 2.5(j)) and V for H3N2 only exhibit CRN values between 2.11 and 2.50, respectively. In these regions, a severe outbreak will occur in phase two (during Hajj ritual) for region IV and during the last days of the arrival phase for region V.

In conclusion, the existence and time of an outbreak of influenza in Hajj depend on mismatch reduced rates (q_{ij}). In this situation, we may have different possible outcomes. The best scenario has vaccine strains for both groups well match circulating strains, where averaged vaccine effectiveness (VE) will be 71% (57% to 86%). In this scenario, mismatch reduced rates will range from 0.14 to 0.43, with an average of 0.29, which places us in region I for H1N1 and region II for H3N2. Hence, there will be no outbreak for H1N1, and a small outbreak for H3N2 whose peak of the absolute number of cases occurs on the last day of the Hajj worship phase, causing approximately 6500 new infections. Another scenario has vaccine strains match their target strains and mismatch the other strains. In this instance, average q_{ii} and q_{ij} will be 0.29 and 0.43, respectively ($\forall i, j = 1, 2, i \neq j$), which places us at the same regions and peak occurrence for H1N1 and H3N2 with approximately 10,000 additional infections for H3N2 than the first scenario. Furthermore, we consider a scenario in which both strains included in the influenza vaccine for both groups mismatch circulating strains, where averaged VE will be 57% (43% to 71%). Under these circumstances, mismatch reduced rates will range from 0.29 to 0.57, with an average of 0.43, which places us in region II for H1N1 and region III for H3N2. Consequently, there will be an outbreak for both strains that peaks on the last day of the Hajj worship phase with 2,000 new cases for H1N1, and at the departure phase with approximately 6,000 more infections for H3N2 than the second scenario. These numbers represent cases in Saudi Arabia during Hajj before pilgrims leave. Additional numbers of cases will arise in the pilgrims' home countries.

However, if the next influenza pandemic arrives, then the VE would be at its worst

case, and the seasonal vaccine will have no protection against novel pandemic strains [16]. Hence, vaccination rates (ϕ_1 and ϕ_2) are irrelevant. In that connection, we may witness a severe outbreak for H3N2 that peaks before everyone has arrived in Makkah (regions IV and V) with approximately 235,500 additional infections, and for H1N1 that peaks after the Hajj worship phase and before everyone returns home (regions III) with approximately 116,000 additional infections (including over 9,000 co-infections).

As long as the influenza vaccines match their target strains, there will be no outbreak of strain H1N1, and only a small outbreak of strain H3N2. In the case of mismatching for non-target strains, it causes about 10,000 new H3N2 cases. In the case of mismatching for both strains, it causes about 2,000 new H1N1 cases and 6,000 additional H3N2 cases. Complete mismatch in a pandemic scenario may infect over 342,000 additional pilgrims (13.75%) and cause more cases in their home countries. These numbers could help the Saudi Ministry of Health (Saudi MOH) to estimate what additional primary health facilities are needed. Besides the size of an expected outbreak, Saudi MOH could make the influenza vaccine mandatory for all pilgrims in order to obtain a Hajj VISA. Further, Saudi MOH could require all arriving pilgrims to pass a health screening before entering the country in order to minimize the number of infected pilgrims.

Our findings can help decision-makers to assess the risk of mismatching between the influenza vaccine and circulating strains and choose containment strategies to mitigate an outbreak. However, the results are limited by the assumption that pilgrims from the Northern/Southern hemisphere have the same exposure. The heterogeneity of individuals arriving for Hajj is more than merely whether they come from the Northern/Southern hemisphere. Further, the amount of data available to estimate parameter values was limited, and our parameter estimates could be better if we have more data to estimate. In the future, a model can be developed to include more heterogeneity in the arriving populations, such as tropical vs. temperate zones. Our model can also be extended to

include several strains to apply to a broader range of influenza viruses. Furthermore, a clinical work can be done to examine how genetically closely related two influenza strains must be in order for the vaccine for one strain to make an individual more susceptible to the other strain.

Chapter 3

How the nature of behavior change affects the impact of asymptomatic coronavirus transmission

3.1 Introduction

Beta coronavirus (β-CoV) has caused three severe epidemic outbreaks over the last 20 years (SARS-CoV, MERS-CoV, and COVID-19). β-CoV is one of four genera of coronavirus (CoV), (alpha-, beta-, gamma-, delta-CoV), and divided into four lineages: lineage A (e.g., OC43 and HKU1), lineage B (e.g., SARS-CoV and SARS-CoV-2), lineage C (e.g., MERS-CoV), and lineage D (e.g., HKU9) [11, 12, 13]. Coronavirus disease 2019 (COVID-19) is caused by a coronavirus called severe acute respiratory syndrome coronavirus 2 (SARS-CoV-2). It is spread through close contact from one individual to another (within about 6 feet), airborne respiratory droplets (coughs, sneezes, or talks), and aerosol transmission [10].

A serial interval is defined to be the duration from illness onset in a primary case (infector/infective) to illness onset in a secondary case (infectee). An incubation period is defined to be the period between infection and the emergence of symptoms [90, 91]. Recent studies showed that the median serial interval for COVID-19 was estimated at 4.0 days (95% credible interval [CrI]: 3.1, 4.9), and the median incubation period 5.2 days (95% confidence interval [CI], 4.1 to 7.0) [92, 93]. Pre-symptomatic transmissions occur

and may occur more often than symptomatic transmissions due to the serial interval being shorter than the incubation period [92].

Asymptomatic cases are defined as patients who have shown no symptoms for the whole course of the infection. There is mixed evidence on the proportion of asymptomatic cases. Recent studies from Italy and China estimated the proportion of asymptomatic infections at up to 75% and 80%, respectively [94, 95, 96]. Other studies have shown a smaller proportion of asymptomatic infections: 41.6% among Japanese nationals evacuated from Wuhan [97], 18% among passengers on the Diamond Princess cruise ship [98], and 10% among children [99]. Several studies have shown that asymptomatic and symptomatic infections have the same relative infectivity [98, 100, 101, 102].

Asymptomatic infections are likely to play a significant role in the transmission of COVID-19 for different reasons. First, to predict disease burden when the virus spreads within a population, the proportion of asymptomatic infections is crucial [98]. Second, comprehending how asymptomatic infections contribute to transmission is fundamental to the success of control strategies [103]. In the initial spread of COVID-19, asymptomatic cases can affect the estimated basic reproduction number [104].

Individuals change their behavior during an epidemic, and their behavior has been intricately linked with the spread of infectious diseases historically [105]. Infected individuals may reduce their contact with others due to the physical weakening effects of their illness or government officials' orders to stay home to prevent new cases. Susceptible individuals may take precautionary measures to reduce the number of contact with others to avoid the risk of being infected. Mitigation strategies based on behavior changes are possibly among the only options available in the early stages of an emerging epidemic. Evidence on behavior changes had strong effects during past pandemics [106, 107, 108, 109].

The COVID-19 global pandemic has prompted researchers to analyze and predict its evolution. Mathematical models are a useful tool that can help to predict the epidemic's

dynamic and control infectious diseases. Ndairou et al. have used a mathematical model, with special focus on super-spreader individuals' transmissibility, to try to replicate the observed data in Wuhan, China [110]. An early study by Wu et al. presented an SEIR meta-population model to simulate the COVID-19 infection across China. They included non-infectious pre-symptomatic cases, but no transmission without symptoms [111]. Another study used the SEIR mathematical model with a quarantine class and governmental intervention measures to mitigate disease transmission. They suggest that governmental intervention strategies can play an essential role in reducing COVID-19 transmission [112].

A recent study by Dobrovolny determined the role of asymptomatic cases in the spread of COVID-19 by using an SAIR mathematical model. Dobrovolny used a different infection rate for asymptomatic individuals determined by a proportionality constant, and a fraction of individuals remain asymptomatic for the whole course of the infection. She concluded that the relative infectiousness of individuals with no symptoms has more impact than asymptomatic proportion on the time course and size of the epidemic [113].

Several recent studies have used mathematical models to illustrate the significant effect of behavior change on the epidemic process. A recent systematic review showed that individual-level models are increasingly used and useful to model behavior changes [114]. Del Valle et al. used simple and agent-based models to assess the impact of behavioral changes in response to an emerging epidemic. They concluded that changes in behavior can be effective in reducing the spread of disease, and a second wave of infection can occur when interventions are stopped too soon [115]. Poletti et al. used a classic SIR model to investigate spontaneous behavioral change, following cost/benefit considerations, on the spread of an epidemic. They proved that their model accounts for multiple waves and can show asymmetric waves when the behavioral changes and disease dynamics occur on vastly different time scales. They also found that behavioral dynamics results in the

reduction of the final attack rate [116]. Buonomo constructed an information index (an additional state variable) that incorporates not only current prevalence but some degree of exponentially decaying memory of recent prevalence, finding that when the information coverage is high enough, the overall incidence is reduced [117].

In this theoretical study, we consider how varying the proportion of asymptomatic (but equally infectious) cases in an epidemic may affect its size when individuals change their risk behavior, using the current COVID-19 outbreak as a case study. Previous published COVID-19 studies have described at most a single wave of preventive measures to the best of our knowledge. Asymptomatic cases play an essential role in the transmission, but they also do not contribute to the perceived disease prevalence, which drives behavior change during an epidemic. Behavior change can be continuous in response to daily news, or discrete as governments announce policies that last for a month or longer. We seek to identify the theoretical impact of the proportion of asymptomatic COVID-19 infections on the magnitude of an epidemic under three different behavior change scenarios. To this end, we develop a compartmental model using a nonlinear dynamical system.

3.2 Model Development

We use a modified SEIR model, but with three possible courses of infection: [permanently] asymptomatic, mild symptomatic, and severe symptomatic cases. All of these are assumed equally infectious, but only severe cases go to a hospital. We distinguish between asymptomatic (infectives who never develop any symptoms) and pre-symptomatic individuals (who will eventually develop symptoms). We consider the case where asymptomatic and symptomatic infections have the same relative infectivity. The constant population size, N, is classified into eight epidemiological classes: susceptible class (S), exposed class (E), infectious but pre-symptomatic class (A_P), infectious but asymptomatic class (A_L),

infected with mild symptoms class (I_M), infected with severe symptoms class (I_S), hospitalized class (H), and recovery class (R, assumed permanent). The model is described as follows (illustrated in Fig. 3.1):

$$\begin{cases} \frac{dS}{dt} = \Lambda - \frac{\beta S}{N}\left[\theta(A_L + A_P) + \tau(I_M + I_S)\right] - \mu S, \\ \frac{dE}{dt} = \frac{\beta S}{N}\left[\theta(A_L + A_P) + \tau(I_M + I_S)\right] - (\eta + \mu)E, \\ \frac{dA_L}{dt} = p\eta E - (\gamma_A + \mu)A_L, \\ \frac{dA_P}{dt} = (1-p)\eta E - (\delta + \mu)A_P, \\ \frac{dI_M}{dt} = q\delta A_P - (\gamma_M + \mu)I_M, \\ \frac{dI_S}{dt} = (1-q)\delta A_P - (\epsilon + \mu)I_S, \\ \frac{dH}{dt} = \epsilon I_S - (\gamma_H + \mu)H, \\ \frac{dR}{dt} = \gamma_A A_L + \gamma_M I_M + \gamma_H H - \mu R, \end{cases} \tag{3.1}$$

where β is the human-to-human infection rate; θ and τ are average reduction factors for asymptomatic and symptomatic infection. Here η is the rate at which an individual departs the exposed class by becoming infectious (pre-symptomatic, symptomatic, or asymptomatic); p is the proportion of infected individuals who remain asymptomatic for the whole course of the infection. δ^{-1} is the mean time from onset of infectivity to onset of symptoms, for those infectives who eventually develop symptoms; q is the proportion of pre-symptomatic infected who eventually develop mild symptoms. ϵ is the average rate at which infected with severe symptoms become isolated or hospitalized. γ_A, γ_M, and γ_H are the recovery rates of asymptomatic, infected with mild symptoms, and hospitalized individuals, respectively. To consider how the timespan of a potentially extended outbreak affects the epidemic, we include some demographic effects in the model (not represented in Fig. 3.1). There is a proportional natural mortality rate μ in each of the eight classes, and Λ represents the constant inflow of susceptible individuals.

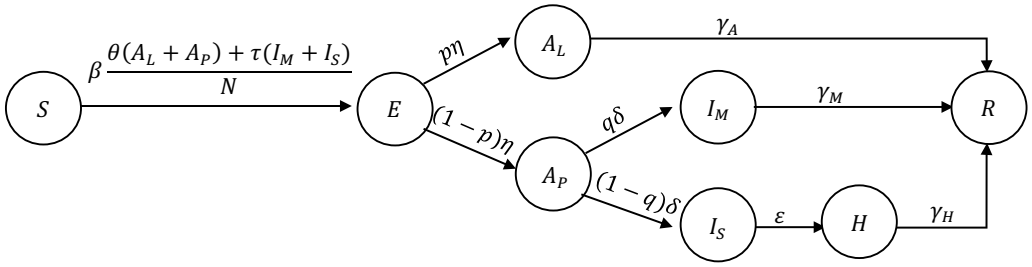

Figure 3.1: Flowchart of model (3.1)

	Notation	Definition
State variables	$S(t)$	Number of susceptible individuals at time t
	$E(t)$	Number of exposed individuals at time t
	$A_L(t)$	Number of asymptomatic infected individuals who remain asymptomatic for the whole course of infection at time t
	$A_P(t)$	Number of pre-symptomatic infected individuals at time t
	$I_M(t)$	Number of symptomatic infected individuals with mild symptoms at time t
	$I_S(t)$	Number of symptomatic infected individuals with severe symptoms at time t
	$H(t)$	Number of hospitalized infected individuals at time t
	$R(t)$	Number of recovered individuals at time t
Parameters	Λ	Recruitment rate (individual/time)
	μ	Per capita natural mortality rate (1/time)
	β	COVID-19 infection rate (1/time)
	θ	Reduction factor for asymptomatic infection (dimensionless)
	τ	Reduction factor for symptomatic infection (dimensionless)
	p	The proportion of individuals who remain asymptomatic for the whole course of infection (dimensionless)
	q	The proportion of infected with mild symptoms (dimensionless)
	η	1/The duration time from exposure to onset of infectivity (1/time)
	δ	1/The infectiousness period while individuals are pre-symptomatic (1/time)
	ϵ	1/Average hospitalized period for infected with severe symptoms (1/time)
	γ_A	Recovery rate of asymptomatic infected individuals (1/time)
	γ_M	Recovery rate of individuals infected with mild symptoms (1/time)
	γ_H	Recovery rate of hospitalized infected individuals (1/time)

Table 3.1: State variable and parameter definitions and their units.

Since there are not any measurements for how asymptomatic and symptomatic cases react while they are infected, we assume that non-symptomatic individuals change their

behavior less than symptomatic individuals do: non-symptomatic individuals reduce their potentially infectious contact rate by a factor of θ, while symptomatic individuals reduce it by a factor of τ, with $0 \leq \tau \leq \theta \leq 1$. We consider the two factors connected, $\theta(\tau)$. These factors may remain constant, or may vary over the course of an epidemic, due either to individual reactions to news or to government policies, according to the different scenarios to be considered. Also, we assume perfect isolation in the hospital compartment.

The relationship between behavior change in asymptomatic, θ, and behavior change in symptomatic individuals, τ, is assumed to be as follows: when symptomatic individuals reduce their contact by 50% ($\tau = 0.5$), asymptomatic individuals only reduce their contact by 1% ($\theta = 0.99$). Furthermore, only when symptomatic individuals reduce their contact by more than 50%, asymptomatic individuals reduce their contact significantly. Hence, an exponentially decaying function is chosen to describe the relationship between θ and τ and match points (0,0), (0.5,0.99) and (1,1), given as follows: (shown in Fig. 3.2):

$$\theta = \left(1 - (1-\tau)^{6.6439}\right).$$

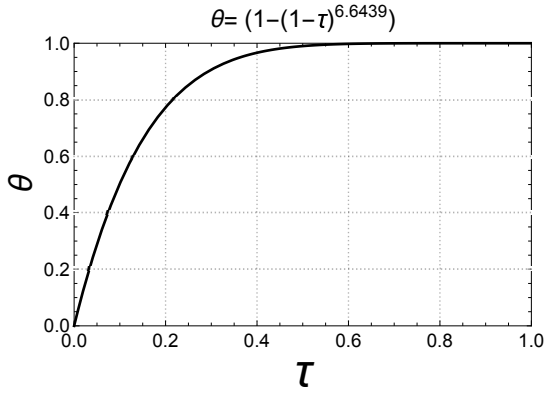

Figure 3.2: relationship between θ and τ

We consider three different behavior change scenarios in this study. Case one is con-

stant reduction rates, where an environment that is not influenced by the gravity or the magnitude of the epidemic is assumed. It is based on background information that the community has, so it is a constant reduction. Case two assumes reduction rates as a function of the instantaneous prevalence. In this case, we have a completely individual-based or media-based reduction rate, which models the impact of just individuals seeing the news every day and making their decisions. Case three uses piecewise constant reduction rates. This case reflects changes by government mandate, which typically do not bounce back and forth instantaneously from one day to another. They tend to be rolled out in phases.

In this type of model, individuals within the same compartments are considered homogeneous. That is, individuals do not differ based on characteristics such as infectiousness period, behavior changes, age, and or other characteristics. In this model, we consider population-level trends.

3.3 Analysis

The control reproduction number, $\mathcal{R}_c$, is one of the most significant thresholds, which measures the infection's ability to spread. We use $\mathcal{R}_c$ instead of using the basic reproduction number, $\mathcal{R}_0$, because we incorporate control measures (τ and θ) in the model. In this section, we perform an equilibrium analysis in order to derive the $\mathcal{R}_c$ for model (3.1). For case two and three, in which behavior change only starts after the outbreak reaches a certain level, the initial values of θ and τ are taken to be one, which simplifies $\mathcal{R}_c$ to $\mathcal{R}_0$

The point where no diseases is present in the population is called the disease-free equilibrium (DFE), which occurs for model (3.1) when $A_L = A_P = I_M = I_S = 0$. Setting all differential equations in (3.1) equal to zero, we find the DFE of the form $(\frac{\Lambda}{\mu}, 0, 0, 0, 0, 0, 0, 0)$.

To drive the $\mathcal{R}_c$ for model (3.1), we use the next-generation operator method proposed

by Diekmann and Heesterbeck [66]. We begin with separating the model's classes into uninfected (X), noninfectious infected (Y), and infectious (Z) classes;

$$X = \begin{pmatrix} S \\ R \end{pmatrix}, Y = \begin{pmatrix} E \\ H \end{pmatrix}, Z = \begin{pmatrix} A_L \\ A_P \\ I_M \\ I_S \end{pmatrix}.$$

After substituting the equilibrium values of the noninfectious infected classes (Y) into the differential equations for the infectious (Z) classes, we compute the Jacobian matrix

$$A = \frac{\partial}{\partial Z}\left(\frac{\partial Z}{\partial t}\right).$$

Computing A at the DFE for model (3.1), we obtain A= M - D, with

$$M = \begin{pmatrix} \frac{\beta\eta\theta p}{\eta+\mu} & \frac{\beta\eta\theta p}{\eta+\mu} & \frac{\beta\eta p\tau}{\eta+\mu} & \frac{\beta\eta p\tau}{\eta+\mu} \\ \frac{\beta\eta\theta(1-p)}{\eta+\mu} & \frac{\beta\eta\theta(1-p)}{\eta+\mu} & \frac{\beta\eta(1-p)\tau}{\eta+\mu} & \frac{\beta\eta(1-p)\tau}{\eta+\mu} \\ 0 & \delta q & 0 & 0 \\ 0 & \delta(1-q) & 0 & 0 \end{pmatrix},$$

and

$$D = \begin{pmatrix} \gamma_A + \mu & 0 & 0 & 0 \\ 0 & \delta + \mu & 0 & 0 \\ 0 & 0 & \gamma_S + \mu & 0 \\ 0 & 0 & 0 & \epsilon + \mu \end{pmatrix}.$$

The control reproduction number $\mathcal{R}_c$ is obtained as the spectral radius of $M \cdot D^{-1}$, precisely,

$$\mathcal{R}_c = \frac{1}{2}\left(a + \sqrt{a^2 + 4b}\right), \tag{3.2}$$

where

$$a = \frac{\beta\eta\theta p}{(\eta+\mu)(\gamma_a+\mu)} + \frac{\beta\eta\theta(1-p)}{(\delta+\mu)(\eta+\mu)},$$
$$b = \frac{\beta\delta\eta(1-p)q\tau}{(\delta+\mu)(\eta+\mu)(\mu+\gamma_s)} + \frac{\beta\delta\eta(1-p)(1-q)\tau}{(\delta+\mu)(\eta+\mu)(\mu+\epsilon)}.$$

The first term of a refers to the contribution of asymptomatic individuals, who remain asymptomatic for the whole course of the infection, while the second term of a refers to pre-symptomatic infection. Furthermore, the first and second terms of b refer to the contribution to infection by individuals with mild and severe symptoms. Numerical simulation will be performed on $\mathcal{R}_c$ in the next section using estimated parameter values.

3.4 Numerical simulation

We find parameter values either from previous literature or by estimation. We consider three different behavior change cases, τ, in this section—the first case when τ is constant over time, the second case when τ is continuously changing over time, and the third case when τ is piecewise constant changing over time.

3.4.1 Parameter Estimates

Some parameter values were obtained directly from previously published studies, as listed in Table 3.2, while the others were estimated in this study.

Table 3.2: Summary of estimated model parameters

Par. (unit)	Value	Range
Λ (individual/day)	0	-
μ (days^{-1})	0	-
β (days^{-1})	0.399322	0.299216 – 0.530679
η (days^{-1})	0.668558	0.641876 – 0.822624
δ (days^{-1})	0.269961	0.183754 – 0.346695
q (dimensionless)	0.8 [118, 119]	-
ϵ (days^{-1})	1/10 [120]	-
γ_A (days^{-1})	1/7	1/9 – 1/6
γ_M (days^{-1})	1/21	-
γ_H (days^{-1})	1/14	-

The average time to recovery ranged from seven to 32 days for mild cases and 21 to 32 days for severe cases [119, 121, 122, 123, 124]. We pick seven days as the recovery time for asymptomatic cases ($\gamma_A = 1/7$), 21 days for mild cases ($\gamma_M = 1/21$), and 24 days for severe cases. After applying the average isolation days for severe cases ($\epsilon = 1/10$), we get $\gamma_H = 1/14$.

To estimate the remaining parameters in this model (β, η, and δ), we use the average reported basic reproduction number (averaged from published estimates of $\mathcal{R}_0$ is 3.28 [125]), serial interval (estimated at 4.0 days [92]), and incubation period (estimated at 5.2 days [93]) for COVID-19. Then, we use a two-part process: first linking these parameters to each other, then using a back-estimation approach to calculate those parameters. The serial interval is the average waiting time before the first infection happens ($1/\beta$), adding to the average duration time from exposure to infectivity onset ($1/\eta$). The incubation period is $1/\eta$, adding to the infectiousness period, while individuals are pre-symptomatic ($1/\delta$). Therefore, we use the relation $\frac{1}{\eta} + \frac{1}{\beta} = 4$ and $\frac{1}{\eta} + \frac{1}{\delta} = 5.2$ to obtain β and δ as functions of η. This made (3.2) an equation to a function of η alone (with $\tau = \theta = 1$). This allows us to obtain estimates for η, β and δ. All the parameter estimates are summarized in Table 3.2.

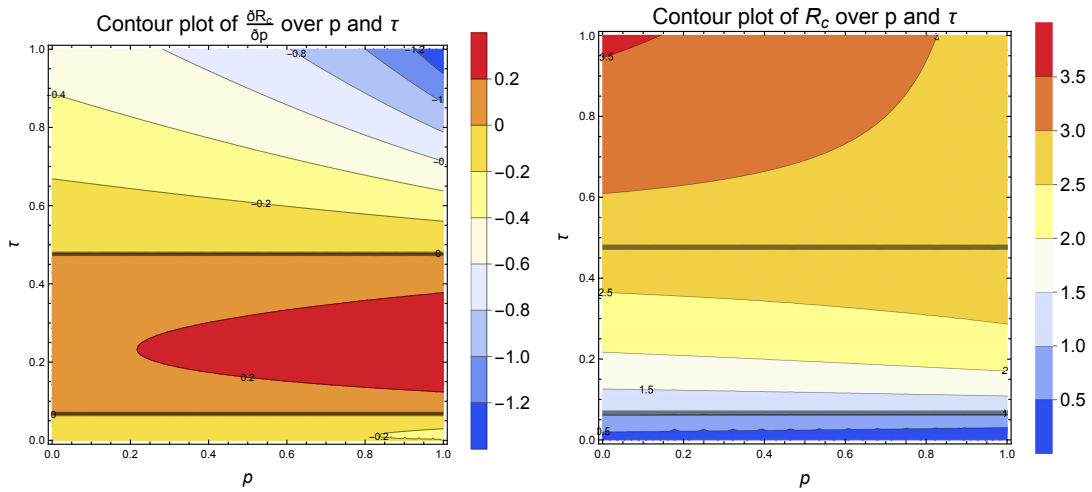

Figure 3.3: Contour plot of CRN over p and τ

3.4.2 Case one: constant reduction in contact rates

When behavior change is constant, independent of the course of the epidemic, $\mathcal{R}_c$ provides one measure of its initial growth. We, therefore, consider how $\mathcal{R}_c$ is affected by the proportion of asymptomatic infections (p), in conjunction with the magnitude of behavior change as represented by τ. By substituting parameter values from table 2 into CRN and considering τ and p to be constants that vary between zero and one, contour plots of $\frac{\partial \mathcal{R}_c}{\partial p}$ and $\mathcal{R}_c$ over p and τ were generated, Figs. 3.3(a) and 3.3(b), respectively.

Figure 3.3(a) shows the contour plot of the partial derivative of $\mathcal{R}_c$ with respect to p as τ and p vary. In this figure, there are three regions. Region one, when τ is between 0.5 and one, shows that as p increases, $\frac{\partial \mathcal{R}_c}{\partial p}$ decreases with negative slopes. Region two, when τ is between 0.05 and 0.5, indicates that $\frac{\partial \mathcal{R}_c}{\partial p}$ goes up as p goes up with positive slopes. Lastly, region three, when τ is between 0 and 0.05, depicts the same behavior as region one.

Figure 3.3(b) shows the contour plot of $\mathcal{R}_c$ over p and τ. By applying the three regions from Fig. 3.3(a), we get the top region where symptomatic individuals do not

reduce their contacts by more than 50%, and almost no behavior change in individuals with no symptoms (i.e., $\tau \in (0.5,1)$, $\theta \in (0.99,1)$). In this region, we notice that $\mathcal{R}_c$ is the highest when $p = 0$. Plus, as p increases, $\mathcal{R}_c$ decreases. In this connection, symptomatic individuals are contributing more to the initial spread of the disease than asymptomatic individuals.

In the next region, region two, as in reality, when people aware of the outbreak, symptomatic individuals will be isolated more since initial recommendations were that people who have symptoms should isolate themselves. In this matter, symptomatic individuals are reducing their contacts more than 50%, while individuals with no symptoms are reducing their contacts, but less than individuals with symptoms ($\tau \in (0.05,0.5)$ and $\theta \in (0.3,1)$). In this region, we discern that as p increases, $\mathcal{R}_c$ increases. Thus, asymptomatic individuals are contributing more to the initial spread of the disease than symptomatic individuals. Further, symptomatic individuals are reducing their contacts by a higher factor than their ability to spread the disease better.

In region three, individuals with symptoms are reducing their contacts by more than 95%, while asymptomatic individuals are reducing their contacts by more than 70% ($\tau \in (0,0.05)$ and $\theta \in (0,0.3)$). In this setting, as p increases, $\mathcal{R}_c$ decreases. Further, symptomatic individuals are contributing more than individuals with no symptoms.

We also perform numerical simulations of the model to see how the entire course of the epidemic varies depending on p and τ, using our best estimates of the parameter values. We computed the number of active cases throughout the outbreak, for different values of p and τ. Figure 3.4 illustrates the range of results over time for all values of p, for $\tau = 0.25$, a representative value from region two in which symptomatic individuals reduce their contact rate by a factor of four.

We have a couple of results that may appear to contradict the control reproduction number (CRN). One is that the height of the peak of prevalence decreases with p (espe-

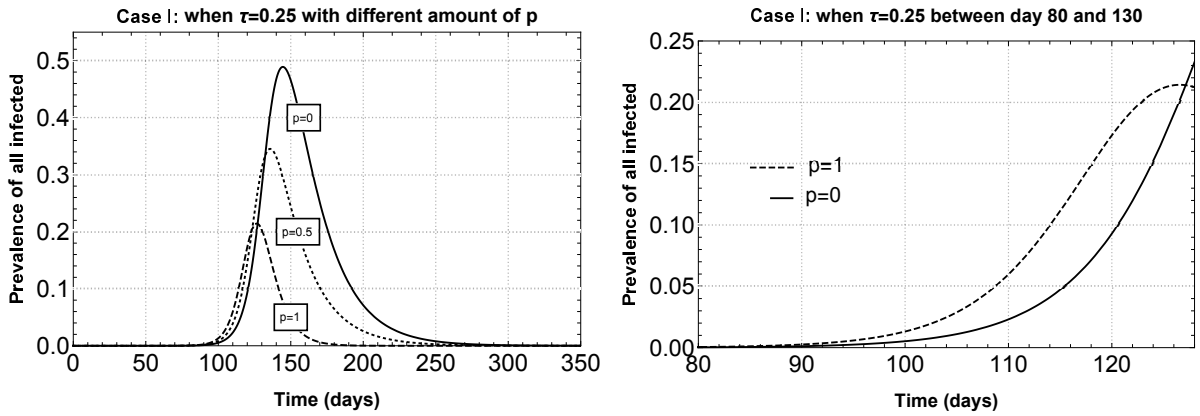

(a) (b)

Figure 3.4: Height of prevalence with different amount of p when $\tau = 0.25$ for case one

cially, if $\tau \in$ region 2 see Fig. 3.4(a)). Further, the fraction of individuals who never get infected increases with p for all values of τ (see Fig. 3.4(b) when $\tau \in$ region 2). These results seem to contradict the contour plot of the CRN and what has been said about the three regions (see Fig. 3.3(b)). However, the CRN describes the rate of spread of disease at the edge of an outbreak. Figure 3.4(a) is representing the peak of an epidemic, which is far away from the boundary of the epidemic. Namely, the CRN is not a good measure of how well the disease spreads when there are many infected individuals. In addition to that, the fraction of asymptomatic individuals is more significant away from the edge of the epidemic. Thus, the CRN tells about the spread of the disease at the beginning of the outbreak. The peak of prevalence and the final fraction of susceptibles depend on events far away from the beginning of the epidemic. So, they do not necessarily follow the same pattern as the CRN.

Therefore, there are multiple possible measures by which we may take an optimum value of p. By saying an optimum value of p, we refer (implicitly) to the evolutionary perspective of the pathogen. Hence, the optimum value of p means the most infection possible, which is chosen to maximize the CRN, maximize the peak of prevalence, and minimize the fraction of susceptibles at the final time. Consequently, the value of p

that maximizes CRN is zero for τ in regions one and three and one for τ in region two. However, to maximize the height of prevalence and minimize the fraction of susceptibles at the final time, p should be zero for all values of τ.

Hence, most pathogen success measures are maximized when p is zero, which implies that there are no asymptomatic infections, except when τ in region two. When τ is in region two, $p = 1$ maximizes only the outbreak's initial spread since asymptomatic infections remain less infectious than symptomatic infections.

3.4.3 Case two: continuous infection reducing rates as a function of the prevalence

In this case, symptomatic reduction rate (τ) is considered as a function of the believed prevalence (symptomatic infected prevalence). τ is assumed to be between 1 and 0.5 if the believed prevalence is between 0 and 5%. τ is below 0.5 if the believed prevalence is above 5% (see Fig. 3.5). A mathematical description for such a function that describes the relationship between τ and the believed prevalence is

$$\tau(t) = e^{k\frac{I(t)}{N(t)}}, \tag{3.3}$$

where k is the fright parameter for an individual that matches the above description, $k = -13.2803$. We choose k to fit the point when $\frac{I}{N} = 0.05$, $\tau = 0.5$.

Figure 3.6(a) indicates the prevalence over time of all infected with varying proportions of asymptomatic infections (p) between zero and one. The height of the peak of the prevalence increases for p between 0 and 0.59, and then it decreases for higher p. For lower p, we notice that the epidemic's shape is asymmetric because most of the cases are observed. Moreover, for high values of p, most of the cases are unobserved and, therefore, there is not much behavior change; consequently, we see the shape of the epidemic is

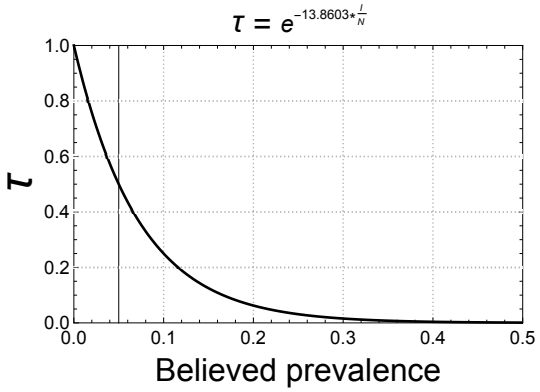

Figure 3.5: τ as a function of the believed prevalence

symmetric. The optimum value, $p = 0.59$, maximizes the highest peak of the epidemic since behavior changes react to less than half of the infections. In contrast, when $p = 0$, behavior changes work at the best capacity. Lastly, when $p = 1$, there are no behavior changes.

Figure 3.6(b) illustrates the fraction of susceptibles, who never get infected, at the final time with varying p between zero and one. The lower curve depicts the case with no behavior change, which is similar to case one. The upper curve shows the case two with behavior changes. In this case, the final fraction of susceptibles increases for p between zero and 0.52, but then it turns around and gets low for higher p until it reaches the lowest point at $p = 0.885$. For p between 0 and 0.52, behavior changes work well with the gradual increases of p to minimize the final fraction of susceptibles. On the other hand, when p is between 0.52 and 0.885, more than half of the infection is unobserved, indicating fewer behavior changes. For $p > 0.885$, most of the infection is asymptomatic, so the final fraction of susceptibles is approaching to match the case with no behavior change. From the pathogen's evolutionary perspective, the lower the uninfected fraction at the final time, the stronger the outbreak was.

Unlike case one, we notice in case two that a higher peak does not necessarily mean the worst outbreak, i.e., the height of the prevalence peaks when $p = 0.59$ whereas the

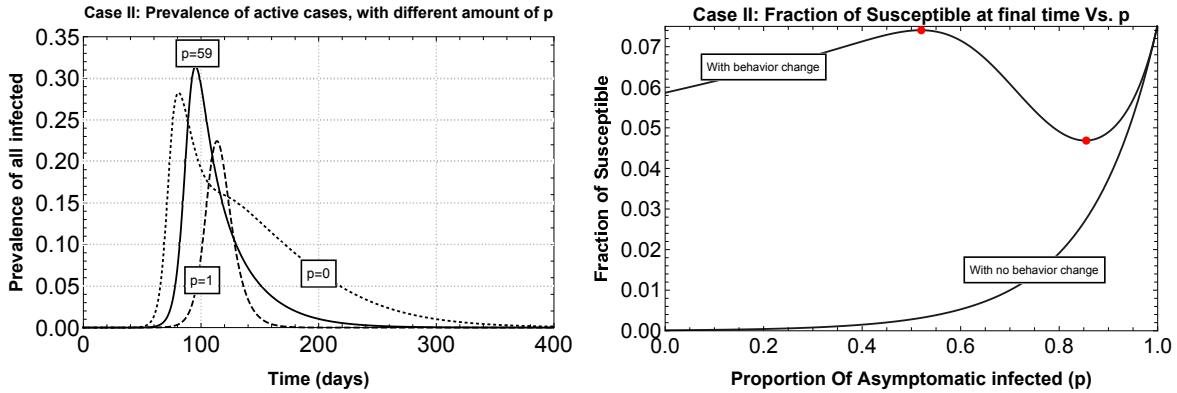

(a) (b)

Figure 3.6: Height of prevalence and fraction of susceptibles at final time with different amount of p when τ varies over time with the perceived prevalence

lowest fraction of susceptibles is when $p = 0.885$. Behavior change reduces the infection more when p is low since the symptomatic prevalence represents most of the infections. The entire course of the epidemic produces the highest peak with the smallest overall outbreak for p between 0.52 and 0.59. For $p = 0.885$, the epidemic displays a relatively lower peak but with the largest overall outbreak. For $p = 1$, the epidemic exhibits both the lowest peak and the smallest overall outbreak.

3.4.4 Case three: piecewise constant reduction in contact rates

In this case, we model the changes by government mandate policies. In the real world, some asymptomatic cases will be diagnosed, but we assume an environment in which testing is not universal. This model includes the hypothesis of limiting testing availability. Here we assume, for simplification, the government does not know about any of the asymptomatic cases, and policies are made based on the believed prevalence (symptomatic infection prevalence only). The first phase of the outbreak occurs only at the beginning of the infection, where the believed prevalence does not exceed 0.1% (the first threshold). In this phase, there is no reduction in symptomatic infection ($\tau = 1$). The second phase occurs

once the believed prevalence exceeds 0.1% (the first threshold). Therefore, a lockdown starts. The government policy is for symptomatic individuals to quarantine completely, but we assume this quarantine (as implemented) is only 95% effective ($\tau = 0.05$). The lockdown remains activated until the believed prevalence rate goes below 0.01% (the second threshold). Thenceforward the lockdown is released gradually, and the believed prevalence rechecked every 30 days. For the first 30 days, $\tau = 0.1$, and for the next 30 days (if the believed prevalence does not exceed the first threshold) $\tau = 0.2$, etc. In this manner, the lockdown will continue to be released gradually until the first threshold is reached; thereafter, another lockdown will be activated.

Numerical simulations of the case three model are performed. We compute the total infection prevalence with different amounts of the proportion of asymptomatic infection (p) and the behavior changes ($\tau(t)$) by government mandate policies.

Figure 3.7(a) indicates the total infection prevalence changes over time due to government policies (the lockdown). Regardless of the proportion of asymptomatic infected (only if $p < 1$), the government policies invoked during a lockdown produce enough behavior change ($\tau(t)$) to pull down the total infections to the second threshold. When $p = 0$, which means all infected individuals are symptomatic, government intervention policies are well designed to the perceived prevalence. For $p > 0.5$, the policies are implemented in response to half or less of the total infections. For higher p, since perceived prevalence takes a longer time to reach the first threshold, government policies take a longer time to be implemented. A higher value of p makes the initial peak higher and later than the lower value of p because the government does not perceive the asymptomatic infections. Also, a higher value of p means the epidemic takes longer to spread. However, the duration between waves is shorter when p is high because the asymptomatic infections do not last as long as symptomatic ones. Furthermore, any effective government policies prolong the outbreak for at least five years (if $p \leq 0.75$), during which time there will continue to

be regular peaks. Through the first five years, the peak of each wave is not diminishing. This isolation behavior will continue for a long enough time scale that demographics will start to be significant. For $0.99 < p < 0.997$, there are at most two phases of government lockdown, while for $p > 0.9977$, hardly any symptomatic infections are noticed, and therefore no government policy is implemented.

Figure 3.7(b) shows the fraction of susceptibles, after the third wave of the infection, with varying p between zero and one. In contrast to cases one and two, the fraction of susceptibles decreases with p since the behavior change reacts less with more asymptomatic infections. For p between zero and 0.75, the fraction of susceptibles decreases slowly to reach 0.9 due to behavior changes, which indicates that only less than 10% of individuals have been infected. Meanwhile, if $0.75 < p < 0.95$, the fraction of susceptibles decreases from 0.9 to 0.6 since the behavior changes only respond to less than 25% of the total infection. For $p > 0.9977$, there is no behavior change, and the final fraction of susceptibles is approaching the case with no behavior change.

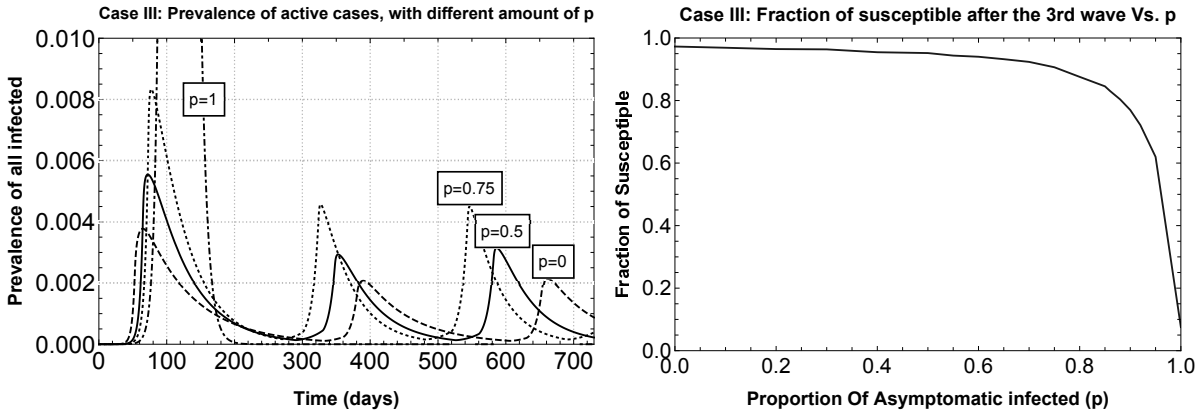

(a) (b)

Figure 3.7: Height of prevalence and fraction of susceptibles at final time with different amount of p when τ piecewise constant varies over time

We further compute the highest point of the first wave's prevalence as a function of the proportion of asymptomatic infections (p). Figure 3.8 shows that the general trend

of the peak is going up with p. However, as p increases in a tiny amount, the peak goes up and down, not in a monotone way because of the discretization of the lockdown's starting day. The lockdown day is not the exact instant of passing the first threshold; it is at the next integer value day after. Moreover, as p increases in a tiny amount, the increased proportion of asymptomatic cases reduces the first wave's peak, making the graph go down until the point where the government policy is implemented a day later causing the sudden jump. The peak prevalence decreases gradually with small increases in p because the asymptomatic infections spread the virus less than symptomatic infections. However, at some point, the decrease in perceived prevalence postpones the onset of behavior changes by a day, causing an abrupt jump in Fig. 3.8. Therefore, the time elapsed between the instant in time when it passed the first threshold and the next day when the census is taken varies as p varies in tiny amounts.

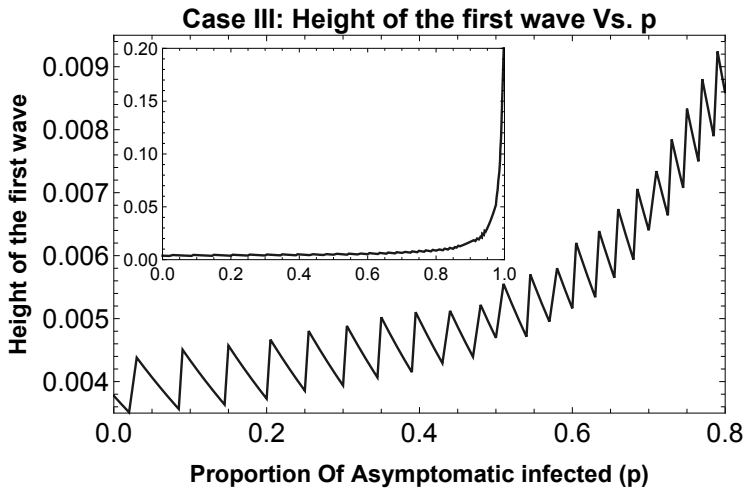

Figure 3.8: The peak of the first wave as a function of the proportion of asymptomatic infections (for $0 \leq p \leq 0.8$)

When the proportion of asymptomatic infections (p) is low, the epidemic spreads faster. This implies that the control measures are implemented relatively soon, and the epidemic peak is relatively low. Then, as p increases, the epidemic spreads more slowly initially, since asymptomatic infections spread it less. Besides, since fewer cases are

observed, the lockdown starts even later, which indicates that the peak is more heightened. Further, when p is high enough, there will never be enough perceived cases to initiate the lockdown, and the epidemic matches the case with no behavior changes.

Although not shown here, we obtained qualitatively identical results for the dependence of symptomatic prevalence and severe cases on p.

3.4.5 Sensitivity and uncertainty analysis

The goal of this subsection is to verify that our qualitative results are independent of the parameter values. We performed a sensitivity analysis of the CRN (Fig. 3.9(a)) and the fraction of susceptibles at final time (S^*_{tf}) (Fig. 3.9(b)) to determine how variations in parameter values impact $\mathcal{R}_c$ and S^*_{tf}. Namely, we increase each parameter by 0.1% (while preserving other parameters at the baseline values obtained in Table 3.2) and calculate the normalized sensitivity index. The results of the sensitivity analysis shown in Figs. 3.9 indicate the CRN is most sensitive to the infection rate (β), the reduction factor for symptomatic infection (τ), 1/the infectious period while individuals are pre-symptomatic (δ), the recovery rate of asymptomatic infected individuals (γ_A), and the proportion of infected with mild symptoms (q). S^*_{tf} is also influenced by β, q, τ, the proportion of individuals who remain asymptomatic for the whole course of infection (p), γ_A, and δ. Remarkably, both measures (CRN and S^*_{tf}) are highly sensitive to τ and p, which are scrutinized in this study. Among the parameters with higher sensitivity indices to both (CRN and S^*_{tf}), the proportion of infected with mild symptoms (q) is well-known [118, 119, 126].

Using ranges for the serial interval, incubation period, and basic reproductive number and the same method as section 4.1, we can estimate the ranges of parameter values (shown in Table 3.2). Figure 3.10 indicates the S^*_{tf} for case one (at the bottom of the figure) and case two (at the top of the figure) with δ over its range. The qualitative results

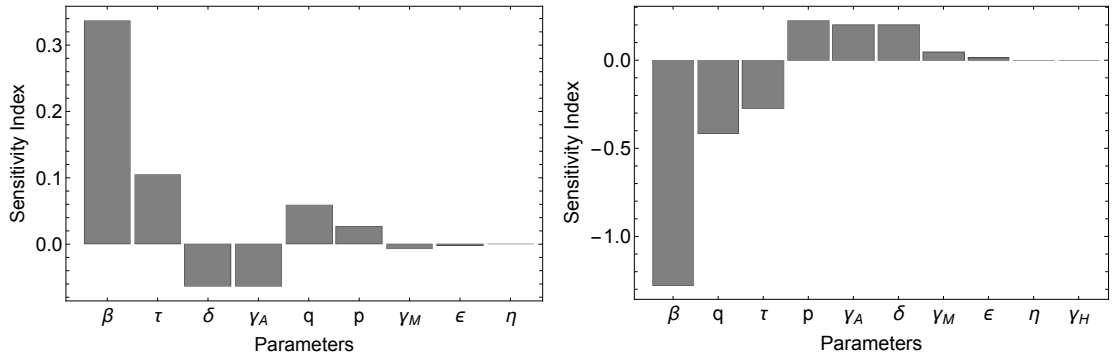

(a) (b)

Figure 3.9: Sensitivity Analysis for $\mathcal{R}_c$ (3.9(a)) and S^*_{tf} (3.9(b)): Sensitivity indices are listed in order of decreasing magnitude

for all three cases remain the same, which shows that our results are not dependent on parameter estimates. Hence, our qualitative results are robust and independent of parameter values.

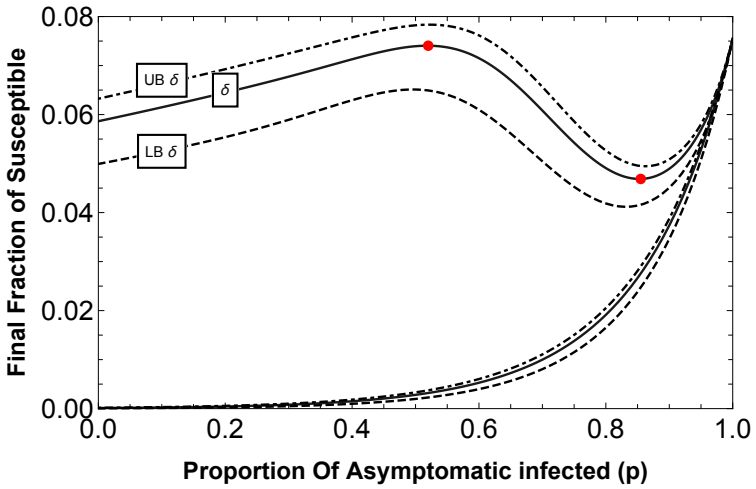

Figure 3.10: S^*_{tf} for case one (bottom) and case two (top) with δ over its range: dashed lines indicate the lower bound for δ; dot-dashed lines indicate the upper bound for δ; solid lines indicate the baseline value for δ

Figure 3.11(a) indicates three different functions representing the assumed relationship between θ and τ. Indeed, the two new functions work as extreme cases. One is a less reactive change where asymptomatic individuals only change their behavior when symp-

tomatic individuals are already nearly wholly isolated, while the other is the least reactive convex function possible. Figure 3.11(b) shows S^*_{tf} with the different $\theta(\tau)$ functions shown in Fig. 3.11(a). The dot-dashed curve in Fig. 3.11(b) (represented by the piecewise linear function (dot-dashed line in Fig. 3.11(a))) shows that the more asymptomatic individuals change their behavior relative to symptomatic individuals ($\theta(\tau)$), the more complex the dependence on p for the size of the epidemic - specifically, the more pronounced the non-monotone variation is for the epidemic size. All three functions describing the behavior change of asymptomatic individuals yield the same type of dependence of S^*_{tf} on p, showing that our qualitative results are robust.

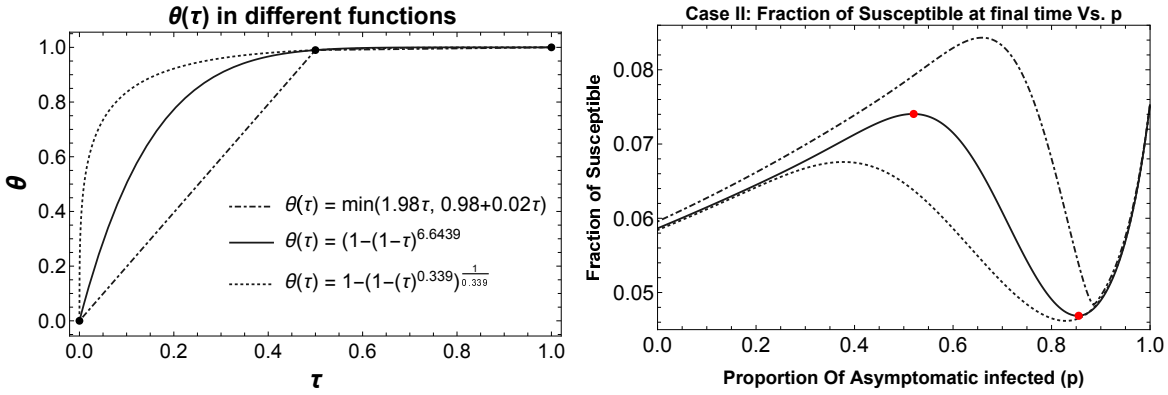

(a) (b)

Figure 3.11: 3.11(a) Different functions represent the relationship between θ and τ; 3.11(b) S^*_{tf} for case two with different functions of $\theta(\tau)$

3.5 Conclusion

We analyzed a deterministic compartmental model to evaluate and predict the impact of the proportion of asymptomatic infections (p) under three different behavior change scenarios finding that p plays a large role in changing the size and the time of the epidemic. Although the model is still too simplistic in directly guiding policymakers to mitigate the effects of p, and it is not intended to do so, the qualitative trends predicted by

our simulations can be beneficial in designing studies to quantify the influence of these asymptomatic infections. Our parameter estimates suggest that symptomatic infections spread the disease more than asymptomatic ones because the infectious period lasts longer, even considering effective isolation following diagnosis.

If behavior change is considered constant, which may occur based on background information that a community has, then the epidemic size is maximized, and the final fraction of susceptibles is minimized, when p is low. On the other hand, a high value of p maximizes only the outbreak's initial spread when the behavior change (τ) ranges between 0.05 and 0.5.

If, instead, behavior change occurs due to an instantaneous response to the disease's perceived prevalence, then the highest peak with the smallest overall outbreak occurs when p is between 0.52 and 0.59. Further, the epidemic reveals a relatively lower peak but with the largest overall outbreak when $p = 0.885$. The lowest peak with the smallest epidemic is shown when $p = 1$.

Finally, if behavior change occurs in response to government policies, then a higher value of p plays a significant role in changing the epidemic's duration, and maximizes the epidemic size. In contrast, a lower value of p means a significant behavior change is implemented since most of the infected individuals are observed. Therefore, the epidemic shows both the lowest peak and the smallest overall outbreak.

If p is high, that maximizes the epidemic size and plays a significant role in changing the epidemic's duration under scenario case three. Furthermore, a higher value of p contributes only to the infection's initial spread of the disease if the behavior change (τ) remains constant and ranges between 0.05 and 0.5. Moreover, if the behavior change is considered changing continually as in case two, then a higher value of p minimizes the disease's initial spread and the epidemic size.

A lower value of p maximizes the epidemic size if the behavior change (τ) is a constant

(case one). Suppose τ is considered to be as in case two and three. In that case, a lower value of p means a significant behavior change is implemented since most of the infected individuals are observed. Therefore, the epidemic shows both the lowest peak and the smallest overall outbreak.

Intermediate values of p, which are essential only under instantaneous behavior change, produce the highest peak and minimize the epidemic size.

In reality, behavior change occurs through all three of these mechanisms. There is a priori information. There are instantaneous behavior changes when individuals make their own decisions. There are also behavior changes that individuals may make when mandated by government policies. In this study, we have seen the effects of each of those forces separately. As the COVID-19 pandemic has spread across the world, we have seen government policies and individuals' behavior vary significantly from one country to another and from one state to another within the United States. It is essential to understand that the pandemic will play out differently depending on the dominant force behind people's behavior change.

In [116], the authors used a time scale argument and asymptotic expansion to show when the spontaneous behavioral changes and diseases dynamics occur on vastly different time scales, then their model observes multiple epidemic waves. In our model, delays in behavior change are necessary to show many waves within the same outbreak and asymmetric shapes of the epidemic, i.e., rising and decaying phases of the epidemic are different in shape, similar to [116]. Further, the present study model shows that the final fraction of susceptibles varies as p varies with significant behavior change. Our results are consistent with [115] that the second wave of infection, in case three, can occur when interventions are stopped too soon.

One of the limitations of this study is that we have assumed a consistent government policy. However, we have seen in the United States and some other countries that there are

multiple waves, but they differ. The second wave is higher than the first one because the government policies have been changing throughout the outbreak. Government policies have been inconsistent, making the shape of the pandemic irregular. Another limitation is that little to nothing was known about the characteristics of SARS-CoV-2 at the beginning of the current outbreak, which has produced a great variety of estimates about the disease's epidemiological characteristics as recovery time and proportion of asymptomatic infections. This limits the quantitative accuracy of our predictions, but the qualitative results hold even for other parameter values. In the future, we hope to extend our model to include two different diseases under different behavior change scenarios. Varying the relative infectiousness between asymptomatic and symptomatic infection is also a potential extension of this study. An Agent-Based Model (ABM) can be developed to allow such variations in individuals in epidemiological characteristics and behavioral. Further, models like our case two model can be extended to include a degree of memory using such an information index.

Chapter 4

How influenza vaccination and virus interference may impact combined influenza-coronavirus disease burden

4.1 Introduction

The current pandemic of coronavirus disease 2019 (COVID-19) is caused by infection with a new coronavirus (called SARS-CoV-2). Influenza (flu) is a contagious respiratory disease caused by influenza viruses. Both diseases are infectious respiratory illnesses. There are some critical differences between flu and COVID-19. COVID-19 differs from influenza in the mortality rate, infectiousness by individuals with no symptoms, and spreading more quickly. While there has long been a vaccine to protect against influenza, vaccines for COVID-19 are just beginning to be distributed around the world.

Even though the influenza vaccine gives no protection against COVID-19 [127], demand for influenza vaccine rose as countries planned for the second COVID-19 wave over the winter months of 2020-2021. High coverage of the vaccine can significantly reduce morbidity and mortality of the burden of influenza.

Although the influenza vaccine may protect against the risk of influenza, natural influenza infection may reduce the risk of noninfluenza respiratory viruses (NRV) by activating short-term non-specific immunity against these viruses, a phenomenon known as virus interference. In other words, individuals who have received the influenza vaccine

may be at higher risk for NRV infections than individuals who have had influenza infections because they do not exhibit the non-specific immunity associated with natural infection [128, 129, 130, 131, 132]. Studies in children and adults support the idea that the influenza vaccine may increase the risk of NRV infections compared to individuals recently recovered from influenza. A recent Dutch study among older adults showed an increased incidence of NRV infections in vaccinated versus unvaccinated persons [133]. A study in children who received the influenza vaccine reported four times more NRV infections [131]. In the case of adults, one study found a 36% increase in risk related to coronavirus infections [134].

It is still not clear whether COVID-19 infection causes similar interference with influenza or other respiratory viruses. Further, there is no definitive evidence about whether the influenza vaccine prevents virus interference with COVID-19. Limited knowledge has been available regarding whether the influenza vaccine affects COVID-19 infection risk. There are conflicting studies concerning this aspect. While some studies found that the influenza vaccination coverage rates correlated negatively with all COVID-19 outcomes [135, 136], other studies found that influenza vaccination coverage rates are associated significantly with recently observed COVID-19 infection rates [137, 138].

Ozaras et al. demonstrated that COVID-19 and influenza co-infection is rare. During their study period, 1103 patients were diagnosed with COVID-19. Among them, six patients (0.54%) were diagnosed co-infected with influenza [139]. Ding et al. confirmed that few patients were co-infected by both diseases. A total of 5 of the 115 patients confirmed with COVID-19 were also diagnosed with influenza virus infection, with three influenza A cases and two influenza B [140].

Mathematical models have been developed to improve our knowledge of respiratory virus transmission and study different aspects of viral interference dynamics, such as influenza-influenza interactions and influenza-NRV interactions. Despite the mounting

evidence of influenza and NRV interactions, mathematical models on influenza and NRV interference are rare [141]. A recent study by Velasco-Hernández et al. explained the interaction observed between influenza and respiratory syncytial virus (RSV) by using an SEIRS model and provided some evidence that RSV dominates influenza. Their model is a superinfection model where RSV infection takes over influenza infection. Furthermore, in their model, individuals already infected with influenza are less susceptible to RSV infection than healthy individuals because the authors assume that infected individuals will be taking some precautionary measures [142]. Merler et al. used a mathematical model to illustrate the role of acute respiratory infections in the transmission dynamics of the 1918 influenza pandemic. The authors proposed that co-infection with other respiratory pathogens leads to enhanced influenza transmission. Their model produced results that agree with mortality excess data during 1918 pandemic influenza [143]. None of these studies have to do with the virus interference phenomenon and vaccination. There is no mathematical study that incorporates both virus interference and influenza vaccine to the best of our knowledge.

This study aims to evaluate whether the influenza vaccine increases the combined disease burden of influenza and COVID-19 in a dual epidemic by using a mathematical compartmental model with differential equations. In this study, the well-known concept of DALY (Disability-Adjusted Life Years) is used to measure the combined disease burden. This calculation has two components for each disease: DALY for the survivals and DALY for non-survivals. We use dynamical systems models as tools to compare the outcomes of the influenza vaccine on the population.

4.2 Model Development

The model is developed to analyze respiratory infection, in which we consider two distinct diseases; disease 1 indicates influenza, and disease 2 indicates COVID-19. We divide the total population into susceptible (S), vaccinated (V), exposed (E_1 and E_2), infected (I_1 and I_2), and recovered (R_1 and R_2) compartments for each disease. Those vaccinated individuals infected by COVID-19 retain partial protection against influenza, requiring a separate chain of exposed (F_2), infective (K_2), and recovered (W_2) compartments. Individuals who recovered from disease 1 or 2 remain susceptible to the other disease, also requiring a separate chain of exposed (G_1 and G_2) and infective (J_1 and J_2) for each disease and recovered (R_3) compartments. Susceptible and vaccinated individuals can be infected by disease 1 (with a reduced rate for vaccinated individuals because of the vaccine's protection) through their contact with infected individuals in classes I_1 and J_1, or by disease 2 through their contact with infected individuals in classes I_2, K_2 and J_2 (with no vaccine protection). Following the observation that co-infection is rare, we assume that no one acquires a secondary infection during a primary infection. The model is described as follows:

$$
\begin{cases}
\frac{dS}{dt} = (1-\phi)\Lambda - \left[\beta_1 \frac{I_1+J_1}{N} + \beta_2 \frac{I_2+J_2+K_2}{N} + \mu\right] S, \\
\frac{dV}{dt} = \phi\Lambda - \left[\kappa\beta_1 \frac{I_1+J_1}{N} + \beta_2 \frac{I_2+J_2+K_2}{N} + \mu\right] V, \\
\frac{dE_1}{dt} = \beta_1 \frac{I_1+J_1}{N} S + \kappa\beta_1 \frac{I_1+J_1}{N} V - (\eta_1+\mu) E_1, \\
\frac{dE_2}{dt} = \beta_2 \frac{I_2+J_2+K_2}{N} S - (\eta_2+\mu) E_2, \\
\frac{dF_2}{dt} = \beta_2 \frac{I_2+J_2+K_2}{N} V - (\eta_2+\mu) F_2, \\
\frac{dI_1}{dt} = \eta_1 E_1 - (\gamma_1+\mu) I_1, \\
\frac{dI_2}{dt} = \eta_2 E_2 - (\gamma_2+\mu) I_2, \\
\frac{dK_2}{dt} = \eta_2 F_2 - (\gamma_2+\mu) K_2, , \\
\frac{dR_1}{dt} = \gamma_1 I_1 - \mu R_1 - \tau_1\beta_2 \frac{I_2+J_2+K_2}{N} R_1, \\
\frac{dR_2}{dt} = \gamma_2 I_2 - \mu R_2 - \tau_2\beta_1 \frac{I_1+J_1}{N} R_2, \\
\frac{dW_2}{dt} = \gamma_2 K_2 - \mu W_2 - \kappa\tau_2\beta_1 \frac{I_1+J_1}{N} W_2, \\
\frac{dG_1}{dt} = \tau_2\beta_1 \frac{I_1+J_1}{N} R_2 + \kappa\tau_2\beta_1 \frac{I_1+J_1}{N} W_2 - (\eta_1+\mu) G_1, \\
\frac{dG_2}{dt} = \tau_1\beta_2 \frac{I_2+J_2+K_2}{N} R_1 - (\eta_2+\mu) G_2, \\
\frac{dJ_1}{dt} = \eta_1 G_1 - (\gamma_1+\mu) J_1, \\
\frac{dJ_2}{dt} = \eta_2 G_2 - (\gamma_2+\mu) J_2, \\
\frac{dR_3}{dt} = \gamma_1 J_1 + \gamma_2 J_2 - \mu R_3,
\end{cases}
\tag{4.1}
$$

where β_1 and β_2 are influenza and COVID-19 infection rates, respectively. These infections are spreading in a large population; therefore, we assume that the contact rates are already saturated. Hence, we use standard incidence in this model instead of mass action. κ is the reduced susceptibility factor due to influenza vaccine protection, a dimensionless value between zero and one. Here η_1 and η_2 are the rates at which an individual departs exposed classes by becoming infectious. γ_1 and γ_2 are the recovery rates of influenza and COVID-

19, respectively.

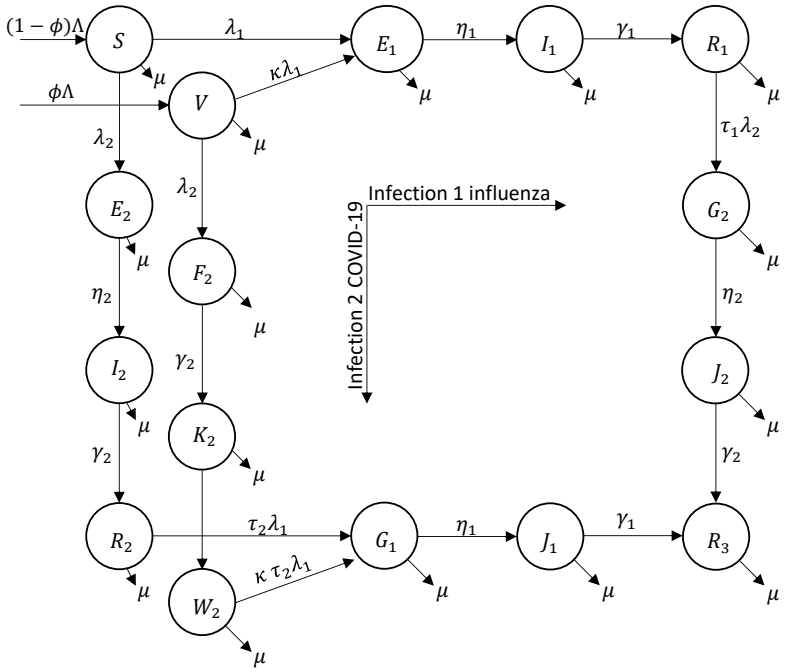

Figure 4.1: Flowchart of model (4.1), where $\lambda_1 = \beta_1 \frac{I_1+J_1}{N}$ and $\lambda_2 = \beta_2 \frac{I_2+J_2+K_2}{N}$

We consider that individuals who recover from disease 1 or 2 (R_1 or R_2) will be less susceptible to the other disease due to virus interference. We incorporate the phenomenon of virus interference as parameters τ_1 and τ_2 that can tune between 0 and 1. τ_1 (τ_2) is the factor by which individuals who have recovered from disease 1 (disease 2) are less susceptible to a disease 2 (disease 1) infection.

By adding equation (4.1), we get

$$\frac{dN}{dt} = \Lambda - \mu N$$

and

$$N(t) = \frac{\Lambda}{\mu} + e^{-\mu t}\left(N_0 - \frac{\Lambda}{\mu}\right),$$

	Notation	Definition
State variables	$S(t)$	Number of susceptible individuals at time t
	$V(t)$	Number of individuals who have received the influenza vaccine at time t
	$E_i(t)$	Number of individuals who have been exposed to disease i at time t
	$I_i(t)$	Number of individuals who have been infected by disease i at time t
	$F_2(t)$	Number of individuals who have received the influenza vaccine and exposed to disease 2 at time t
	$K_2(t)$	Number of individuals who have received the influenza vaccine and infected by disease 2 at time t
	$R_i(t)$	Number of individuals who have recovered from disease i at time t
	$W_2(t)$	Number of individuals who have received the influenza vaccine and recovered from disease 2 at time t
	$G_i(t)$	Number individuals who have been exposed to disease 2 and immunized by the other disease due to recovery at time t
	$J_i(t)$	Number individuals who have been infected by disease i and immunized by the other disease due to recovery at time t
	$R_3(t)$	Number of individuals who have recovered from both diseases at time t
Parameters	Λ	Recruitment rate (Individual/Time)
	μ	Per capita natural mortality rate (1/Time)
	β_i	disease i infection rate (1/Time)
	ϕ	The proportion of individuals who have received the flu vaccine (Dimensionless)
	κ	Influenza vaccine efficacy. (Dimensionless)
	κ	Reduced susceptibility factor due to the flu vaccine protection (Dimensionless)
	η_i	1/The duration time from exposure to onset of infectivity for disease i (1/Time)
	γ_i	Disease i recovery rate (1/Time)
	τ_i	Virus interference reduced rate after recovery from disease i (Dimensionless)

Table 4.1: State variable and parameter definitions and their units.

where N_0 is the initial total population of the system. Then, taking the limit as $t \to \infty$:

$$\lim_{t\to\infty} N(t) = \frac{\Lambda}{\mu}.$$

Since we are aiming at a constant population and not interested in the demographic

growth in this study, we assume that N is a constant population by taking $N(0) = \frac{\Lambda}{\mu}$. Therefore, the total population is constant for all t.

In this study, we have two additional differential equations to calculate the cumulative number of infections of disease 1, $C_1(t)$, and disease 2, $C_2(t)$

$$\begin{aligned}
\frac{dC_1}{dt} &= \beta_1 \frac{I_1 + J_1}{N} S + \kappa\beta_1 \frac{I_1 + J_1}{N} V + \tau_2\beta_1 \frac{I_1 + J_1}{N} R_2 + \kappa\tau_2\beta_1 \frac{I_1 + J_1}{N} W_2, \\
\frac{dC_2}{dt} &= \beta_2 \frac{I_2 + J_2 + K_2}{N} S + \beta_2 \frac{I_2 + J_2 + K_2}{N} V + \tau_1\beta_2 \frac{I_2 + J_2 + K_2}{N} R_1.
\end{aligned}$$

The combined disease burden can be estimated by using a cost function determined by the cumulative number of infections and the total number of deaths for each disease. The cost function determines the number of Disability Adjusted Life Years (DALY), which can be considered a loss of healthy life. The DALY is formed of Years of Life lived with Disability (YLD), resulting from infections, and Years of Life Lost (YLL) caused by death [144]. To estimate DALY components, we have

$$YLD_i = (1 - d_i) C_i(t) DW_i \frac{1}{\gamma_i},$$

where d_i is the case fatality ratio for disease i, $C_i(t)$ is the cumulative number of infections for disease i at time t, $\frac{1}{\gamma_i}$ is the average duration (in years) of infection for disease i, and DW_i is the disease weight. The term DW_i is assumed to be one for each disease. Further, we have

$$YLL_i = d_i C_i(t) L_i,$$

where L_i is the standard life expectancy at the age of death for disease i (average life

expectancy at birth − average age of infection). Therefore, for each disease i we have

$$\begin{aligned} DALY_i &= YLD_i + YLL_i \\ &= (1-d_i)C_i(t)DW_i\frac{1}{\gamma_i} + d_iC_i(t)L_i \\ &= C_i(t)[(1-d_i)DW_i\frac{1}{\gamma_i} + d_iL_i]. \end{aligned}$$

Then, finally the combined disease burden cost function is

$$DB(t) = C_1(t)\left[(1-d_1)DW_1\frac{1}{\gamma_1} + d_1L_1\right] + C_2(t)\left[(1-d_2)DW_2\frac{1}{\gamma_2} + d_2L_2\right].$$

4.3 Analysis

4.3.1 Disease Free Equilibrium and Control Reproductive Numbers

In this section, we compute the control reproductive number (CRN) which is one of the most significant thresholds that measures the infection's ability to spread. We use $\mathcal{R}_c$ instead of using the basic reproduction number, $\mathcal{R}_0$, because it includes vaccination as a control measure. In order to derive the $\mathcal{R}_c$ for model (4.1), we perform an equilibrium analysis.

The disease-free equilibrium (DFE) is a point where no disease is present in the population and occurs for model (4.1) when $I_i^* = J_i^* = K_2^* = 0$ for all $i = 1, 2$. By setting all differential equations in (4.1) equal to zero, we find the DFE of the form $\frac{\Lambda}{\mu}((1-\phi), \phi, 0, 0, 0, 0, 0, 0, 0, 0, 0, 0, 0, 0, 0, 0, 0)$.

To determine under what conditions infection with disease 1 or disease 2 can persist

in the population, we determine the control reproductive numbers for each infection. The control reproductive number is a threshold condition defined to be the average number of secondary infections caused by one primary infected individual in a wholly uninfected population under a control strategy. We compute $\mathcal{R}_1$ for disease 1, $\mathcal{R}_2$ for disease 2, and $\mathcal{R}_c$ for the presence of any infection with either disease.

To drive the various reproductive numbers of the diseases in the model, we use the next-generation operator method [145]. We find $\mathcal{R}_c = \max\{\mathcal{R}_1, \mathcal{R}_2\}$ where

$$\mathcal{R}_1 = \frac{\eta_1}{\eta_1 + \mu}\frac{\beta_1}{\gamma_1 + \mu}\left[(1-\phi) + \kappa\phi\right], \quad \mathcal{R}_2 = \frac{\eta_2}{\eta_2 + \mu}\frac{\beta_2}{\gamma_2 + \mu}.$$

The first two parts of $\mathcal{R}_1$ and $\mathcal{R}_2$ can be interpreted as the following. The first fraction $(\frac{\eta_i}{\eta_i+\mu})$ is the proportion of exposed individuals who did not die before they progress to infectious status. The second fraction $(\frac{\beta_i}{\gamma_i+\mu})$ is the product of the disease i infection rate and the average time an individual remains infected with disease i. The additional part of $\mathcal{R}_1$ is the proportion of vaccinated individuals (ϕ) times the reduced susceptibility factor (κ) due to the vaccine effectiveness added to the proportion of individuals who have not received the vaccine $(1-\phi)$.

We see that reduced infection factors of recovered individuals due to virus interference (τ_1 and τ_2) do not appear in the CRN because each of them occurs when the other infection is persistent. In an initial outbreak scenario, neither infection would be persisting in the population. Therefore, τ_1 and τ_2 should not be expected to appear in the CRN, but in the invasion reproductive numbers (IRNs).

4.3.2 Endemic Equilibria and Invasion Reproductive Numbers

We find another equilibrium when there is no infection with disease 2. In this case, $I_2^* = K_2^* = J_2^* = 0$. By setting all the nonlinear differential equations in model (4.1) equations equal to zero, we get $E_2^* = F_2^* = G_2^* = W_2^* = R_2^* = G_1^* = J_1^* = R_3^* = 0$ and the equilibrium is $EE_1 = \frac{\Lambda}{\mu}\big(\frac{1-\phi}{1+m}, \frac{\phi}{1+\kappa m}, \frac{(\gamma_1+\mu)m\mu}{\eta_1\beta_1}, 0, 0, \frac{m\mu}{\beta_1}, 0, 0, \frac{\gamma_1 m}{\beta_1}, 0, 0, 0, 0, 0, 0, 0\big)$, where

$$m = \frac{\kappa(\mathcal{R}_1 - 1) - (1 - (1-\kappa^2)\phi) + \sqrt{((1-(1-\kappa^2)\phi) - \kappa(\mathcal{R}_1 - 1))^2 + 4\kappa(1-(1-\kappa)\phi)(\mathcal{R}_1 - 1)}}{2\kappa(1-(1-\kappa)\phi)}.$$

Observe that this equilibrium makes biological sense only when $\mathcal{R}_1 > 1$. Further, the sum of uninfected compartments at EE_1 is $\frac{1+m(\kappa(1-\phi)+\phi)}{(1+m)(1+\kappa m)}$ and infected compartments is $\frac{m(1-(1-\kappa)\phi)}{\mathcal{R}_1}$.

The second single-disease equilibrium is found when there is no infection with disease 1. In this case, $I_1^* = J_1^* = 0$. By setting all differential equations in model 4.1 equal zero, we get $E_1^* = G_1^* = R_1^* = G_2^* = J_2^* = R_3^* = 0$ and and the equilibrium is $EE_2 = \frac{\Lambda}{\mu}$ $(\frac{1-\phi}{\mathcal{R}_2}$, $\frac{\phi}{\mathcal{R}_2}$, 0, $\frac{(\mathcal{R}_2-1)(1-\phi)(\gamma_2+\mu)\mu}{\beta_2\eta_2}$, $\frac{(\mathcal{R}_2-1)\phi(\gamma_2+\mu)\mu}{\beta_2\eta_2}$, 0, $\frac{(\mathcal{R}_2-1)(1-\phi)\mu}{\beta_2}$, $\frac{(\mathcal{R}_2-1)\phi(\gamma_2+\mu)\mu}{\beta_2}$, 0, $\frac{(\mathcal{R}_2-1)(1-\phi)\gamma_2}{\beta_2}$, $\frac{(\mathcal{R}_2-1)\phi\gamma_2}{\beta_2}$, 0, 0, 0, 0, 0).

We observe that the total population at EE_2 is $\frac{\Lambda}{\mu}$ (the sum of uninfected compartments is $\frac{1}{\mathcal{R}_2}$ and infected compartments is $1 - \frac{1}{\mathcal{R}_2}$) . Further, this equilibrium makes biological sense only when $\mathcal{R}_2 > 1$.

The invasion reproductive number (IRN), which is defined to be the average number of secondary infections caused by one primary infected individual with one disease in an environment where the other disease is endemic, measures the ability of a disease to invade while another disease is present and at equilibrium [146, 60, 147, 148].

We define IRN $\tilde{\mathcal{R}}_1$ to be the average number of secondary disease 1 infections caused by an infected individual introduced into a population at EE_2. $\tilde{\mathcal{R}}_2$ is defined similarly.

$\tilde{\mathcal{R}}_1$ is found through the next-generation operator method at EE_2, where we calculate the spectral radius of the matrix $F_1V_1^{-1}$ [145]. In this method, we assume implicitly that $\mathcal{R}_2 > 1$. We compute the spectral radius of $F_1V_1^{-1}$ is given by

$$\tilde{\mathcal{R}}_1 = \mathcal{R}_1\left[\frac{1}{\mathcal{R}_2} + \tau_2\left(\frac{\gamma_2}{\gamma_2+\mu}\frac{\eta_2}{\eta_2+\mu}\right)\left(1-\frac{1}{\mathcal{R}_2}\right)\right].$$

We observe that $\tilde{\mathcal{R}}_1$ is essentially $\mathcal{R}_1$ multiplied by a term representing a weighted average susceptibility to infection: the uninfected proportion at EE_2 ($\frac{1}{\mathcal{R}_2}$) weighting relative (unchanged) susceptibility 1, and the infected proportion ($1-\frac{1}{\mathcal{R}_2}$) weighting their average susceptibility τ_2 multiplied by the proportion of infecteds who do not die while infected (since by assumption the infected are unavailable for infection until they recover).

We also consider the IRN $\tilde{\mathcal{R}}_2$. $\tilde{\mathcal{R}}_2$ represents the ability of disease 2 to invade a susceptible population at EE_1. $\tilde{\mathcal{R}}_2$ is found similar to $\tilde{\mathcal{R}}_1$ and given by

$$\tilde{\mathcal{R}}_2 = \mathcal{R}_2\left[\left(\frac{1+m(\kappa(1-\phi)+\phi)}{(1+m)(1+\kappa m)}\right) + \tau_1\left(\frac{\gamma_1}{\gamma_1+\mu}\frac{\eta_1}{\eta_1+\mu}\right)\left(\frac{m(1-(1-\kappa)\phi)}{\mathcal{R}_1}\right)\right].$$

$\tilde{\mathcal{R}}_2$ can be interpreted term by term similarly to those for $\tilde{\mathcal{R}}_1$. From this view, we can see that $\tilde{\mathcal{R}}_2$ is $\mathcal{R}_2$ multiplied by a weighted average susceptibility to infection: the uninfected proportion at EE_1 ($\frac{1+m(\kappa(1-\phi)+\phi)}{(1+m)(1+\kappa m)}$) weighting relative (unchanged) susceptibility 1, and the infected proportion ($\frac{m(1-(1-\kappa)\phi)}{\mathcal{R}_1}$) weighting their average susceptibility τ_1 multiplied by the proportion of infecteds who do not die while infected.

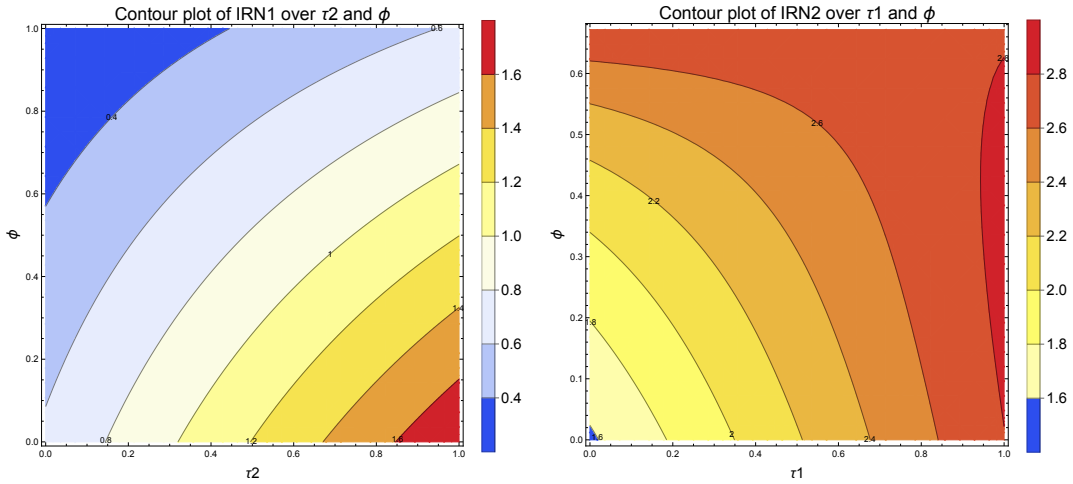

(a) (b)

Figure 4.2: Contour plot of IRN1 (IRN2) over ϕ and τ_2 and (τ_1)

4.4 Numerical Simulations

To address this study's goal, we take parameter values directly from Table 3 of [149] and Table 3.2. We consider disease 1 to be influenza H3N2 and disease 2 is COVID-19. Further, we allow the proportion of individuals who have received the vaccine (ϕ) to vary between 0 and 1 as a control measure.

For the estimation of parameter values of our cost function, we have the average age of the infection of influenza in the U.S. as 32.36 [150] and COVID-19 as 41.1 [10], and the average life expectancy at birth for the total U.S. population as 77.8 years [151]. That gives $L_1 = 77.8 - 32.36 = 45.44$ and $L_2 = 77.8 - 41.1 = 36.7$. We estimate case fatality ratios for influenza and COVID-19 by calculating the case fatality ratio for each age group from [150, 10] and then multiplying each age group's case fatality ratio by the proportion of the whole population in that age group, and summing the results [151], which gives $d_1 = 0.031\%$ and $d_2 = 1.96\%$. All these parameters give us an estimate of 0.02 DALY for one average case of influenza and 0.73 DALY for one average case of COVID-19.

Figure 4.2(a) (Fig. 4.2(b)) is a contour plot of $\tilde{\mathcal{R}}_1$ ($\tilde{\mathcal{R}}_2$) over τ_2 (τ_1) and ϕ. First, for

Fig. 4.2(a), we observed that $\tilde{\mathcal{R}}_1$ increases with τ_2, which indicates that virus interference plays a major role in reducing $\tilde{\mathcal{R}}_1$. Besides, $\tilde{\mathcal{R}}_1$ decreases with ϕ, indicating that as the proportion of individuals who received the influenza vaccine increased, the ability of influenza to spread becomes difficult. Then, for Fig. 4.2(b), we observed that $\tilde{\mathcal{R}}_2$ increases with τ_1 and ϕ, except if τ_1 is close to one. $\tilde{\mathcal{R}}_2$ increases with ϕ can be interpreted as the more individuals who have received the influenza vaccine results to the more of them are available for infection with COVID-19. However, the closer ϕ to making $\mathcal{R}_1 = 1$, the fewer individuals are infected with influenza. Therefore, the ability of virus interference to affect COVID-19 transmission is irrelevant at the top of Fig. 4.2(b). τ_1 describes an altered characteristic of individuals who recovered from influenza; however, if ϕ is high enough, there are no individuals infected with influenza ($\mathcal{R}_1 < 1$). Therefore, τ_1 is pointless for high values of ϕ.

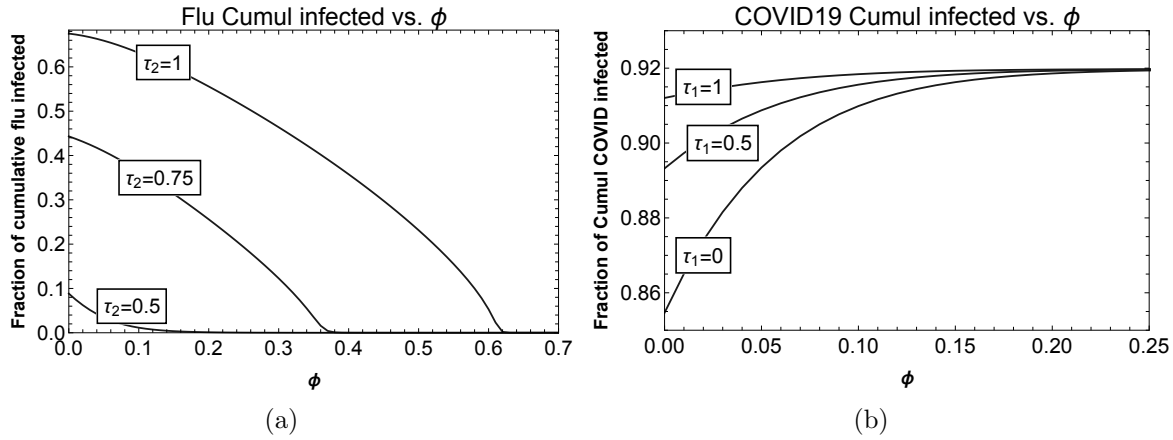

(a) (b)

Figure 4.3: Cumulative infected of disease 1 (disease 2) vs. ϕ with different amount of τ_2 (τ_1)

Figure 4.3(a) (Fig. 4.3(b)) indicates the cumulative proportion of infected with influenza (COVID-19) after 365 days of introducing one infected case with varying ϕ between zero and one, and with different values of τ_2 (τ_1). For Fig. 4.3(a), we noticed that high values of ϕ indicate that $\mathcal{R}_1 < 1$ and virus interference (τ_2) is irrelevant since the influenza

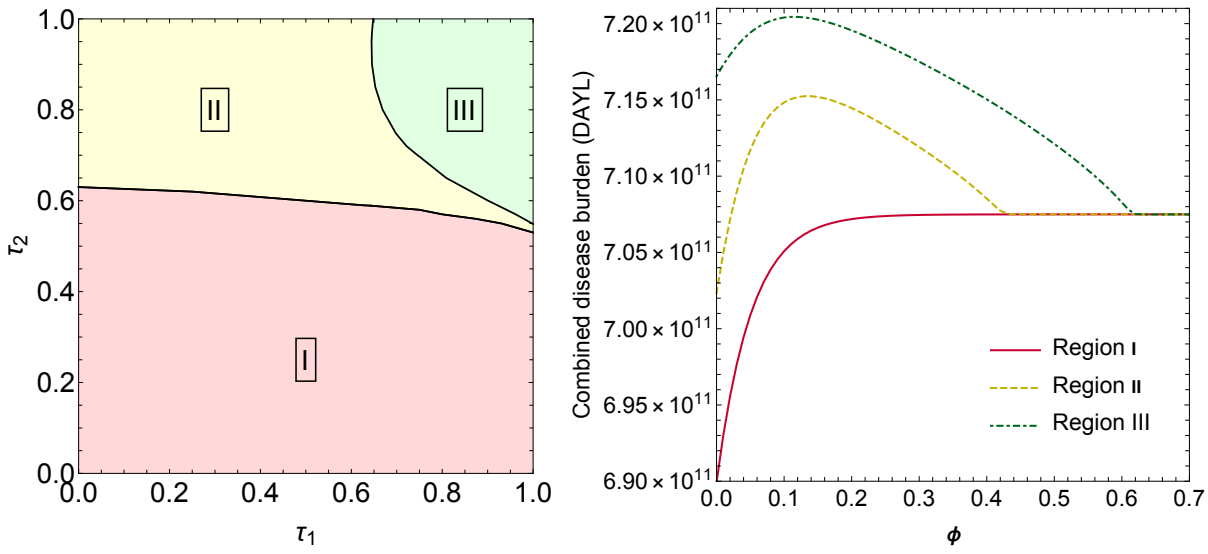

(a) (b)

Figure 4.4: 4.4(a) Variations of virus interference factors (τ_1 and τ_2) against the combined disease burden; 4.4(b) The combined disease burden vs. ϕ) with varying amounts of τ_1 and τ_2

is not going to spread, which is consistent with Fig. 4.2(a). Further, for lower values of ϕ, τ_2 plays a significant role in reducing the cumulative proportion of infected since by preventing individuals who have had COVID-19 and recovered from getting influenza, that is also preventing them from infecting other individuals. For Fig. 4.3(b), we observed that as $\phi > 0.2$, τ_1 is irrelevant whereas if no one gets vaccinated ($\phi = 0$), then natural virus interference makes about 5% difference.

We provide numerical simulations of the combined disease burden with varying amounts of influenza vaccine proportion (ϕ) and virus interference factors (τ_1 and τ_2). Figure 4.4(a) indicates how variations in virus interference factors (τ_1 and τ_2) affect the combined disease burden characteristics when the amount of influenza vaccine proportion (ϕ) varies. The horizontal axis is virus interference by influenza against COVID-19 (τ_1). The vertical axis is virus interference by COVID-19 against influenza (τ_2). Figure 4.4(a) is created by incrementing τ_2 along the vertical axis, and then for each value of τ_2 increasing τ_1 along

the horizontal axis until the threshold characteristic is observed. The first threshold, between region I and II, is whether the disease burden exceeds the asymptotic line, i.e., the first point where the non-monotone increase occurs. The second threshold is between region II and III, where the combined disease burden at $\phi = 0$ exceeds the asymptotic line for $\phi > 0.6$.

Increasing ϕ from 0 to around 0.2 increases overall COVID-19 incidence due to reduced virus interference; this increases the overall disease burden. At the same time, influenza incidence is decreasing due to vaccination, but the decrease in overall disease burden is outweighed by the increase in COVID-19 until the point where COVID-19 incidence plateaus. After that, flu incidence decreases (as ϕ increases) until it drops to zero as $\mathcal{R}_1$ reaches 1. In region I, this occurs before COVID-19 incidence plateaus, but in regions II and III there is a drop in overall disease burden after COVID-19 incidence plateaus. For virus interference factors (τ_1 and τ_2) in region I, increasing ϕ always raises the combined disease burden (see the solid curve in Fig. 4.4(b)). For τ_1 and τ_2 in region II, increasing ϕ increases the combined disease burden until the point where the cumulative number of COVID-19 infections stops rising, then combined disease burden decreases until it reaches the asymptotic level, which is the point where the cumulative number of influenza infections is zero. However, in this region, influenza vaccination always increases the combined disease burden relative to vaccinating no one (see the dashed curve in Fig. 4.4(b)). For τ_1 and τ_2 in region III, increasing ϕ will share the same characteristics as in region II. Still, vaccinating two-thirds or more of the population decreases the combined disease burden relative to vaccinating no one (see the dash-dotted curve in Fig. 4.4(b)).

Another way to illustrate the net virus interference is by a mathematical description

$$r = \sqrt{(1-\tau_1)^2 + (1-\tau_2)^2},$$

where r is a measure of the net virus interference. (It is the Euclidean distance from (τ_1, τ_2)=(1,1), the top right corner of Fig. 4.4(a), which represents no virus interference.) Therefore, very roughly, region III is the region when $r < 0.35$, which can be described as low net virus interference. Region II has $r > 0.35$ but $\tau_2 > 0.6$, which can be explained as significant net virus interference but limited COVID-19-on-influenza interference. Finally, region I has $\tau_2 < 0.6$, which can be described as high COVID-19-on-influenza interference.

4.5 Discussion and Conclusions

Mathematical models help forecast disease dynamics and estimate significant quantities such as disease burden that can be incorporated to evaluate disease control measures such as vaccination. This study analyzed deterministic models to investigate whether the influenza vaccine increases the combined disease burden of influenza and COVID-19 in a dual epidemic due to a virus interference phenomenon that reduces susceptibility to secondary infections in those who recover from natural primary infections (rather than being vaccinated). The control reproductive numbers $\mathcal{R}_1$ and $\mathcal{R}_1$ as well as the invasion reproductive numbers $\tilde{\mathcal{R}}_1$ and $\tilde{\mathcal{R}}_2$ were computed in this study. Together, these quantities measure a disease's ability to spread in a completely susceptible population or to invade while another disease is present and at equilibrium.

According to this study, the combined disease burden's behavior depends on virus interference factors (τ_1 and τ_2), representing reduced susceptibility, and on the proportion of the population vaccinated against influenza (ϕ). Regardless of virus interference levels, vaccinating two-thirds or more of the population against influenza eliminates the flu outbreak ($\mathcal{R}_1 < 1$). In this case, the cumulative number of influenza infections drops off, and the cumulative number of COVID-19 infections levels off in ϕ, so that for vaccine coverage ϕ of 60% or more, there is effectively no change in the combined disease burden

as virus interference levels vary (see Fig. 4.4(b)). However, virus interference still plays a strategic role, as it affects disease burden at lower vaccine coverage levels, and thus affects whether the combined disease burden is lower for high or low coverage. Depending on the degree of virus interference, the combined disease burden either increases monotonically in ϕ, or rises and then falls to an asymptotic level. As seen in Fig. 4.4(b), these effects divide virus interference levels into three regions.

If τ_1 and τ_2 fall in region I, indicating that for all values of τ_1 virus interference by COVID-19 (τ_2) gives a 40% or more protection against influenza, then the influenza vaccine is always unhelpful, and the lowest value of the combined disease burden is when no one has received the flu vaccine ($\phi = 0$). In this region (region I), the combined disease burden only increases when the vaccine coverage (ϕ) is between 0% and 20% since, in this interval, the cumulative number of COVID-19 infections increases and the cumulative number of flu infections dies out. Further, when the vaccine coverage (ϕ) is more than 20%, there is no change in the combined disease burden due to no changes in the cumulative number of flu and COVID-19 infections and (see the solid curve in Fig. 4.4(b)).

If τ_1 and τ_2 fall in region II, indicating that virus interference by the flu gives at least 30% protection against COVID-19 and virus interference by COVID-19 gives at most 40% protection against the flu, then influenza vaccine is not beneficial since the combined disease burden is lower for no vaccine coverage $\phi = 0$ than for vaccine coverage ϕ of 60%. Under this condition, the combined disease burden's lowest value is when $\phi = 0$. In this region, the combined disease burden increases with ϕ when vaccine coverage (ϕ) is between 0% and 20% since the cumulative number of COVID-19 infections increases at a much larger scale than the cumulative number of flu infections decreases. Further, when vaccine coverage (ϕ) is between 20% and 60%, the combined disease burden falls approaching the asymptotic level since the cumulative number of flu infections decreases

and no changes in the cumulative number of COVID-19 infections. However, the end results in this region are that vaccinating no one is better than vaccinating two-thirds of the population (see the dashed curve in Fig. 4.4(b)).

For low net virus interference (region III), influenza vaccination is only beneficial if two-thirds of the population or more have received the influenza vaccine ($\phi > 0.6$) because the combined disease burden is lower for vaccine coverage ϕ of 60% or more than for no vaccine coverage $\phi = 0$. Under this condition, the combined disease burden shares the same qualitative trends as in region II, but the lowest value is when $\phi \geq 0.6$ (see the dash-dotted curve in Fig. 4.4(b)).

In general, influenza vaccination only lowers the overall disease burden when net virus interference is relatively low (region III) and vaccine coverage is high enough that the reduction in influenza cases more than compensates for any increase in COVID-19 cases. Influenza vaccination may increase the overall disease burden because the average disease burden for one case of COVID-19 is significantly higher than the average disease burden for one case of influenza. Additionally, the actual degree of virus interference in each direction remains a source of some debate, and further studies are needed to measure these factors. However, according to [134], influenza-on-COVID-19 interference (τ_1) is 0.64, which places us either in region I or region II, depending on what COVID-19-on-influenza interference (τ_2) is. Regardless of COVID-19-on-influenza interference (τ_2), the combined disease burden is always higher relatively when vaccinating two-thirds or more of the population.

In cases where two co-circulating diseases have separate burdens and case fatality ratios, vaccinating only a few individuals against one of the diseases may make the other disease increase the combined disease burden more than the vaccine reduces due to virus interference being a part of the cause. It is essential to get a proper amount of vaccine coverage to overcome the range of increasing overall disease burden. The model structure

that we developed could also be used to evaluate the risk of vaccination increasing disease burden by preventing virus interference for other diseases. Hence, it would be important to develop estimates for the degree to which the respective infections interfere with each other by stimulating the body's nonspecific immune response.

One of the limitations of this study is that the actual degree of virus interference is still being debated. As all the epidemiological parameters in the study become better known, we will have not just a better idea of where the region boundaries are, but a better idea of which region we are in. In the future, a study can be extended to consider vaccination in both diseases since vaccinating the world's population against COVID-19 is currently a primary focus of world public health. Only when a large proportion of the population has been vaccinated will we begin to observe effects such as those outlined in this study.

Chapter 5

Conclusion

In this dissertation, we used mathematical models to assess the effects of some characteristics of respiratory diseases like influenza and COVID-19 either alone or co-circulating and how might influenza vaccine affect this interplay. Our work in Chapter 2 is the first to incorporate both: two different populations, with the possibility that a proportion of each population is vaccinated, and two different strains of influenza. We illustrate how the mismatch between vaccine strains and circulating strains affects the existence and duration of an influenza outbreak during Hajj. Besides, the qualitative trends of Chapter 3 predicted by our simulations can help design studies to quantify the influence of these asymptomatic infections.

In Chapter 2, we developed a deterministic model consisting of two populations and two influenza strains to evaluate the impact of mismatch between influenza vaccine strains and circulating strains. Our results showed that the existence and duration of an influenza outbreak during Hajj depend on the influenza vaccine effectiveness. Hence, we considered four scenarios: vaccine strains for both populations match/mismatch circulating strains, and vaccine strains match their target strains and mismatch the other strains. Further, a scenario where a novel pandemic strain arises. We showed that if the influenza vaccines match their target strains, there will be only a small outbreak of strain H3N2 and no

outbreak of strain H1N1. Mismatching for non-target strains causes about 10,000 new H3N2 cases, and mismatching for both strains causes about 2,000 more new H1N1 cases and 6,000 additional H3N2 cases during Hajj. Complete mismatch in a pandemic scenario may infect over 342,000 additional pilgrims (13.75%) and cause more cases in their home countries.

In Chapter 3, we analyzed a deterministic compartmental model to evaluate and predict the impact of the proportion of asymptomatic infections under three different behavior change scenarios. We also see that the proportion of asymptomatic infection plays a significant role in changing the size and the time of the epidemic. Further, it is essential to understand that the pandemic will play out differently depending on the dominant force behind people's behavior change. Our results showed that a high proportion of asymptomatic infections plays a vital role in changing the epidemic's duration and maximizes the epidemic size if the behavior change occurs in response to government policies. Further, an intermediate proportion of asymptomatic infections maximizes the epidemic size in the case of continually adjusted behavior change. Finally, a low proportion of asymptomatic infections maximizes the epidemic size in the case of constant behavior change.

In Chapter 4, we analyzed deterministic models to investigate whether the influenza vaccine increases the combined disease burden of influenza and COVID-19 in a dual epidemic due to a virus interference phenomenon that reduces susceptibility to secondary infections in those who recover from natural primary infections (rather than being vaccinated). We showed that the combined disease burden's behavior depends on virus interference factors and the proportion of the population vaccinated against influenza. Furthermore, influenza vaccination only lowers the overall disease burden when net virus interference is relatively low, and vaccine coverage is high enough to reduce influenza cases more than compensates for any increase in COVID-19 cases. Additionally, the actual de-

gree of virus interference in each direction remains a source of some debate, and further studies are needed to measure these factors.

Consolidating the various chapters of this dissertation leads to two conclusions on the study of respiratory diseases and behavior changes. From Chapters 2 and 4, it is clear that virus interference can occur in the influenza vaccine mismatch. Since the cause of virus interference is not the vaccine failure but the natural influenza infection. Therefore, in the influenza vaccine mismatch case, we expect that increasing the influenza vaccine coverage will not increase the combined disease burden because the vaccine fails to protect against natural influenza infection. From Chapters 3 and 4, behavior changes during a dual outbreak of influenza and COVID-19 would reduce the number of infections since both diseases are airborne diseases with the exact infection mechanisms. In addition to this, in a significant behavior change that reduces contacts, we expect that virus interference would be less crucial.

Bibliography

[1] Fred Brauer and Carlos Castillo-Chavez. *Mathematical Models in Population Biology and Epidemiology*. Springer, New York City, NY, second edition, 2012.

[2] David L Smith, Katherine E Battle, Simon I Hay, Christopher M Barker, Thomas W Scott, and F Ellis McKenzie. Ross, Macdonald, and a theory for the dynamics and control of mosquito-transmitted pathogens. *PLoS Pathog*, 8(4):e1002588, 2012.

[3] World Health Organization (2018) Influenza Fact Sheet. http://www.who.int/influenza, Access date: September 2019.

[4] Fred M Davenport. Current knowledge of influenza vaccine. *JAMA*, 182(1):11–13, 1962.

[5] Anthony E Fiore, Timothy M Uyeki, Karen Broder, Lyn Finelli, Gary L Euler, James A Singleton, John K Iskander, Pascale M Wortley, David K Shay, Joseph S Bresee, et al. Prevention and control of influenza with vaccines: recommendations of the Advisory Committee on Immunization Practices (ACIP). 2010.

[6] Robert B Couch and Julius A Kasel. Immunity to Influenza in Man. *Annual Review of Microbiology*, 37(1):529–549, 1983.

[7] Tadao Sonoguchi, Hiroshi Naito, Masaru Hara, Yasue Takeuchi, and Hideo Fukumi. Cross-subtype protection in humans during sequential, overlapping, and/or concur-

rent epidemics caused by H3N2 and H1N1 influenza viruses. *Journal of Infectious Diseases*, 151(1):81–88, 1985.

[8] Neil M Ferguson, Alison P Galvani, and Robin M Bush. Ecological and immunological determinants of influenza evolution. *Nature*, 422(6930):428, 2003.

[9] Michael T Osterholm, Nicholas S Kelley, Alfred Sommer, and Edward A Belongia. Efficacy and effectiveness of influenza vaccines: a systematic review and meta-analysis. *The Lancet Infectious Diseases*, 12(1):36–44, 2012.

[10] Centers for Disease Control and Prevention. Coronavirus Disease 2019 (COVID-19). https://www.cdc.gov/coronavirus/2019-ncov/prevent-getting-sick/how-covid-spreads.html, Access date: September 2020.

[11] Susan R Weiss and Sonia Navas-Martin. Coronavirus pathogenesis and the emerging pathogen severe acute respiratory syndrome coronavirus. *Microbiol. Mol. Biol. Rev.*, 69(4):635–664, 2005.

[12] Shuo Su, Gary Wong, Weifeng Shi, Jun Liu, Alexander CK Lai, Jiyong Zhou, Wenjun Liu, Yuhai Bi, and George F Gao. Epidemiology, genetic recombination, and pathogenesis of coronaviruses. *Trends in Microbiology*, 24(6):490–502, 2016.

[13] Yongshi Yang, Fujun Peng, Runsheng Wang, Kai Guan, Taijiao Jiang, Guogang Xu, Jinlyu Sun, and Christopher Chang. The deadly coronaviruses: The 2003 SARS pandemic and the 2020 novel coronavirus epidemic in China. *Journal of Autoimmunity*, page 102434, 2020.

[14] Nancy J Cox and Kanta Subbarao. Influenza. *The Lancet*, 354(9186):1277–1282, 1999.

[15] Andrea C Tricco, Ayman Chit, Charlene Soobiah, David Hallett, Genevieve Meier, Maggie H Chen, Mariam Tashkandi, Chris T Bauch, and Mark Loeb. Comparing influenza vaccine efficacy against mismatched and matched strains: a systematic review and meta-analysis. *BMC Medicine*, 11(1):153, 2013.

[16] H Kelly and K Grant. Interim analysis of pandemic influenza (h1n1) 2009 in australia: surveillance trends, age of infection and effectiveness of seasonal vaccination. *Eurosurveillance*, 14(31):19288, 2009.

[17] Vittorio Demicheli, Tom Jefferson, Eliana Ferroni, Alessandro Rivetti, and Carlo Di Pietrantonj. Vaccines for preventing influenza in healthy adults. *Cochrane Database of Systematic Reviews*, (2), 2018.

[18] Tom Jefferson, Carlo Di Pietrantonj, Lubna A Al-Ansary, Eliana Ferroni, Sarah Thorning, and Roger E Thomas. Vaccines for preventing influenza in the elderly. *Cochrane Database of Systematic Reviews*, (2), 2010.

[19] Tadao Sonoguchi, Mitsuo Sakoh, Nobuharu Kunita, Kiyoaki Satsuta, Hideo Noriki, and Hideo Fukumi. Reinfection with influenza A (H2N2, H3N2, and H1N1) viruses in soldiers and students in Japan. *Journal of Infectious Diseases*, 153(1):33–40, 1986.

[20] Shin'ichi Shimada, Kenji Sadamasu, Takayuki Shinkai, Osamu Kakuta, Yoshinori Kikuchi, Michiyo Shinohara, Kazue Uchida, Rie Doi, Kyoko Kohmoto, Miho Shimizu, et al. Virological analysis of a case of dual infection by influenza A (H3N2) and B viruses. *Japanese Journal of Infectious Diseases*, 59(1):67–68, 2006.

[21] Shoichi Toda, Reiko Okamoto, Tomoko Nishida, Toshiki Nakao, Masatoshi Yoshikawa, Eitaro Suzuki, and Shigenori Miyamura. Isolation of influenza A/H3

and B viruses from an influenza patient: confirmation of co-infection by two influenza viruses. *Japanese Journal of Infectious Diseases*, 59(2):142–143, 2006.

[22] Alessandra Falchi, Christophe Arena, Laurent Andreoletti, Julien Jacques, N Leveque, Thierry Blanchon, B Lina, Clement Turbelin, Yves Dorleans, Antoine Flahault, et al. Dual infections by influenza A/H3N2 and B viruses and by influenza A/H3N2 and A/H1N1 viruses during winter 2007, Corsica Island, France. *Journal of Clinical Virology*, 41(2):148–151, 2008.

[23] Elodie Ghedin, Adam Fitch, Alex Boyne, Sara Griesemer, Jay DePasse, Jayati Bera, Xu Zhang, Rebecca A Halpin, Marita Smit, Lance Jennings, et al. Mixed infection and the genesis of influenza virus diversity. *Journal of Virology*, 83(17):8832–8841, 2009.

[24] Nelson Lee, Paul KS Chan, WaiYip Lam, Cheuk-chun C Szeto, David SC Hui, et al. Co-infection with pandemic H1N1 and seasonal H3N2 influenza viruses. *Annals of Internal Medicine*, 152(9):618–619, 2010.

[25] Liwen Ju, Lufang Jiang, Jixing Yang, Qing Shi, Qingwu Jiang, Huiguo Shen, Yiyun Tan, and Yuanan Lu. Co-infection with influenza A/H1N1 and A/H3N2 viruses in a patient with influenza-like illness during the winter/spring of 2008 in Shanghai, China. *Journal of Medical Virology*, 82(8):1299–1305, 2010.

[26] Matthew Peacey, Richard J Hall, Stephanie Sonnberg, Mariette Ducatez, Shevaun Paine, Mackenzie Nicol, Jacqui C Ralston, Don Bandaranayake, Virginia Hope, Richard J Webby, et al. Pandemic (H1N1) 2009 and seasonal influenza A (H1N1) co-infection, New Zealand, 2009. *Emerging Infectious Diseases*, 16(10):1618, 2010.

[27] Arianna Calistri, Cristiano Salata, Marina Cosentino, Samuele Asnicar, Elisa Franchin, Riccardo Cusinato, Monia Pacenti, Isabella Donatelli, and Giorgio Palù.

Report of two cases of influenza virus A/H1N1v and B co-infection during the 2010/2011 epidemics in the Italian Veneto Region. *Virology Journal*, 8(1):502, 2011.

[28] JM Liu, DY Liu, YJ Yang, MQ Huang, LX Lin, and CM Xie. Investigation of mixed infection with influenza A (H1N1) and seasonal B viruses in medical staff. *Chin J Nosocomiology*, 15:052, 2011.

[29] Christopher A Myers, Matthew R Kasper, Chadwick Y Yasuda, Chin Savuth, David J Spiro, Rebecca Halpin, Dennis J Faix, Robert Coon, Shannon D Putnam, Thomas F Wierzba, et al. Dual infection of novel influenza viruses A/H1N1 and A/H3N2 in a cluster of Cambodian patients. *The American Journal of Tropical Medicine and Hygiene*, 85(5):961–963, 2011.

[30] Fahad N Almajhdi and Ghazanfar Ali. Report on influenza A and B viruses: their coinfection in a Saudi leukemia patient. *BioMed Research International*, 2013, 2013.

[31] Yefei Zhu, Xian Qi, Lunbiao Cui, Minghao Zhou, and Hua Wang. Human co-infection with novel avian influenza A H7N9 and influenza A H3N2 viruses in Jiangsu province, China. *The Lancet*, 381(9883):2134, 2013.

[32] Fabio Tramuto, Carmelo Massimo Maida, Francesco Magliozzo, Emanuele Amodio, and Francesco Vitale. Occurrence of a case of influenza A (H1N1) pdm09 and B co-infection during the epidemic season 2012–2013. *Infection, Genetics and Evolution*, 23:95–98, 2014.

[33] Jun Li, Yu Kou, Xinfen Yu, Yongxiang Sun, Yinyan Zhou, Xiaoying Pu, Tao Jin, Jingcao Pan, and George F Gao. Human co-infection with avian and seasonal influenza viruses, China. *Emerging Infectious Diseases*, 20(11):1953, 2014.

[34] Wanju Zhang, Dongyi Zhu, Di Tian, Lei Xu, Zhaokui Zhu, Zheng Teng, Jing He, Shan Shan, Yi Liu, Wei Wang, et al. Co-infection with avian (H7N9) and pandemic

(H1N1) 2009 influenza viruses, China. *Emerging Infectious Diseases*, 21(4):715, 2015.

[35] F Perez-Garcia, V Vasquez, V de Egea, P Catalán, B Rodríguez-Sánchez, and E Bouza. Influenza A and B co-infection: a case–control study and review of the literature. *European Journal of Clinical Microbiology & Infectious Diseases*, 35(6):941–946, 2016.

[36] Rakefet Pando, Yaron Drori, Nehemya Friedman, Aharona Glatman-Freedman, Hanna Sefty, Tamar Shohat, Ella Mendelson, Musa Hindiyeh, and Michal Mandelboim. Influenza A (H1N1) pdm 2009 and influenza B virus co-infection in hospitalized and non-hospitalized patients during the 2015–2016 epidemic season in Israel. *Journal of Clinical Virology*, 88:12–16, 2017.

[37] Tatiana Schäffer Gregianini, Ivana R Santos Varella, Patricia Fisch, Letícia Garay Martins, and Ana BG Veiga. Dual and triple infections with influenza A and B viruses: a case-control study in Southern Brazil. *The Journal of Infectious Diseases*, 220(6):961–968, 2019.

[38] Wei Liu, Zeng-De Li, Fang Tang, Mao-Ti Wei, Yi-Gang Tong, Lei Zhang, Zhong-Tao Xin, Mai-Juan Ma, Xiao-Ai Zhang, Li-Juan Liu, et al. Mixed infections of pandemic H1N1 and seasonal H3N2 viruses in 1 outbreak. *Clinical Infectious Diseases*, 50(10):1359–1365, 2010.

[39] Saudi Ministry of Health. Hajj and Umrah Health Regulations (2020/1441H). https://www.moh.gov.sa/en/Hajj/HealthGuidelines/HealthGuidelinesDuringHajj/Pages/HealthRequirements.aspx, Access date: March 2020.

[40] Mohammad Alfelali, Gulam Khandaker, Robert Booy, and Harunor Rashid. Mismatching between circulating strains and vaccine strains of influenza: Effect on Hajj pilgrims from both hemispheres. *Human vaccines & immunotherapeutics*, 12(3):709–715, 2016.

[41] Carlos Castillo-Chavez, Herbert W Hethcote, Viggo Andreasen, Simon A Levin, and Wei M Liu. Epidemiological models with age structure, proportionate mixing, and cross-immunity. *Journal of Mathematical Biology*, 27(3):233–258, 1989.

[42] Sunetra Gupta, Martin CJ Maiden, Ian M Feavers, Sean Nee, Robert M May, and Roy M Anderson. The maintenance of strain structure in populations of recombining infectious agents. *Nature Medicine*, 2(4):437, 1996.

[43] Viggo Andreasen, Juan Lin, and Simon A Levin. The dynamics of cocirculating influenza strains conferring partial cross-immunity. *Journal of Mathematical Biology*, 35(7):825–842, 1997.

[44] Sunetra Gupta, Neil Ferguson, and Roy Anderson. Chaos, persistence, and evolution of strain structure in antigenically diverse infectious agents. *Science*, 280(5365):912–915, 1998.

[45] Juan Lin, Viggo Andreasen, and Simon A Levin. Dynamics of influenza A drift: the linear three-strain model. *Mathematical Biosciences*, 162(1-2):33–51, 1999.

[46] JR Gog and J Swinton. A status-based approach to multiple strain dynamics. *Journal of Mathematical Biology*, 44(2):169–184, 2002.

[47] Julia R Gog and Bryan T Grenfell. Dynamics and selection of many-strain pathogens. *Proceedings of the National Academy of Sciences*, 99(26):17209–17214, 2002.

[48] Masashi Kamo and Akira Sasaki. The effect of cross-immunity and seasonal forcing in a multi-strain epidemic model. *Physica D: Nonlinear Phenomena*, 165(3-4):228–241, 2002.

[49] Juan Lin, Viggo Andreasen, Renato Casagrandi, and Simon A Levin. Traveling waves in a model of influenza A drift. *Journal of Theoretical Biology*, 222(4):437–445, 2003.

[50] Maciej F Boni, Julia R Gog, Viggo Andreasen, and Freddy B Christiansen. Influenza drift and epidemic size: the race between generating and escaping immunity. *Theoretical Population Biology*, 65(2):179–191, 2004.

[51] Olivier Restif and Bryan T Grenfell. Integrating life history and cross-immunity into the evolutionary dynamics of pathogens. *Proceedings of The Royal Society B: Biological Sciences*, 273(1585):409–416, 2005.

[52] M Nuno, Zhilan Feng, Maia Martcheva, and Carlos Castillo-Chavez. Dynamics of two-strain influenza with isolation and partial cross-immunity. *SIAM Journal on Applied Mathematics*, 65(3):964–982, 2005.

[53] Ben Adams and Akira Sasaki. Cross-immunity, invasion and coexistence of pathogen strains in epidemiological models with one-dimensional antigenic space. *Mathematical Biosciences*, 210(2):680–699, 2007.

[54] Pavlo Minayev and Neil Ferguson. Improving the realism of deterministic multi-strain models: implications for modelling influenza A. *Journal of The Royal Society Interface*, 6(35):509–518, 2008.

[55] F Chamchod and Nicholas F Britton. On the dynamics of a two-strain influenza model with isolation. *Mathematical Modelling of Natural Phenomena*, 7(3):49–61, 2012.

[56] KW Chung and Roger Lui. Dynamics of two-strain influenza model with cross-immunity and no quarantine class. *Journal of Mathematical Biology*, 73(6-7):1467–1489, 2016.

[57] Shingo Iwami, Yasuhiro Takeuchi, and Xianning Liu. Avian–human influenza epidemic model. *Mathematical Biosciences*, 207(1):1–25, 2007.

[58] Mohamed Derouich and Abdesslam Boutayeb. An avian influenza mathematical model. *Applied Mathematical Sciences*, 2(36):1749–1760, 2008.

[59] Hans J Bremermann and HR Thieme. A competitive exclusion principle for pathogen virulence. *Journal of Mathematical Biology*, 27(2):179–190, 1989.

[60] Christopher M Kribs-Zaleta and Anuj Mubayi. The role of adaptations in two-strain competition for sylvatic Trypanosoma cruzi transmission. *Journal of Biological Dynamics*, 6(2):813–835, 2012.

[61] Perrine Pelosse and Christopher M Kribs-Zaleta. The role of the ratio of vector and host densities in the evolution of transmission modes in vector-borne diseases. The example of sylvatic Trypanosoma cruzi. *Journal of Theoretical Biology*, 312:133–142, 2012.

[62] Christopher M Kribs-Zaleta. Graphical analysis of evolutionary trade-off in sylvatic Trypanosoma cruzi transmission modes. *Journal of Theoretical Biology*, 353:34–43, 2014.

[63] Raul Isea, Karl E. Lonngren. A preliminary mathematical model for the dynamic transmission of Dengue, Chikungunya and Zika. *American Journal of Modern Physics and Application*, 3(2):11–15, 2016.

[64] Kamaldeen O Okuneye, Jorge X Velasco-Hernandez, and Abba B Gumel. The "unholy" chikungunya–dengue–zika trinity: A theoretical analysis. *Journal of Biological Systems*, 25(04):545–585, 2017.

[65] US Department of State Bureau of Consular Affairs: Pilgrimage Travelers (Hajj and Umrah). https://travel.state.gov/content/travel/en/international-travel/before-you-go/travelers-with-special-considerations/hajj-umrah.html, Access date: February 2020.

[66] Odo Diekmann, Johan Andre Peter Heesterbeek, and Johan AJ Metz. On the definition and the computation of the basic reproduction ratio R 0 in models for infectious diseases in heterogeneous populations. *Journal of Mathematical Biology*, 28(4):365–382, 1990.

[67] Nidhi Parikh, Mina Youssef, Samarth Swarup, and Stephen Eubank. Modeling the effect of transient populations on epidemics in Washington DC. *Scientific Reports*, 3:3152, 2013.

[68] Y Hsieh, H Chen, J Yen, D Liu, L Chang, C Lu, P Shao, C Lee, and L Huang. Influenza in Taiwan: seasonality and vaccine strain match. *Journal of Microbiology Immunology and Infection*, 38(4):238, 2005.

[69] Y Al-Maghderi, A Al-Joudi, A Choudhry, A Al-Rabeah, M Ibrahim, and A Turkistani. Behavioral risk factors for diseases during Hajj 1422 H. *Saudi Epidemiology Bulletin*, 9(3):19–20, 2002.

[70] Randa Nooh and Abdul Jamil. Effect of health education advice on Saudi Hajjis, Hajj 1423 H (2003 G). *Saudi Epidemiology Bulletin*, 11:2–11, 2004.

[71] K AlMudmeigh, A AlNaji, M AlEnezi, et al. Incidence of Hajj related acute respiratory infection among pilgrims from Riyadh, 1423 H (2003 G). *Saudi Epidemiology Bulletin*, 10:25–26, 2003.

[72] Dr Kholeidi, Mohammed F Baksh, Abdul Aziz Al Mazam, and G Ashry. Seropositive in Clinical Influenza Cases Among Pilgrims During Hajj, 1421 Ha. *Saudi Epidemiology Bulletin*, 8(4), 2001.

[73] H Rashid, S Shafi, R Booy, H El Bashir, K Ali, MC Zambon, ZA Memish, J Ellis, PG Coen, and E Haworth. Influenza and respiratory syncytial virus infections in British Hajj pilgrims. *Emerging Health Threats Journal*, 1(1):7072, 2008.

[74] H Rashid, S Shafi, E Haworth, H El Bashir, ZA Memish, M Sudhanva, M Smith, H Auburn, and R Booy. Viral respiratory infections at the Hajj: comparison between UK and Saudi pilgrims. *Clinical Microbiology and Infection*, 14(6):569–574, 2008.

[75] Harunor Rashid, Shuja Shafi, Elizabeth Haworth, Ziad A Memish, Haitham El Bashir, Kamal A Ali, and Robert Booy. Influenza vaccine in Hajj pilgrims: policy issues from field studies. *Vaccine*, 26(37):4809–4812, 2008.

[76] Fahad S Al-Jasser, Ibrahim A Kabbash, Mohammad A AlMazroa, and Ziad A Memish. Patterns of Diseases and Preventive Measures Among Domestic Hajjis From Central, Saudi Arabia. *Saudi Med J*, 33(8):879–86, 2012.

[77] Afagh Moattari, Amir Emami, Mohsen Moghadami, and Behnam Honarvar. Influenza viral infections among the Iranian Hajj pilgrims returning to Shiraz, Fars province, Iran. *Influenza and other respiratory viruses*, 6(6):e77–e79, 2012.

[78] Mazyar Ziyaeyan, Abdolvahab Alborzi, Marziyeh Jamalidoust, Mahsa Moeini, Gholam R Pouladfar, Bahman Pourabbas, Mandana Namayandeh, Mohsen Moghadami,

Kamran Bagheri-Lankarani, and Talat Mokhtari-Azad. Pandemic 2009 influenza A (H1N1) infection among 2009 Hajj Pilgrims from Southern Iran: a real-time RT-PCR-based study. *Influenza and other respiratory viruses*, 6(6):e80–e84, 2012.

[79] Philippe Gautret, Vinh Vu Hai, Seydou Sani, Mahamadou Doutchi, Philippe Parola, and Philippe Brouqui. Protective measures against acute respiratory symptoms in French pilgrims participating in the Hajj of 2009. *Journal of travel medicine*, 18(1):53–55, 2010.

[80] Osamah Barasheed, Harunor Rashid, Leon Heron, Iman Ridda, Elizabeth Haworth, Jonathan Nguyen-Van-Tam, Dominic E Dwyer, Robert Booy, and Hajj Research Team. Influenza vaccination among Australian Hajj pilgrims: uptake, attitudes, and barriers. *Journal of travel medicine*, 21(6):384–390, 2014.

[81] Mohammad Hassan Emamian, Ali Mohammad Hassani, and Mansooreh Fateh. Respiratory tract infections and its preventive measures among Hajj pilgrims, 2010: A nested case control study. *International journal of preventive medicine*, 4(9):1030, 2013.

[82] Mohammad Azeem, Mohamed Tashani, Osamah Barasheed, Leon Heron, Grant A Hill-Cawthorne, Elizabeth Haworth, Dominic E Dwyer, Harunor Rashid, and Robert Booy. Knowledge, attitude and practice (KAP) survey concerning antimicrobial use among Australian Hajj pilgrims. *Infectious Disorders-Drug Targets (Formerly Current Drug Targets-Infectious Disorders)*, 14(2):125–132, 2014.

[83] Hajj Statistics 2019. https://www.stats.gov.sa/en/28, Access date: November 2019.

[84] WHO Influenza Vaccination Timing. https://www.who.int/influenza/vaccines/tropics/Vaccinetimingv4.pdf?ua=1, Access date: November 2019.

[85] Ziad A Memish, Abdullah M Assiri, Raheela Hussain, Ibrahim Alomar, and Gwen Stephens. Detection of respiratory viruses among pilgrims in Saudi Arabia during the time of a declared influenza A (H1N1) pandemic. *Journal of travel medicine*, 19(1):15–21, 2011.

[86] Ziad A Memish, Abdullah Assiri, Abdulhafeez Turkestani, Saber Yezli, Malak al Masri, Rémi Charrel, Tassadit Drali, Jean Gaudart, Sophie Edouard, Philippe Parola, et al. Mass gathering and globalization of respiratory pathogens during the 2013 Hajj. *Clinical Microbiology and Infection*, 21(6):571–e1, 2015.

[87] Juliette Stehlé, Nicolas Voirin, Alain Barrat, Ciro Cattuto, Vittoria Colizza, Lorenzo Isella, Corinne Régis, Jean-François Pinton, Nagham Khanafer, Wouter Van den Broeck, et al. Simulation of an SEIR infectious disease model on the dynamic contact network of conference attendees. *BMC Medicine*, 9(1):87, 2011.

[88] Ashleigh R Tuite, Amy L Greer, Michael Whelan, Anne-Luise Winter, Brenda Lee, Ping Yan, Jianhong Wu, Seyed Moghadas, David Buckeridge, Babak Pourbohloul, et al. Estimated epidemiologic parameters and morbidity associated with pandemic H1N1 influenza. *Cmaj*, 182(2):131–136, 2010.

[89] Ira M Longini Jr, Eugene Ackerman, and Lila R Elveback. An optimization model for influenza A epidemics. *Mathematical Biosciences*, 38(1-2):141–157, 1978.

[90] Paul EM Fine. The interval between successive cases of an infectious disease. *American Journal of Epidemiology*, 158(11):1039–1047, 2003.

[91] Åke Svensson. A note on generation times in epidemic models. *Mathematical Biosciences*, 208(1):300–311, 2007.

[92] Hiroshi Nishiura, Natalie M Linton, and Andrei R Akhmetzhanov. Serial interval of novel coronavirus (COVID-19) infections. *International Journal of Infectious Diseases*, 93:284–286, 2020.

[93] Qun Li, Xuhua Guan, Peng Wu, Xiaoye Wang, Lei Zhou, Yeqing Tong, Ruiqi Ren, Kathy SM Leung, Eric HY Lau, Jessica Y Wong, et al. Early transmission dynamics in Wuhan, China, of novel coronavirus–infected pneumonia. *New England Journal of Medicine*, 382:1199–1207, 2020.

[94] Michael Day. Covid-19: identifying and isolating asymptomatic people helped eliminate virus in italian village. *BMJ: British Medical Journal (Online)*, 368:m1165, 2020.

[95] Michael Day. Covid-19: four fifths of cases are asymptomatic, China figures indicate. *BMJ (Clinical research ed.)*, 369:m1375, April 2020.

[96] Ruiyun Li, Sen Pei, Bin Chen, Yimeng Song, Tao Zhang, Wan Yang, and Jeffrey Shaman. Substantial undocumented infection facilitates the rapid dissemination of novel coronavirus (SARS-CoV-2). *Science*, 368(6490):489–493, 2020.

[97] Hiroshi Nishiura, Tetsuro Kobayashi, Takeshi Miyama, Ayako Suzuki, Sung-mok Jung, Katsuma Hayashi, Ryo Kinoshita, Yichi Yang, Baoyin Yuan, Andrei R Akhmetzhanov, et al. Estimation of the asymptomatic ratio of novel coronavirus infections (COVID-19). *International Journal of Infectious Diseases*, 94:154, 2020.

[98] Kenji Mizumoto, Katsushi Kagaya, Alexander Zarebski, and Gerardo Chowell. Estimating the asymptomatic proportion of coronavirus disease 2019 (COVID-19) cases on board the Diamond Princess cruise ship, Yokohama, Japan, 2020. *Eurosurveillance*, 25(10):2000180, 2020.

[99] Yuanyuan Dong, Xi Mo, Yabin Hu, Xin Qi, Fang Jiang, Zhongyi Jiang, and Shilu Tong. Epidemiological characteristics of 2143 pediatric patients with 2019 coronavirus disease in china. *Pediatrics*, 16(16), 2020.

[100] Yi Chen, Aihong Wang, Bo Yi, K Ding, Haibo Wang, Jianmei Wang, and G Xu. The epidemiological characteristics of infection in close contacts of COVID-19 in Ningbo city. *Chin J Epidemiol*, 41(5):668–672, 2020.

[101] Zhiru Gao, Yinghui Xu, Chao Sun, Xu Wang, Ye Guo, Shi Qiu, and Kewei Ma. A systematic review of asymptomatic infections with COVID-19. *Journal of Microbiology, Immunology and Infection*, pages 1684–1182, 2020.

[102] Yan Bai, Lingsheng Yao, Tao Wei, Fei Tian, Dong-Yan Jin, Lijuan Chen, and Meiyun Wang. Presumed asymptomatic carrier transmission of COVID-19. *Jama*, 323(14):1406–1407, 2020.

[103] Christophe Fraser, Steven Riley, Roy M Anderson, and Neil M Ferguson. Factors that make an infectious disease outbreak controllable. *Proceedings of the National Academy of Sciences*, 101(16):6146–6151, 2004.

[104] Sang Woo Park, Daniel M Cornforth, Jonathan Dushoff, and Joshua S Weitz. The time scale of asymptomatic transmission affects estimates of epidemic potential in the COVID-19 outbreak. *Epidemics*, page 100392, 2020.

[105] William Hardy McNeill and William McNeill. *Plagues and peoples*. Anchor Books, New York, USA, 1998.

[106] Martin CJ Bootsma and Neil M Ferguson. The effect of public health measures on the 1918 influenza pandemic in us cities. *Proceedings of the National Academy of Sciences*, 104(18):7588–7593, 2007.

[107] G James Rubin, Richard Amlôt, Lisa Page, and Simon Wessely. Public perceptions, anxiety, and behaviour change in relation to the swine flu outbreak: cross sectional telephone survey. *BMJ*, 339:b2651, 2009.

[108] James Holland Jones and Marcel Salathe. Early assessment of anxiety and behavioral response to novel swine-origin influenza A (H1N1). *PLoS One*, 4(12):e8032, 2009.

[109] Joseph TF Lau, Xilin Yang, HY Tsui, and Ellie Pang. SARS related preventive and risk behaviours practised by Hong Kong-mainland China cross border travellers during the outbreak of the SARS epidemic in Hong Kong. *Journal of Epidemiology & Community Health*, 58(12):988–996, 2004.

[110] Faical Ndairou, Ivan Area, Juan J Nieto, and Delfim FM Torres. Mathematical modeling of COVID-19 transmission dynamics with a case study of Wuhan. *Chaos, Solitons & Fractals*, 135:109846, 2020.

[111] Joseph T Wu, Kathy Leung, and Gabriel M Leung. Nowcasting and forecasting the potential domestic and international spread of the 2019-nCoV outbreak originating in Wuhan, China: a modelling study. *The Lancet*, 395(10225):689–697, 2020.

[112] Manotosh Mandal, Soovoojeet Jana, Swapan Kumar Nandi, Anupam Khatua, Sayani Adak, and TK Kar. A model based study on the dynamics of COVID-19: Prediction and control. *Chaos, Solitons & Fractals*, page 109889, 2020.

[113] Hana M Dobrovolny. Modeling the role of asymptomatics in infection spread with application to SARS-CoV-2. *Plos One*, 15(8):e0236976, 2020.

[114] Frederik Verelst, Lander Willem, and Philippe Beutels. Behavioural change models for infectious disease transmission: a systematic review (2010–2015). *Journal of The Royal Society Interface*, 13(125):20160820, 2016.

[115] Sara Y Del Valle, Susan M Mniszewski, and James M Hyman. Modeling the impact of behavior changes on the spread of pandemic influenza. In Piero Manfredi and Alberto D'Onofrio, editors, *Modeling the interplay between human behavior and the spread of infectious diseases*, pages 59–77. Springer New York, 2013.

[116] Piero Poletti, Bruno Caprile, Marco Ajelli, Andrea Pugliese, and Stefano Merler. Spontaneous behavioural changes in response to epidemics. *Journal of Theoretical Biology*, 260(1):31–40, 2009.

[117] Bruno Buonomo. Effects of information-dependent vaccination behavior on coronavirus outbreak: insights from a SIRI model. *Ricerche di Matematica*, 69(2):483–499, 2020.

[118] Zunyou Wu and Jennifer M McGoogan. Characteristics of and important lessons from the coronavirus disease 2019 (COVID-19) outbreak in China: summary of a report of 72314 cases from the Chinese Center for Disease Control and Prevention. *JAMA*, 323(13):1239–1242, 2020.

[119] Report of the WHO-China Joint Mission on Coronavirus Disease 2019 (COVID-19). https://www.who.int/docs/default-source/coronaviruse/who-china-joint-mission-on-covid-19-final-report.pdf. Published February 16, 2020. Access date: March 2020.

[120] Yan Deng, Wei Liu, Kui Liu, Yuan-Yuan Fang, Jin Shang, Ling Zhou, Ke Wang, Fan Leng, Shuang Wei, Lei Chen, et al. Clinical characteristics of fatal and recovered cases of coronavirus disease 2019 in Wuhan, China: a retrospective study. *Chinese Medical Journal*, 133(11):1261–1267, 2020.

[121] Sasmita Poudel Adhikari, Sha Meng, Yu-Ju Wu, Yu-Ping Mao, Rui-Xue Ye, Qing-Zhi Wang, Chang Sun, Sean Sylvia, Scott Rozelle, Hein Raat, et al. Epidemiology,

causes, clinical manifestation and diagnosis, prevention and control of coronavirus disease (COVID-19) during the early outbreak period: a scoping review. *Infectious Diseases of Poverty*, 9(1):1–12, 2020.

[122] Qifang Bi, Yongsheng Wu, Shujiang Mei, Chenfei Ye, Xuan Zou, Zhen Zhang, Xiaojian Liu, Lan Wei, Shaun A Truelove, Tong Zhang, et al. Epidemiology and transmission of COVID-19 in 391 cases and 1286 of their close contacts in Shenzhen, China: a retrospective cohort study. *The Lancet Infectious Diseases*, 20(8):911–919, 2020.

[123] Dawei Wang, Bo Hu, Chang Hu, Fangfang Zhu, Xing Liu, Jing Zhang, Binbin Wang, Hui Xiang, Zhenshun Cheng, Yong Xiong, et al. Clinical characteristics of 138 hospitalized patients with 2019 novel coronavirus–infected pneumonia in Wuhan, China. *JAMA*, 323(11):1061–1069, 2020.

[124] Lan Lan, Dan Xu, Guangming Ye, Chen Xia, Shaokang Wang, Yirong Li, and Haibo Xu. Positive RT-PCR test results in patients recovered from COVID-19. *JAMA*, 323(15):1502–1503, 2020.

[125] Ying Liu, Albert A Gayle, Annelies Wilder-Smith, and Joacim Rocklöv. The reproductive number of COVID-19 is higher compared to SARS coronavirus. *Journal of Travel Medicine*, 27(2), 2020.

[126] Centers for Disease Control and Prevention. Interim Clinical Guidance for Management of Patients with Confirmed Coronavirus Disease (COVID-19). https://www.cdc.gov/coronavirus/2019-ncov/hcp/clinical-guidance-management-patients.html, Access date: February 2021.

[127] Zainab Shahid, Ricci Kalayanamitra, Brendan McClafferty, Douglas Kepko, Devyani Ramgobin, Ravi Patel, Chander Shekher Aggarwal, Ramarao Vunnam, Nitasa

Sahu, Dhirisha Bhatt, et al. COVID-19 and older adults: what we know. *Journal of the American Geriatrics Society*, 68(5):926–929, 2020.

[128] Shuo Feng, Ashley L Fowlkes, Andrea Steffens, Lyn Finelli, and Benjamin J Cowling. Assessment of virus interference in a test-negative study of influenza vaccine effectiveness. *Epidemiology (Cambridge, Mass.)*, 28(4):514, 2017.

[129] M Suzuki, A Camacho, and K Ariyoshi. Potential effect of virus interference on influenza vaccine effectiveness estimates in test-negative designs. *Epidemiology & Infection*, 142(12):2642–2646, 2014.

[130] Benjamin J Cowling and Hiroshi Nishiura. Virus interference and estimates of influenza vaccine effectiveness from test-negative studies. *Epidemiology*, 23(6):930–931, 2012.

[131] Benjamin J Cowling, Vicky J Fang, Hiroshi Nishiura, Kwok-Hung Chan, Sophia Ng, Dennis KM Ip, Susan S Chiu, Gabriel M Leung, and JS Malik Peiris. Increased risk of noninfluenza respiratory virus infections associated with receipt of inactivated influenza vaccine. *Clinical Infectious Diseases*, 54(12):1778–1783, 2012.

[132] H Kelly, Steven Barry, Karen Laurie, and Geoffry Mercer. Seasonal influenza vaccination and the risk of infection with pandemic influenza: a possible illustration of non-specific temporary immunity following infection. *Eurosurveillance*, 15(47):19722, 2010.

[133] Josine Van Beek, Reinier H Veenhoven, Jacob P Bruin, Renée AJ Van Boxtel, Marit MA De Lange, Adam Meijer, Elisabeth AM Sanders, Nynke Y Rots, and Willem Luytjes. Influenza-like illness incidence is not reduced by influenza vaccination in a cohort of older adults, despite effectively reducing laboratory-confirmed influenza virus infections. *The Journal of Infectious Diseases*, 216(4):415–424, 2017.

[134] Greg G Wolff. Influenza vaccination and respiratory virus interference among department of defense personnel during the 2017–2018 influenza season. *Vaccine*, 38(2):350–354, 2020.

[135] Mauro Amato, José Pablo Werba, Beatrice Frigerio, Daniela Coggi, Daniela Sansaro, Alessio Ravani, Palma Ferrante, Fabrizio Veglia, Elena Tremoli, and Damiano Baldassarre. Relationship between Influenza Vaccination Coverage Rate and COVID-19 Outbreak: An Italian Ecological Study. *Vaccines*, 8(3):535, 2020.

[136] Iván Martínez-Baz, Camino Trobajo-Sanmartín, Irati Arregui, Ana Navascués, Marta Adelantado, Juan Indurain, Ujué Fresán, Carmen Ezpeleta, and Jesús Castilla. Influenza Vaccination and Risk of SARS-CoV-2 Infection in a Cohort of Health Workers. *Vaccines*, 8(4):611, 2020.

[137] Andreas Martin Lisewski. Association between Influenza Vaccination Rates and SARS-CoV-2 Outbreak Infection Rates in OECD Countries. *Social Science Research Network*, 2020.

[138] Ebmphet Consortium et al. COVID-19 severity in Europe and the USA: Could the seasonal influenza vaccination play a role? *Social Science Research Network*, 2020.

[139] Resat Ozaras, Rasim Cirpin, Arif Duran, Habibe Duman, Ozgur Arslan, Yasin Bakcan, Metin Kaya, Huseyin Mutlu, Leyla Isayeva, Fatih Kebanlı, et al. Influenza and COVID-19 Co-infection: Report of 6 cases and review of the Literature. *Journal of Medical Virology*, 92(11):2657–2665, 2020.

[140] Qiang Ding, Panpan Lu, Yuhui Fan, Yujia Xia, and Mei Liu. The clinical characteristics of pneumonia patients coinfected with 2019 novel coronavirus and influenza virus in Wuhan, China. *Journal of Medical Virology*, 92(9):1549–1555, 2020.

[141] Lulla Opatowski, Marc Baguelin, and Rosalind M Eggo. Influenza interaction with cocirculating pathogens and its impact on surveillance, pathogenesis, and epidemic profile: A key role for mathematical modelling. *PLoS Pathogens*, 14(2):e1006770, 2018.

[142] Jorge Xicoténcatl Velasco-Hernández, Mayra Núñez-López, Andreu Comas-García, Daniel Ernesto Noyola Cherpitel, and Marcos Capistrán Ocampo. Superinfection between influenza and RSV alternating patterns in San Luis Potosí State, México. *PloS One*, 10(3):e0115674, 2015.

[143] Stefano Merler, Piero Poletti, Marco Ajelli, Bruno Caprile, and Piero Manfredi. Coinfection can trigger multiple pandemic waves. *Journal of Theoretical Biology*, 254(2):499–507, 2008.

[144] Christopher J Murray. Quantifying the burden of disease: the technical basis for disability-adjusted life years. *Bulletin of the World Health Organization*, 72(3):429, 1994.

[145] Pauline Van den Driessche and James Watmough. Reproduction numbers and sub-threshold endemic equilibria for compartmental models of disease transmission. *Mathematical Biosciences*, 180(1-2):29–48, 2002.

[146] Christopher Mitchell and Christopher Kribs. Invasion reproductive numbers for periodic epidemic models. *Infectious Disease Modelling*, 4:124–141, 2019.

[147] Pei Zhang, Gregory J Sandland, Zhilan Feng, Dashun Xu, and Dennis J Minchella. Evolutionary implications for interactions between multiple strains of host and parasite. *Journal of theoretical biology*, 248(2):225–240, 2007.

[148] Travis C Porco and Sally M Blower. Designing hiv vaccination policies: subtypes and cross-immunity. *Interfaces*, 28(3):167–190, 1998.

[149] Mohammed H Alharbi and Christopher M Kribs. A Mathematical Modeling Study: Assessing Impact of Mismatch Between Influenza Vaccine Strains and Circulating Strains in Hajj. *Bulletin of Mathematical Biology*, 83(1):1–26, 2021.

[150] CDC. Estimated Influenza Illnesses, Medical visits, Hospitalizations, and Deaths in the United States — 2019–2020 Influenza Season. https://www.cdc.gov/flu/about/burden/2019-2020.html#flu-burden-infographic, 2020. Accessed: March 2021.

[151] U.S. Census Bureau (2019). Annual Estimates of the Resident Population for Selected Age Groups by Sex for the United States: April 1, 2010 to July 1, 2019. https://www.census.gov/newsroom/press-kits/2020/population-estimates-detailed.html, 2019. Accessed: March 2021.

BIOGRAPHICAL STATEMENT

Mohammed Hameed Alharbi was born in Jeddah, Saudi Arabia. He earned his Bachelor of Science degree in Mathematics from King Abdulaziz University in 2011. In May 2017, he earned an honors Master of Science in Mathematics at the University of Houston-Clear Lake. After receiving his Master's degree, he entered the mathematics doctoral program at UTA, where he worked under the supervision of Christopher Kribs and performed research in mathematical modeling of infectious diseases. During his doctoral program, he was awarded the Michael B. and Wanda G. Ray Fellowship and Maverick Science Graduate Research Fellowship.